In: Progress in Solid State Chemistry Research
Editors: Ronald W. Buckley, pp. 109-172
ISBN 1-60021-567-X

Chapter 5

ALKALINE EARTH METAL PHOSPHONATES: FROM SYNTHETIC CURIOSITIES TO NANOTECHNOLOGY APPLICATIONS

Konstantinos D. Demadis*
Crystal Engineering, Growth and Design Laboratory,
Department of Chemistry, University of Crete,
Voutes, Heraklion GR-71003, Crete, Greece

ABSTRACT

Metal phosphonate chemistry is going through a renaissance in the last decade. Synthetic chemists, chemical engineers, pharmacists, medical doctors, water technologists, and other application scientists have been involved in this exciting area of chemistry and technology from different perspectives. Metal phosphonate chemistry has found numerous applications in the areas of chemical water treatment, pharmaceutical science, ion exchange, catalysis, medicine, agronomy, etc. In this contribution the chemistry and applications of metal phosphonates are reviewed with emphasis on alkaline earth metal phosphonates and research progress that has originated from our laboratory. In particular synthetic methodologies will be presented for M-phosphonates (M = Mg, Ca, Sr, Ba and Zn). Methods of structural characterization will also be reviewed. Lastly, the role of these metal phosphonates in modern, ground breaking application areas will be presented. These include chemical water treatment, oilfield drilling, desalination, scale inhibition, dispersion, ion exchange, catalysis, treatment of osteoporosis, treatment of osteoarthritis and related pathological conditions, and others. This review will be useful for chemists, chemical engineers, biochemists, medical doctors and graduate students who are involved in modern inorganic and organic synthesis and in biochemical sciences.

Keywords: *alkaline-earth metals, phosphonates, inhibitors, synthesis, nanochemistry.*

* Phone: +30 2810 545051, fax: +30 2810 545001, email: demadis@chemistry.uoc.gr
http://www.chemistry.uoc.gr/demadis

1. INTRODUCTION

Organic phosphonates are important organic compounds that have found widespread use in a multitude of technological applications of industrial and medicinal interest (Table 1).[1]

Table 1. The washing and cleaning agents registered (WRMG) with the Federal Office for Environment Protection, Berlin, Germany, and the complexing agents and substances with complexing characteristics contained therein (updated 6/2001).[a]

Compound	Number of registered products containing this compound	Amount used in washing and cleaning agents in Germany (tons/annum)
DTPA	27	18.5
1,3-PDTA	0	
MGDA	50	126
β-ADA	1	0.15
DHEG	4	0.2
HEDTA	15	5.9
HEIDA	5	0.8
QUADROL	9	59
DTPMP	770	1702
ATMP	691	1639
HEDP	1117	5485
EDTMP	161	877
HDTMP	4	3.8
PBTC	981	1401
S,S-EDDS	28	289
IDS Na salt	69	55
GLUCONIC ACID	302	1181
GLUCOHEPTONIC ACID	1	0.1

[a] Abbreviations: EDTA (ethylene diamine tetra-acetic acid), NTA (nitrilo-tri-acetic acid), DTPA (diethyl triamine penta-acetic acid), PDTA (1,3-propylene diamine penta-acetic acid), MGDA (methyl glycine diacetic acid), β-ADA (β-alanine diacetic acid); b) hydroxy carboxylates: HEIDA (N-(2-hydroxyethyl)imino diacetic acid), DHEG (N,N-bis(2-hydroxyethyl)glycine), HEDTA (hydroxy ethyl-ethylene diamine tri-acetic acid), quadrol (N,N,N′,N′-tetrakis-2-hydroxyisopropyl-ethylendiamine); c) organophosphonates: DTPMP (diethylene triaminopenta (methylene phosphonic acid)), EDTMP (ethylene diaminotetra(methylene phosphonic acid)), HDTMP (hexamethylene diaminotetra (methylene phosphonic acid)), ATMP (aminotrimethylene phosphonic acid), HEDP (hydroxyethane dimethylene phosphonic acid), PBTC (2-butane phosphate 1,2,4-tricarboxylic acid)

These areas include Langmuir-Blodgett film (LB), [2] meso-/microporous materials, [3] ion exchangers,[4] small molecular sensors,5 adsorption/desorption, [6] catalysts, [7] and nonlinear optics.[2,8,13] They have also attracted immense interest from the viewpoint of basic/fundamental research in fields such as organic synthesis, [9] construction of organic-inorganic hybrids [10] and metal-containing coordination polymers. [11] The main structural feature of phosphonates (Figure 1) is that they contain a $–PO_3H_2$ moiety attached to a carbon

atom. Phosphonates may contain several phosphonate groups in different arrangements. The behavior of the –PO3H2 moiety is pH-dependent.[12]

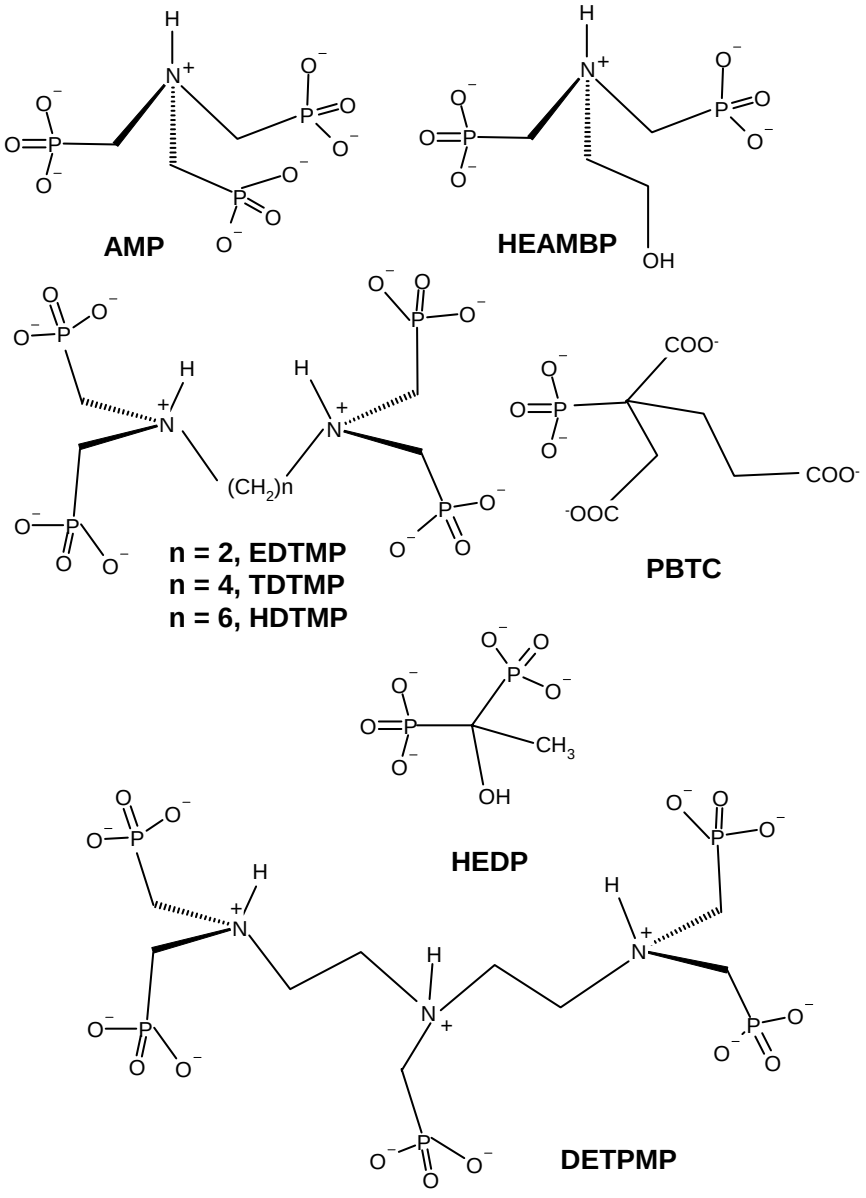

Figure 1. Schematic structures of some representative scale inhibitors used in various industrial applications. Abbreviations are as follows: PBTC 2-phosphonobutane-1,2,4-tricarboxylic acid, HEDP 1-hydroxyethylidene-1,1-diphosphonic acid, AMP amino-*tris*-(methylene-phosphonic acid), HEAMBP 2-hydroxyethyl-amino-*bis*(methylenephosphonic acid), HPAA hydroxyphosphono acetic acid, EDTMP ethylenediamine-*tetrakis*(methylene-phosphonic acid),TDTMP tetramethylenediamine-*tetrakis*(methylene-phosphonic acid), HDTMP hexamethylenediamine-*tetrakis*(methylenephosphonic acid) DETPMP diethylenetriamine-*pentakis*(methylenephosphonic acid). It should be noted that all aminomethylene phosphonate molecules have the N atom protonated at pH regions below ~12

As solution pH increases successive deprotonation processes occur, rendering the $–PO_3H_2$ moiety monoanionic ($–PO_3H^-$) or dianionic ($–PO_3^{2-}$). Therefore, solution pH needs to be mentioned in the context of their solution behavior.

Often phosphonate groups are present in the same molecule with other moieties, such as carboxylates.[13] Some of these molecules will be examined in the present review. Phosphonate polymers are important members of the "phosphonate family" but are beyond the scope of this chapter.

2. STRUCTURAL CHEMISTRY OF PHOSPHONIC ACIDS AND METAL PHOSPHONATES

2.1. Phosphonobutane-1,2,4-Tricarboxylate (PBTC)

PBTC (Figure 1) was first discovered in the Laboratories of Bayer (commercial name Bayhibit)[14] and has survived intense use in the water treatment field for several decades, due to its ease of preparation in large scale and robustness to decomposition.[15] Up until 2005 there was no published structural information on PBTC or its metal complexes. PBTC acid contains one phosphonate and three carboxylate groups. It was crystallized form very concentrated aqueous solutions. The presence of protonated phosphonate and carboxylate groups as well as the water molecule creates an intricate network of hydrogen bonding. The complexity of the structure can be seen in Figures 2, 3 and 4. Hydrogen bonding distances are reported herein as D···A (donor···acceptor) and H-bonds are given notations such as a, b, c, etc. The $-PO_3H_2$ group acts as both donor and acceptor and forms two sets, a total of four, H-bonds. The first set forms between the -P=O (from one molecule), the –P-O(H) (from a neighboring molecule) and two water molecules of crystallization. This H-bonding mode forms an 8-member ring (not counting the H atoms) and is locally centrosymmetric. The O(9)-H(9)···O(10") distance (bond a) is rather short, 2.4622(14) Å. The O(9)-H(9)···O(10") angle is slightly bent, 164.8º. The O_w(10")-H_w(1)···O(7) distance (bond b) is much longer, 2.6736(15) Å. The O_w(10")-H_w(1)···O(7) angle is 161.6º. The second set consists of two hydrogen bonds. These are formed between the P=O portion of the $-PO_3H_2$ group and the –OH group of the carboxylate of a neighboring molecule, and between the second –P-O(H) group and the carbonyl –C=O portion of the same carboxylate. This generates a 6-member ring (not counting the H atoms). The O(7)···H(5')-O(5') distance (bond c) is 2.6171(13) Å and the O(8)–H(8)···O(6)' bond distance is 2.7319(14) Å. The O(7)···H(5')-O(5') angle is 165.7º and the O(8)–H(8)···O(6)' angle is 171.1º. The O(7) atom of the phosphonate –P=O group participates in two H-bonds and acts as a bridge between a water proton and a carboxylate proton. These bonds are dissimilar in length (2.6736(15) Å in the former and 2.7319(14) Å in the latter). It appears that the formation of the 4-member ring facilitates a shorter H-bond compared to that from an 8-member ring. The –COOH group at the 2' position participates in hydrogen bonding interactions with the $-PO_3H_2$ group as described above. The –COOH group at the 4' position forms a commonly seen "dicarboxylate dimer" with a neighboring carboxylate also at the 4' position. This "dimer" sits on a "local" inversion center. The bond distance is 2.6903(14) Å for O(4)-H(4)···O(3'). The O atom of the carboxylate C=O group also forms a very long H-bond with on of the water protons, at a

distance of 2.9552(17) Å. The –COOH group at the 1’ position forms the aforementioned “dicarboxylate dimer” with a neighboring carboxylate (also at the 1’ position) forming a 6-member ring. The H-bonding distance is 2.7674(15) Å. All three carboxylate and the phosphonate groups in PBTC are protonated. The P=O double bond length is 1.4928(10) Å, whereas the P-O single bonds are 1.5294(10) Å and 1.5578(10) Å. The P-C bond length is 1.8465(12) Å and it falls in the normal range (1.8-1.9 Å) for such bonds.[16]

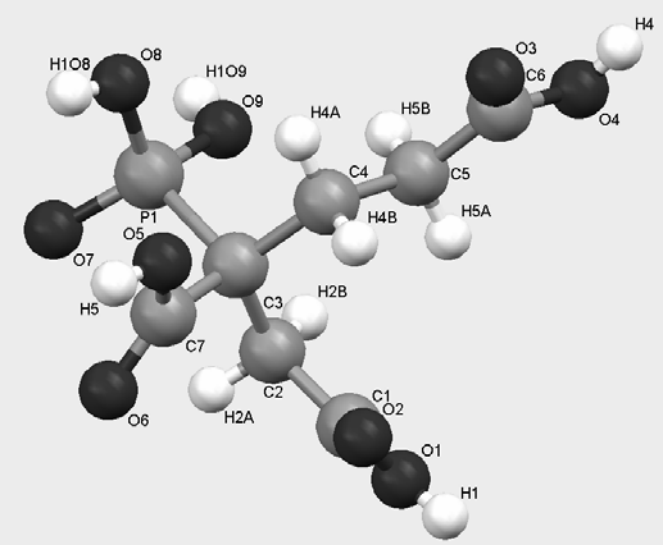

Figure 2. ORTEP diagram of PBTC (50 % ellipsoids)

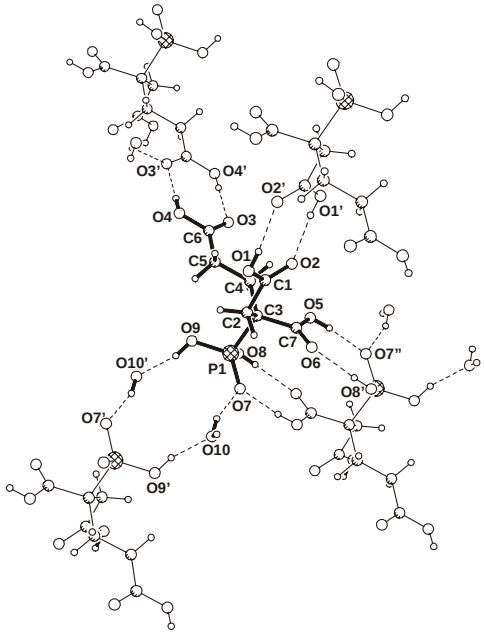

Figure 3. A view of the PBTC·H_2O structure showing all hydrogen bonds

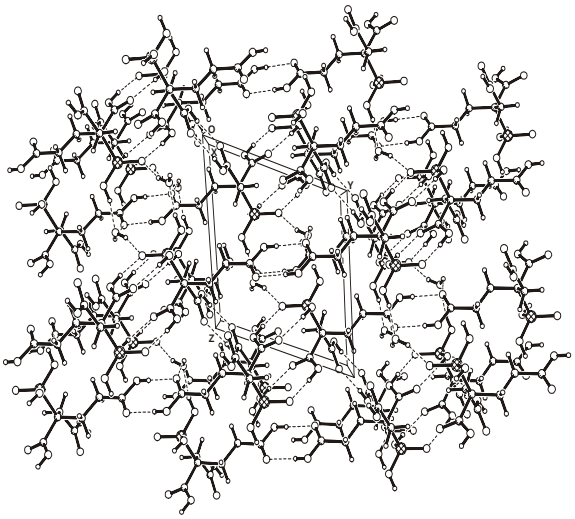

Figure 4. Packing diagram of the PBTC·H_2O structure down the x-axis

2.2. Ethylenediamine-*tetrakis*(methylenephosphonic acid) (EDTMP)

EDTMP is a tetraphosphonate with four methylenephosphonate groups attached to two different N atoms. It is an excellent scale inhibitor for sparingly soluble salts.[17] Its molecular structure is shown in Figure 5. EDTMP is a zwitter-ion in low pH regions. Both N atoms are protonated because of their high basicity, whereas two phosphonate groups (one per N atom) are monodeprotonated. The remaning two phosphonate moieties are fully protonated. EDTMP can be easily synthesized from ethylenediamine, hypophosphorus acid, and formaldehyde in a Manich-type reaction. Several aminomethylenephosphonates can be synthesized in a similar manner.[18]

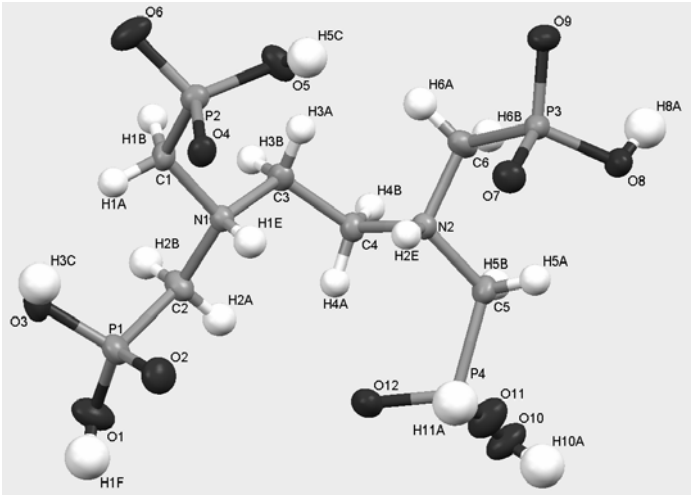

Figure 5. Molecular structure of EDTMP with the numbering scheme.

2.3. Dimethylaminomethylene-bis(phosphonic acid) (DMABP)

DMABP is a diphosphophosphonate that belongs to the "gem-bisphosphonate" family of phosphonates.[19] Both phosphonate groups are linked to the same C atom. The molecular structure of DMABP is shown in Figure 6. As expected, the N atom is protonated and one of the two phosphonate groups is monodeprotonated. DMABP can be prepared from dimethylformamide, phosphorous acid and phosphorus trichloride.[20] Complexation studies have been reported with Indium(III), Gallium(III), Iron(III), Gadolinium(III), and Neodymium(III) ions.[20] Linear coordination polymers with tungstate centers have been reported in which the negatively-charged chains $[(O_3PC(H)N(CH_3)_2PO_3)W_2O_6]^{4-}$ are the repeat units.[21]

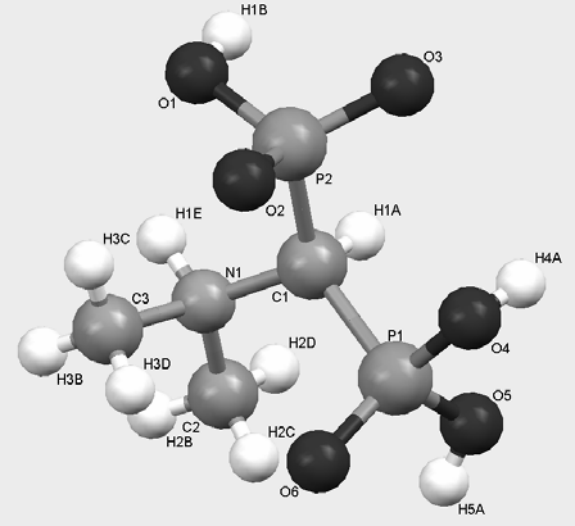

Figure 6. Molecular structure of DMABP with the numbering scheme

2.4. Magnesium-(amino-*tris*-(methylenephosphonate)) and its Zinc Isostructural Analog [22, 23]

These metal-AMP organic-inorganic hybrids are isostructural,[22, 23] so only the crystal structure of the Zn analog will be discussed herein. In the structure of Zn-AMP, each phosphonate group is singly deprotonated, whereas the N atom is protonated. Therefore AMP maintains its "zwitter ion" character in the crystal lattice. Zn^{2+} is coordinated by three phosphonate O's and three H_2O molecules. Notably, there are no lattice H_2O molecules. The asymmetric unit is shown in Figure 7 (upper). AMP forms an 8-member chelate ring with Zn^{2+}. Zn-O(P) bond distances range from 2.0459(13) Å to 2.1218(13) Å. Bond angles point to a slightly distorted octahedral geometry, with the largest deviation being 166.90(6)º for the O12-Zn-O10 angle. The third phosphonate arm is surprisingly *not* coordinated to Zn^{2+}, but is exclusively involved in H-bonding through O1, O2, and O3 (*vide infra*).

A zig-zag chain parallel to the c-axis is formed by Zn^{2+}, Figure 7 (lower). The Zn^{2+} centers are located at the corners of the zig-zag chain, whereas the "linear" portion of the zig-zag is made of the non-coordinated, hydrogen bonded phosphonate groups. Besides the three metal-bonded phosphonate oxygens (O4, O7 and O11), three additional oxygens (O5, O8 and O2) are protonated, and the remaining three O atoms serve as hydrogen bond acceptors.

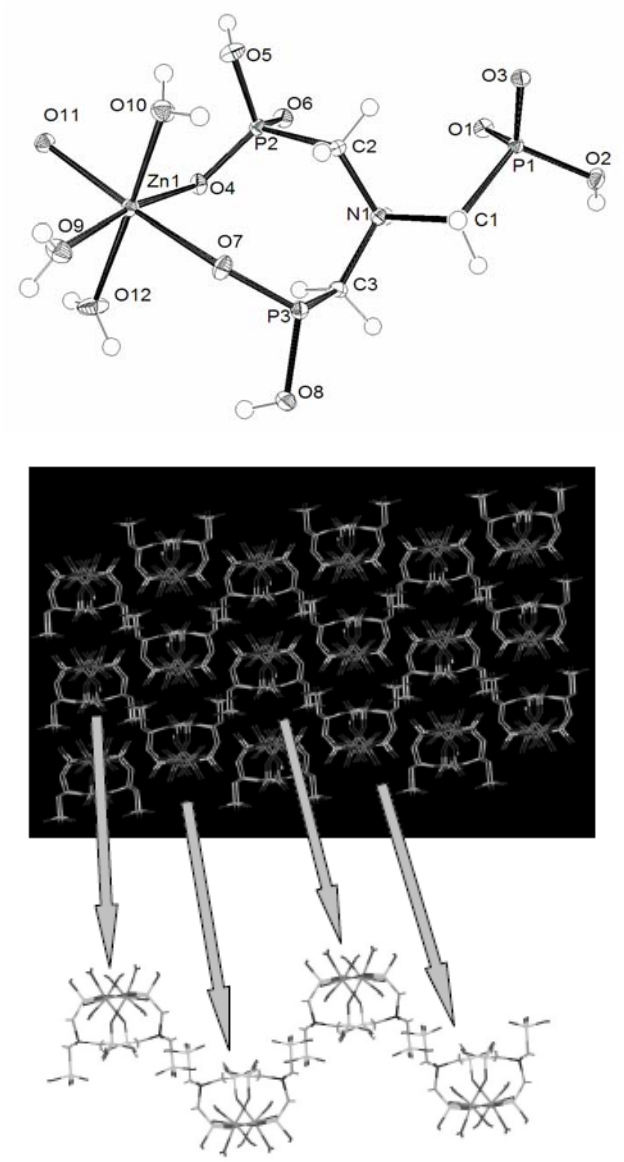

Figure 7. ORTEP of the asymmetric unit of the $Zn[HN(CH_2PO_3H)_3(H_2O)_3]_x$ polymer (upper, 50 % probability ellipsoids). Packing diagram of the Zn-AMP lattice showing the corrugated structure and an isolated zig-zag chain (lower)

There is only one long intramolecular H-bonding interaction (2.469 Å) between O5 (from a Zn-coordinated phosphonate) and O10 from the water located at a *cis* position to it. The presence of a non-coordinated, singly deprotonated phosphonate group in the lattice is

somewhat surprising. This phosphonate moiety participates in a complicated H-bonding network that presumably "relieves" the presence of the negative charge. Based on the bond distances of P1-O1 (1.4998 Å) and P1-O3 (1.5202 Å) the P=O and P-O^- bonds cannot be unequivocally distinguished. These bond distances point to delocalization of the negative charge over the two P-O bonds. The non-coordinating $–PO_3H^-$ moiety participates in six "short" and two "long" hydrogen bonding interactions. The –P1-O2-H9 proton forms a H-bond (1.875 Å) with the O of the P=O moiety that belongs to a phosphonate coordinated to a neighboring Zn^{2+} center. The O3 oxygen of the same moiety interacts *via* three short interactions with the H of a neighboring free –P-O-H group (1.914 Å), with the H the H-O-P group of a neighboring Zn-coordinated phosphonate (1.891 Å) and with the H (1.963 Å) of a neighboring Zn-coordinated water, O12. O3 also forms two "long" interactions with a Zn-bound water (2.569 Å) and the H of a neighboring phosphonate (2.843 Å) that participates in the 8-member chelate. The third O (O1) of the uncoordinated phosphonate interacts with the N-H group (1.843 Å) of a neighboring AMP ligand and with the O=P (1.937 Å) of a Zn-coordinated water. The H-bonding network that involves the uncoordinated phosphonate group is shown in Figure 8.

The H_2O molecule (O9) located *trans* to a coordinated phosphonate (P2) participates in two H-bonds with O6 (1.961 Å) of a Zn-bound phosphonate (P2) and O1 (1.937 Å) of a free phosphonate (P1). Of the other two water molecules that are trans to eachother, O12-H15 interacts with O7 that belongs to phosphonate P3 that bridges two Zn^{2+} centers, and O12-H16 interacts with O3 (1.963 Å) that belongs to a non-coordinated phosphonate. The remaining water (O10) forms an interaction with O4 (2.168 Å) of a neighboring Zn-bound phosphonate group.

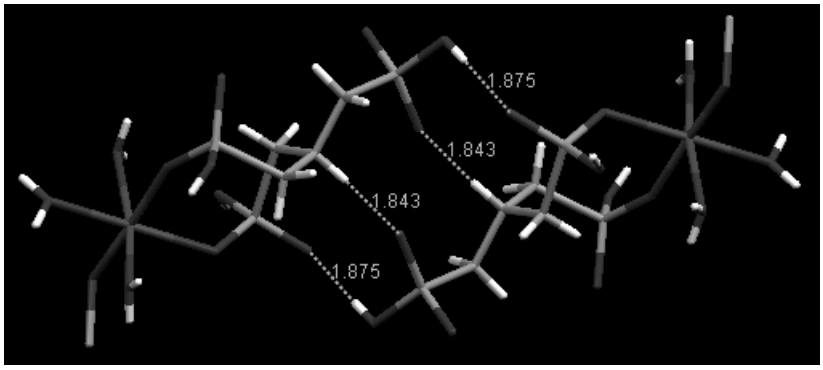

Figure 8. Hydrogen bonding network that connects two Zn-AMP units through the non-coordinated phosphonate group

The three H_2O molecules form their hydrogen bonds, mostly in the a-axis direction. The H-bonds create a 3-D network of H-bonded linear chains. The overall effect is the formation of 2-D corrugated sheets that nest within each other running along the ab diagonal. However, these sheets are made up of individual chains where the non-coordinated phosphonate groups overlap.

The crystal and molecular structure of the $Mg[HN(CH_2PO_3H)_3(H_2O)_3]_x$ coordination polymer is shown in Figures 9 and 10. The M-O(phosphonate) bond distances are very

similar. For the Mg analog they are in the range 2.0213(15)-2.1225(18) Å and for the Zn analog they are 2.0459(13)-2.1456(14) Å.

An isostructural series of $M[HN(CH_2PO_3H)_3(H_2O)_3]_x$ (M = Cd, Ni, Co, Mn) compounds has been prepared by Clearfield *et al*.[24]

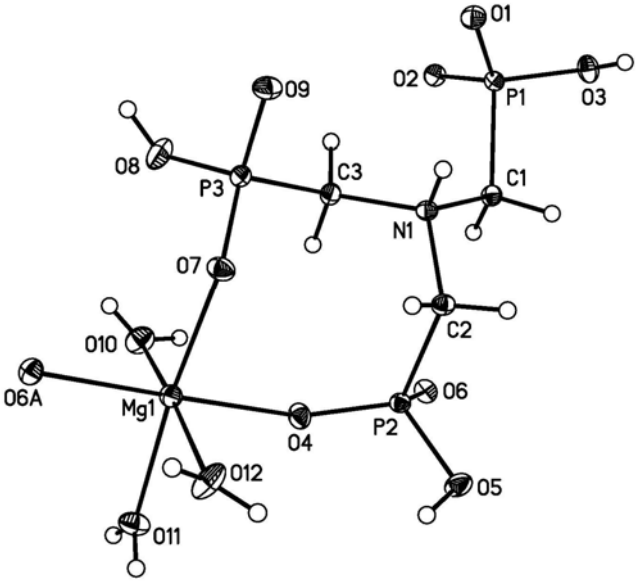

Figure 9. ORTEP of the asymmetric unit of the $Mg[HN(CH_2PO_3H)_3(H_2O)_3]_x$ polymer (upper, 50 % probability ellipsoids)

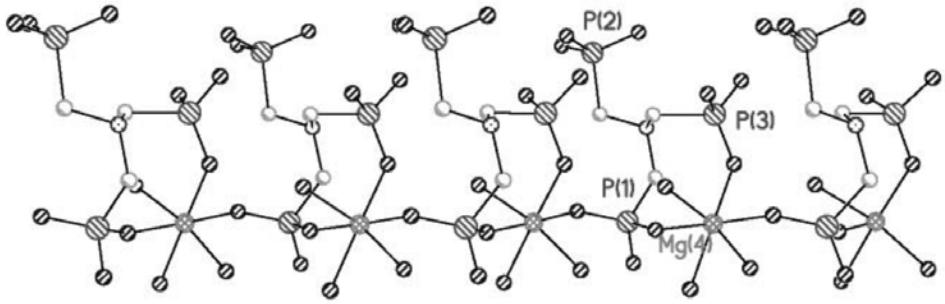

Figure 10. One-dimensional fragment in the structure of the coordination polymer $Mg[HN(CH_2PO_3H)_3(H_2O)_3]_x$

2.5. Calcium-(amino-*tris*-(methylenephosphonate))[25]

The complexity of the polymeric structure can be seen in Figure 11. There are no discrete molecular units of the Ca-AMP complex. Instead, the methylenephosphonate "arms" participate in an intricate network of *inter*molecular and *intra*molecular interactions involving Ca atoms and hydrogen bonds. The result is a complex polymeric three-dimensional structure

caused mainly by multiple bridging of the AMP molecules. Each phosphonate group is monodeprotonated. The protonated O atom (-P-O-H) remains non-coordinated. The remaining two P-O groups bridge two neighboring Ca atoms in a Ca-O-P-O-Ca arrangement. There are four Ca-AMP "units" per unit cell. The overall Ca:AMP molar ratio is 1:1. Electroneutrality is achieved by charge balance between the divalent Ca and the triply deprotonated/monoprotonated AMP ligand. There are also 3½ water molecules in the unit cell. One is coordinated to Ca. Water molecules of crystallization serve as "space fillers" and also participate in extensive hydrogen bonding superstructures.

The intimate coordination environment of the Ca atom is shown in Figure 12. The Ca is surrounded by six oxygens, five from phosphonate groups and one from water. Ca-O(P) distances range from 2.2924(14) to 2.3356(14) Å. The Ca-O(H_2O) distance is 2.3693(17) Å, somewhat longer than Ca-O(P) distances. The Ca atom is situated in a slightly distorted octahedral environment, as judged by the O-Ca-O angles, which show slight deviations from idealized octahedral geometry. Ca-O(P) bond lengths can be compared to similar bonds found in the literature (*vide infra*).

One AMP ligand *per* Ca acts as a bidentate chelate, forming an eight-member ring. Each Ca center is coordinated by four AMP phosphonate oxygens in a monodentate fashion. Each of these methylenephosphonate groups is simultaneously coordinated to a neighboring Ca atom. A water molecule completes the octahedron.

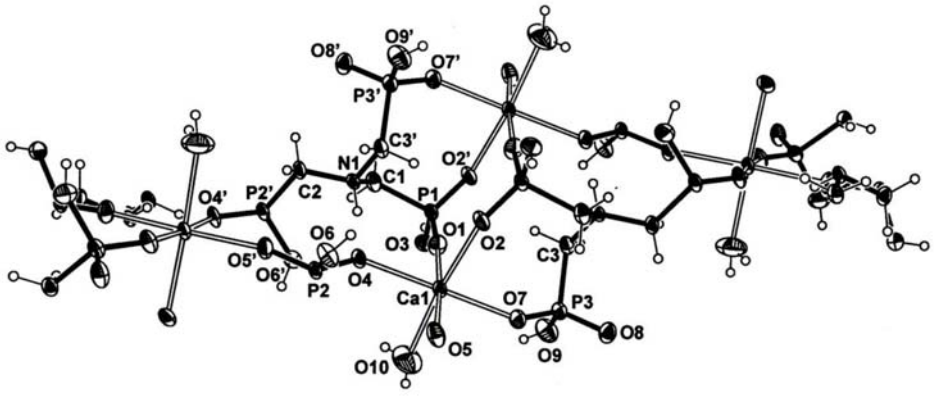

Figure 11. One-dimensional fragment in the structure of $\{Ca[HN(CH_2PO_3H)_3(H_2O)(2.5H_2O)]\}_x$ polymer. Waters of crystallization are not shown for clarity.

All three phosphonate groups in AMP are mono-deprotonated. This formally separates the P-O bonds into three groups: P-O-H (protonated), P=O (phosphoryl), and $P\text{-}O^-$ (deprotonated). The P-O(H) bond lengths are 1.5684(15) Å, 1.5703(16) Å, and 1.5802(14) Å. On the other hand, P=O and $P\text{-}O^-$ bond lengths are crystallographically indistinguishable and are found in the 1.4931(15)-1.5102(14) Å range. This observation coupled with the fact that all Ca-O(P) distances are very similar, point to the conclusion that the negative charge on each $–PO_3H^-$ is delocalized over the O-P-O moiety. It is worth-noting that only the deprotonated P-O groups coordinate to the Ca atoms, whereas the protonated P-OH's remain non-coordinated. P-C bond lengths are unexceptional, 1.8382(20) Å, 1.8347(20) Å and 1.8330(20) Å. N-C bond lengths are 1.5019(25), 1.5155(25) Å, and 1.5094(25) Å. The C-N-C

angles are ~ 112°. The N is protonated (the H atom was located in the difference Fourier map and refined).

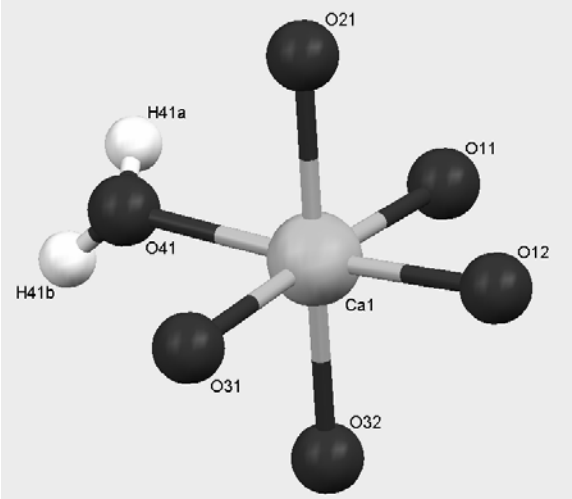

Figure 12. The intimate coordination environment of the 6-coordinated Ca center

2.6. Strontium-(amino-*tris*-(methylenephosphonate)) [23]

Strontium-(amino-*tris*-(methylenephosphonate)) is 3D polymer consisting of $[Sr(AMP)]_n$. The Sr-atoms are 7-coordinate, with five monohapto and one chelating AMP ligands and Sr–O bond lengths ranging from 2.4426(17) to 2.9060(17) Å. The structure can be viewed as Sr "dimers" connected together by AMP ligands (Figure 13). The Sr centers in these "dimmers" are bridged by a phosphonate oxygen. This bridging oxygen, together with a second oxygen atom of the same phosphonate group coordinate in a chelating fashion to the same Sr center. A more detailed view of the coordination environment of the Sr centers is shown in (Figure 14). Each AMP ligand is coordinated to six symmetry related Sr-centers (Figure 15), with two O-atoms of each phosphate group acting as donors. The Sr-atoms form layers separated by AMP ligands, with each AMP bridging four Sr-atoms in one layer and two in the next one; the best-fit planes of Sr-layers are 8.069(2) Å apart (Figure 16). Within each layer, the Sr-atoms form a distorted hexagonal honeycomb lattice with short (4.445(1) Å) and long (6.150(28) Å) distances (Figure 17).

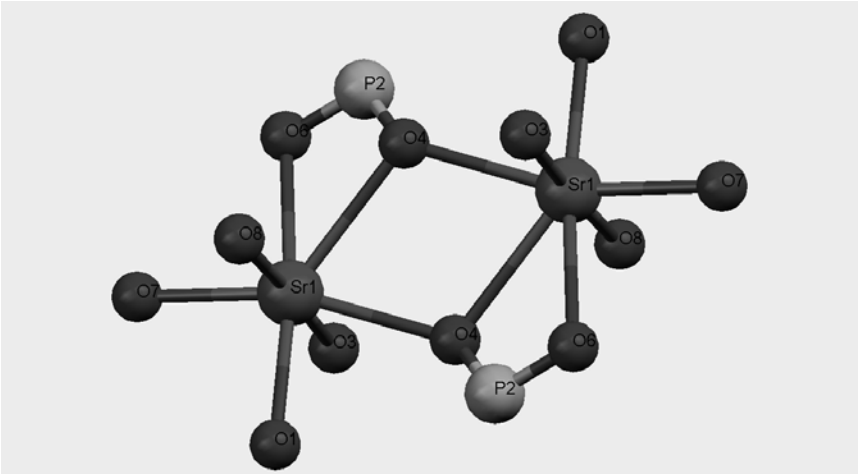

Figure 13. The intimate coordination environment of the Sr "dimer", showing the bridging phosphonate oxygens

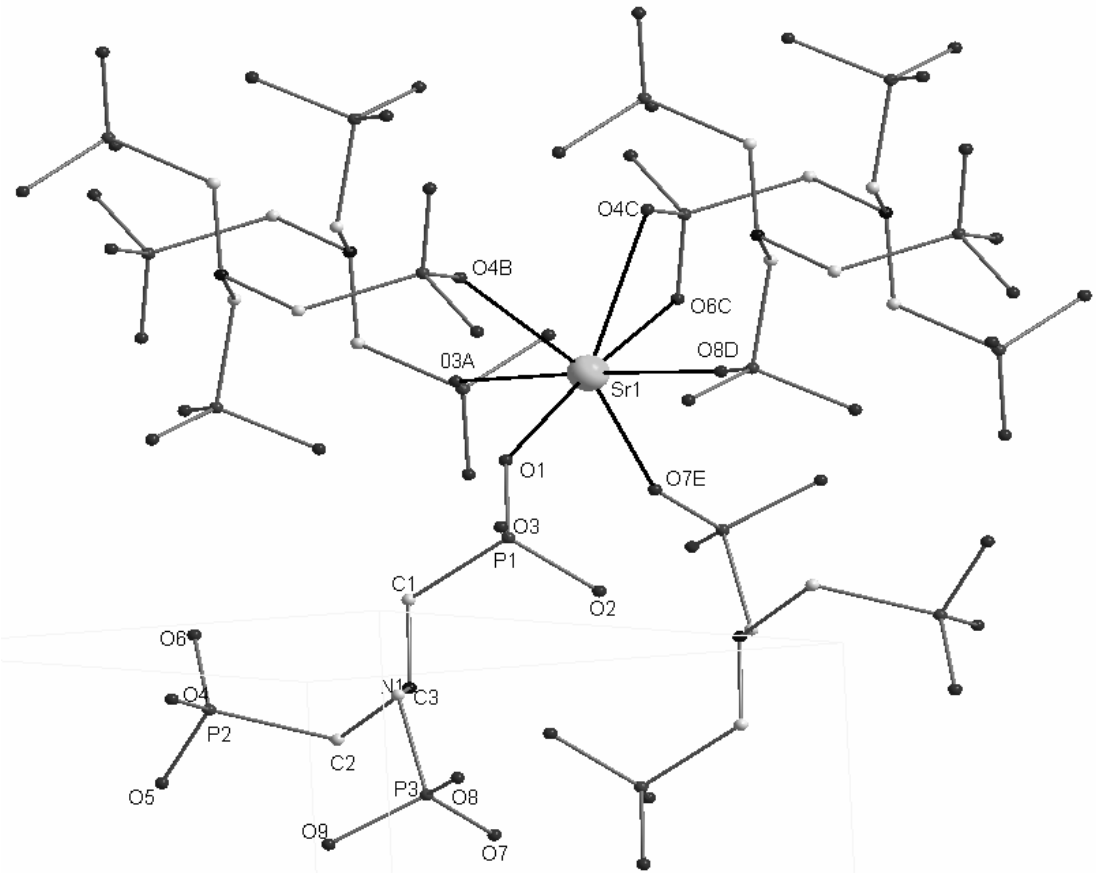

Figure 14. The coordination environment of the Sr center, showing the AMP ligands surrounding it

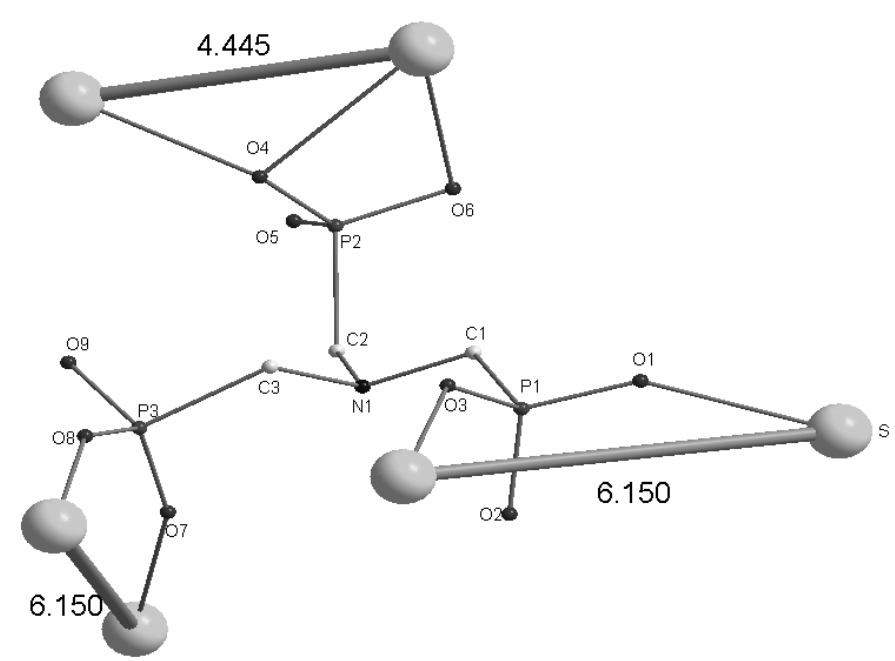

Figure 15. Chelating ability of AMP in the structure of Sr-AMP. Close distances between the Sr atoms are shown

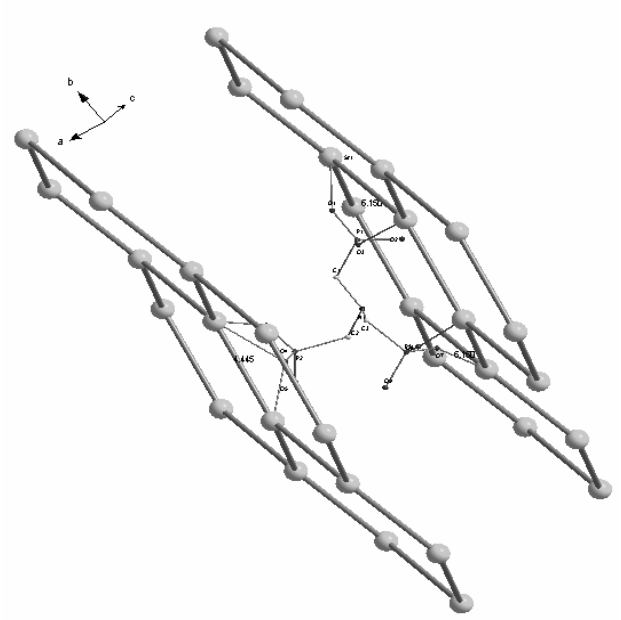

Figure 16. Sr-based layers separated by AMP ligands. Each AMP bridges four Sr-atoms in one layer and two in the neighboring one

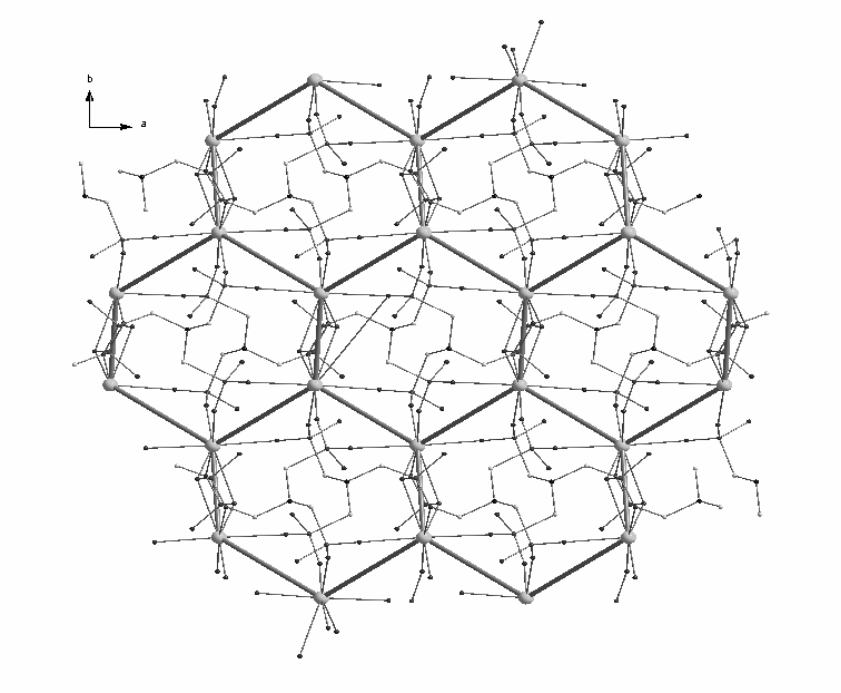

Figure 17. Distorted hexagons formed by Sr^{2+} centers. In this Sr-based, distorted hexagonal honeycomb lattice the short distances are 4.445(1) Å and the long distances are 6.150(28) Å

2.7. Barium-(amino-*tris*-(methylenephosphonate)) [23]

Barium-(amino-tris-(methylenephosphonate)) has a 3D polymeric structure with the formula $\{Ba(AMP)(H_2O)\}_n$ (Figure 18). AMP maintains its "zwitter ion" character in the crystal lattice of Ba-AMP. The coordination modes of both symmetry independent AMP^{2-} octadentate ligands are identical. Metric features of the Ba-coordinated AMP ligand show insignificant variations from those in "free" AMP.[26]

Ba(1) is 9-coordinated, bound by 9 O atoms, 8 originating from phosphonate oxygens and 1 from H_2O, whereas Ba(2) is 10-coordinated, linked by 9 phosphonate and 1 H_2O oxygens, Figure 19. The geometry at Ba^{2+} does not approximate either of the idealized polyhedra, the bicapped square antiprism, or the bicapped dodecahedron; this observation is not surprising in view of the steric requirements of the triphosphonate ligand in the structure. There are no lattice H_2O molecules of crystallization. The closest Ba···Ba contact is 4.3691(10) Å. This Ba···Ba close proximity has its origin in the triple Ba(1)-μ-O-Ba(2) bridge by O atoms from three different AMP ligands. The Ba-O(H_2O) bond distances are Ba(1)-O(51) 2.841(10) Å, and Ba(2)-O(52) 2.956(12) Å. Note that the longer Ba-O(H_2O) bond distance is associated with the 10-coordinate Ba^{2+} center. All bridging O-atoms belong to phosphonate moieties that act as chelates for one Ba^{2+} and form 4-membered rings. This bridging motif has been observed in the structure of Ba-glyphosate, in which Ba is 8-coordinate.[27]

The 3D structure of $\{Ba(AMP)(H_2O)\}_n$ can be seen as a layer of Ba atoms lying in the *bc* plane interconnected *via* AMP ligands in the a direction. Ba···Ba distances between the triply μ-O bridged Ba atoms are 4.637(1) and 4.369(1) Å, while between doubly or singly μ-(O-P-O) bridged Ba atoms they are 7.163(1) or 7.687(1) Å apart (Figure 20).

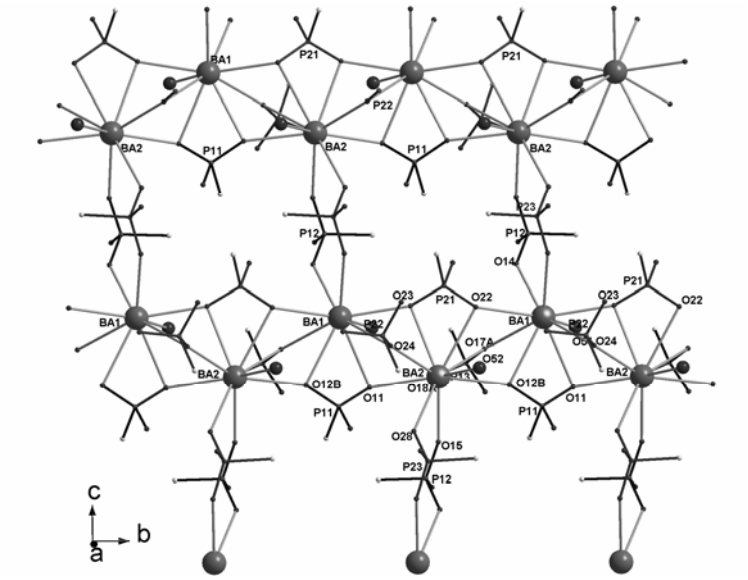

Figure 18. 3D structure of the $\{Ba(AMP)(H_2O)\}_n$ polymer that can be envisioned as a layer of Ba atoms lying in bc plane interconnected via AMP ligands in the a-direction. Only phosphonate groups of AMP ligand are shown for clarity

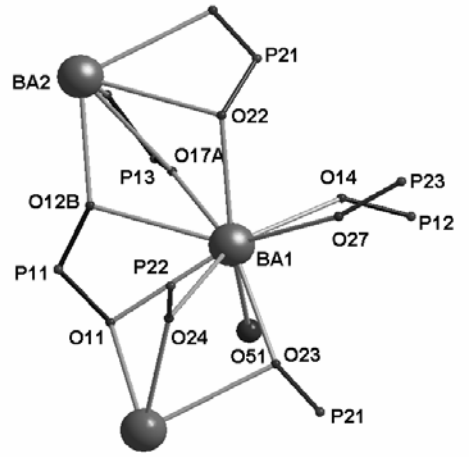

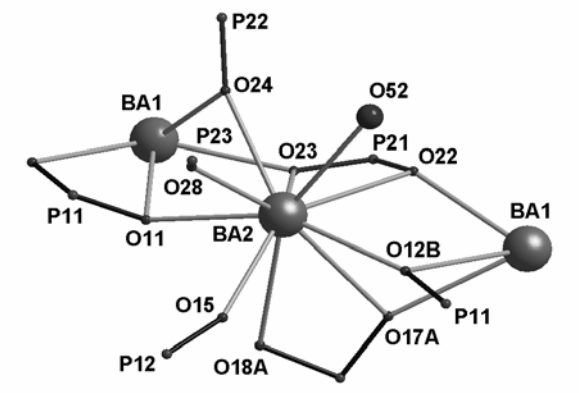

Figure 19. Coordination environments of the two Ba^{2+} centers in the structure of the $\{Ba[(AMP)(H_2O)]\}_n$ polymer: 9-coordinated Ba(1) (top) and 10-coordinated Ba(2) (bottom)

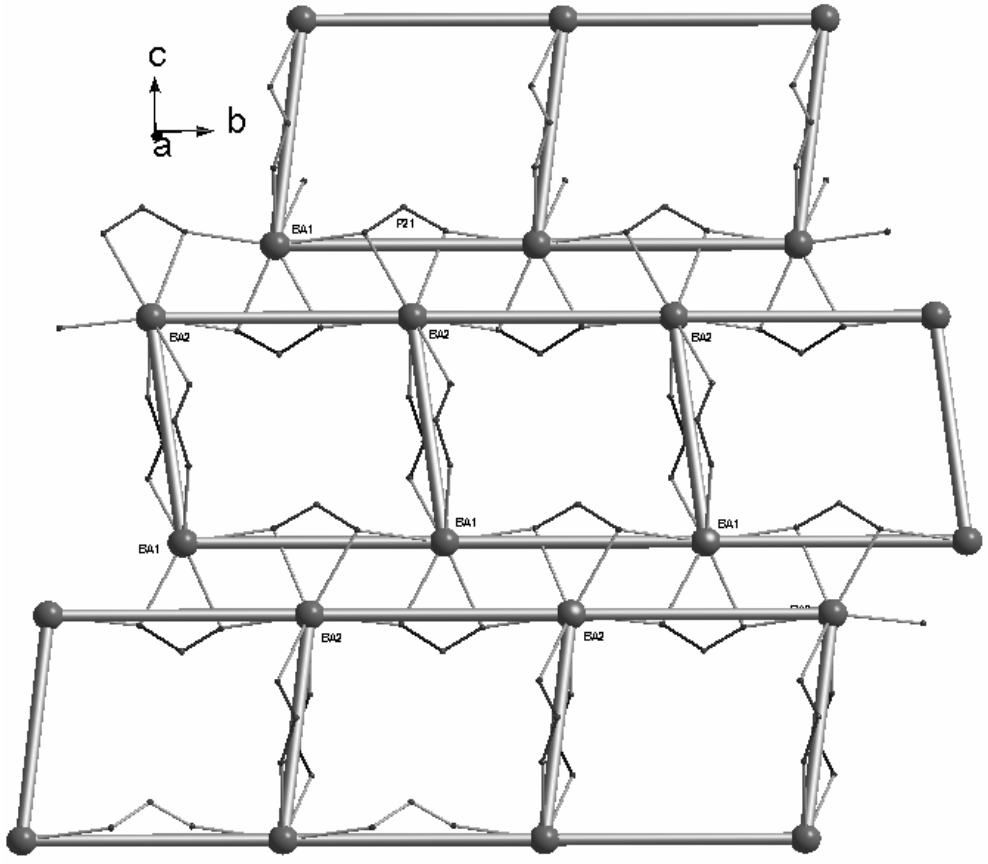

Figure 20. “Brick wall”-like network composed of Ba centers and AMP ligands.

2.8. Zinc-HDTMP [28]

The crystal structure of Zn-HDTMP shows it is a 3D coordination polymer. The Zn-O distances are unexceptional and consistent with other structurally characterized Zn-phosphonates.[29] Zn^{2+} is found in a distorted octahedral environment (Figure 21) formed exclusively by phosphonate oxygens. An interesting feature is that the sixth oxygen ligand for Zn^{2+} originates from a protonated phosphonate oxygen, O(9), and forms a long interaction (2.622(3) Å) with Zn^{2+}. Apparently, this interaction offers local stabilization because of a strong hydrogen bond, O(9)-H(9)···O(3), 1.879 Å. The O(10)-Zn-O(4) angle greatly deviates from linearity (156.03°), compared to the O(7)-Zn-O(1) angle that is almost linear (175.83°). Two Zn^{2+} centers and the aminomethylene-*bis*-phosphonate portions of HDTMP form an 18-membered ring (Figure 22), while there is a concentric 8- membered ring formed by the same Zn^{2+} centers and the protonated methylenephosphonate arm involved in the long Zn···O(9) interaction. The lattice water interacts weakly with O5 (2.700 Å) and O(2) (2.964 Å). The absence of chelate rings is noteworthy, in contrast to several metal animomethylene-phosphonate structures.[30] HDTMP's four phosphonate groups are coordinated to six different Zn^{2+} centers. O1 (from P(1)) and O4 (from P(2)) act as unidentate ligands to Zn^{2+}. O(10) and O(12) (both from P(4)) bridge two Zn^{2+} centers that are 4.395 Å apart. O(7) and O(9) (both from P(3)) also bridge two Zn^{2+} centers but due to the long O(9)···Zn interaction (2.622 Å), their distance is much longer, 5.092 Å.

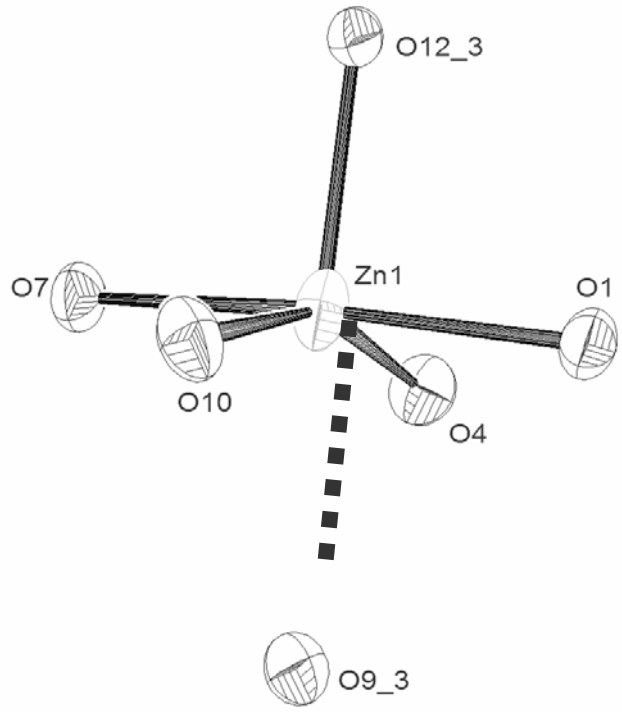

Figure 21. Coordination environment of the Zn^{2+} center displaying important bond distances (in Å). The non-linear O(10)-Zn-O(4) angle is 156.03°

The Zn^{2+} centers reside very close to the unit cell edges and the cell's interior is filled with the organic portion of the tetraphosphonate. The C_6 carbon chain runs almost parallel to the bc diagonal. Also it does not possess the expected zig-zag configuration, but the portion C(2)-C(3)-C(5)-C(6) is in a "*syn*" rather in an "*anti*" configuration.

Structurally characterized metal tetraphosphonate materials are rare. To our knowledge, there is only one published metal HDTMP structure, that of polymeric Co-HDTMP, in which HDTMP is monodentate and bridging two Co(H2O)42+ centers.[31] Some structural details of Zn-tetramethylenediaminetetraphosphonate have been reported.[32] The structure of Zn-HDTMP can be compared to that of $Ca[(HO_3PCH_2)_2N(H)CH_2C_6H_4CH_2N(H)-(CH_2PO_3H)_2]\cdot 2H_2O$ possessing a flexible cyclohexane ring linker.[33] Major structural differences between the two include the bidentate chelation of the tetraphosphonate to the metal center. These are absent in Zn-HDTMP. Similar to the Ca^{2+} structure noted above is the EDTMP-containing material, $Mn[(HO_3PCH_2)_2N(H)(CH_2)_4(H)N(CH_2PO_3H)_2]$.[34]

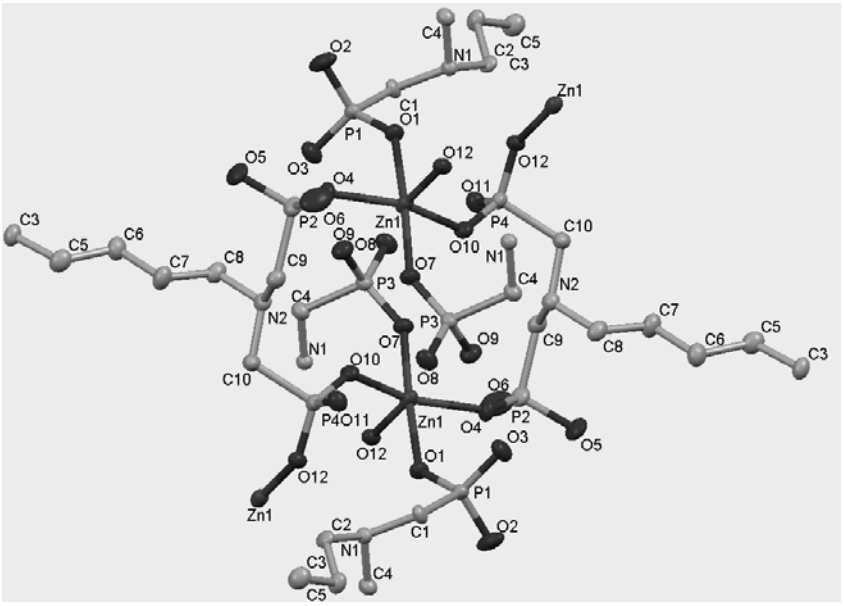

Figure 22. Coordination modes of the tetraphosphonate ligand. The aminomethylene portions of the ligand and the Zn^{2+} centers create a "box" of ~160 Å approximate capacity

2.9. Sr and Ba-HDTMP

Hexamethylenediamine-*tetrakis*(methylenephosphonate) reacts with alkaline-earth metal salts to give polymeric materials as products. The Sr and Ba-HDTMP materials have been prepared in high yields and structurally characterized. They are isostructural, but their structure is notably different from that of Zn-HDTMP discussed above (Section 2.8).

The metal centers are 8-coordinated (Figure 23). Two of the ligands are phosphonate oxygens from two neighboring HDTMP ligands and the remaining six ligands are water molecules. It is important to point out that two phosphonate moieties of HDTMP (one per "side") are monodeprotonated, but not coordinated to a metal ion. They are hydrogen-bonded

to a neighboring water of crystallization. The structure of Sr/Ba-HDTMP could be seen as 2D sheet-like topology made-up by zig-zag chains that form a corrugated sheet (Figure 24). The structure of Sr/Ba-HDTMP can be compared to that of a similar material, Co-HDTMP.[31] The latter is a linear structure, not polymeric because of the *trans* configuration of the two, Co-coordinated phosphonate groups that are bonded to an octahedral Co center.

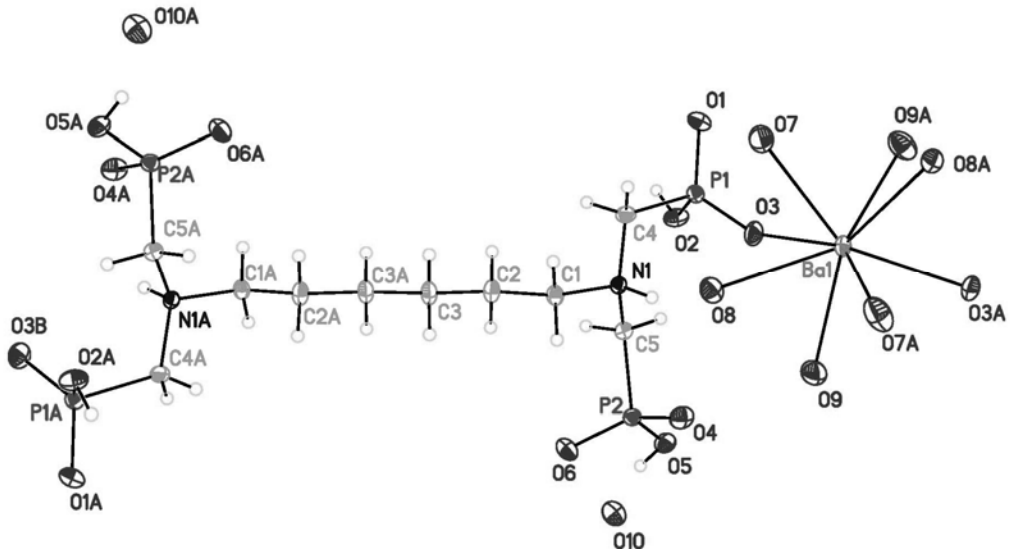

Figure 23. Fragment of the Ba-HDTMP structure. The 8-coordinated Ba center and the two non-coordinated phosphonate moieties can be clearly seen

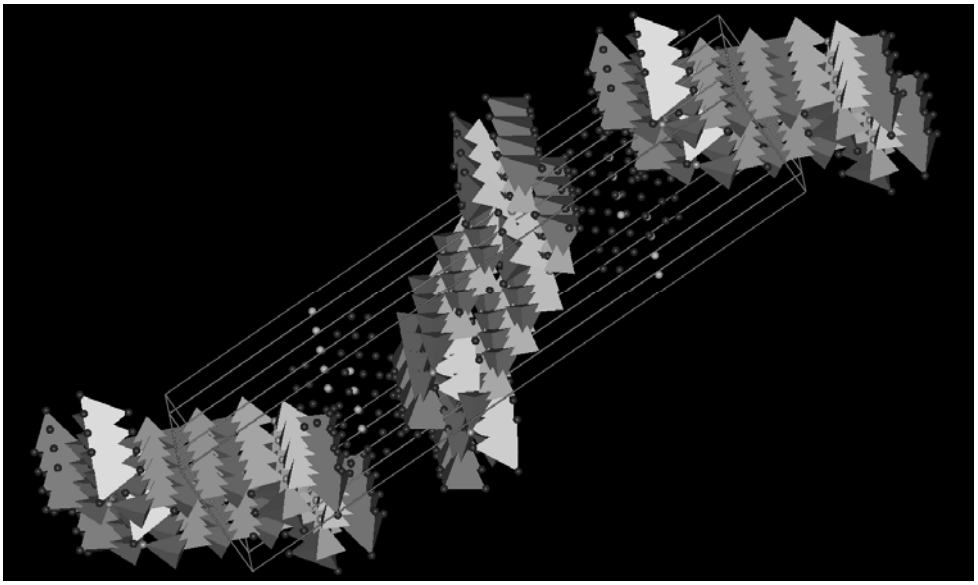

Figure 24. Zig-zag chains in the structure of Sr-HDTMP. The "angles" of the zig-zag are the Sr centers, whereas the "arms" are the C_6 organic linker

2.10. Zn-TDTMP [35]

A systematic approach was undertaken to see the coordination behavior of polymethylenediamine-*tetrakis*(methylenephosphonates) towards metal ions. As mentioned above, reaction of Zn^{2+} with HDTMP afforded a Zn-HDTMP inorganic-organic hybrid coordination polymer. However, a reaction under the same conditions between Zn^{2+} and TDTMP gave a dramatically different material in which Zn^{2+} is not coordinated to the tetraphosphonate, but is found in an octahedral hexaaqua coordination environment (Figure 25).

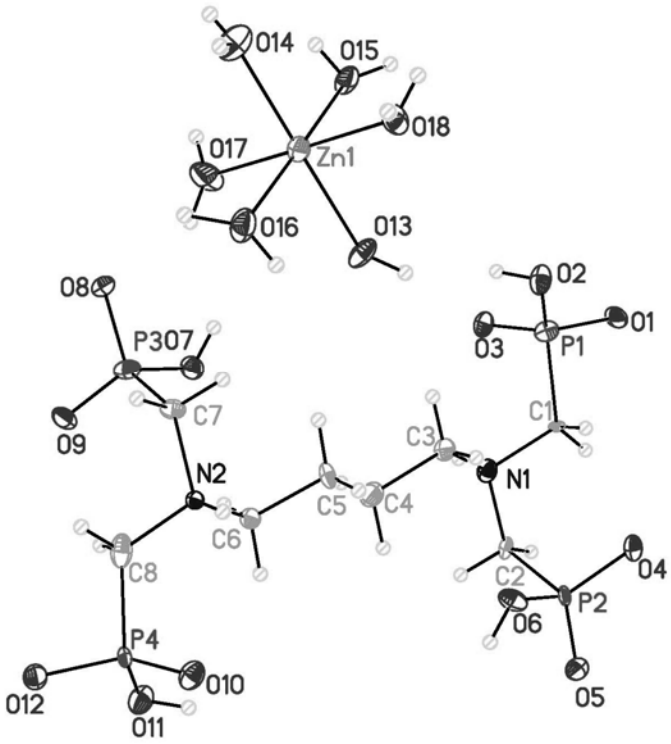

Figure 25. The asymmetric unit of Zn-TDTMP material

It appears that water coordinates more strongly to Zn^{2+} than TDTMP. Presence of phosphonates and metal ions that are not coordinated to them is rarely encountered in the literature.[36]

2.11. Sr-EDTMP and Ca-EDTMP

In contrast to Zn^{2+}, EDTMP reacts with soluble Sr^{2+} salts to give 1D coordination polymers (Figure 26). In the structure of Sr-EDTMP the tetraphosphonate acts as a chelate for a Sr center with two of its phosphonate groups (originating from different N atoms), whereas it bridges two different Sr centers with two phosphonate moieties (originating from the same N atom). The Sr centers are octahedral with phosphonate oxygens occupying the basal positions and water oxygens completing the octahedron in the axial positions. The result of Sr

chelation is a rare 11-membered ring. Bridging creates 1D "rods" (Figure 27). The Ca-EDTMP material is isostructural to Sr-EDTMP.

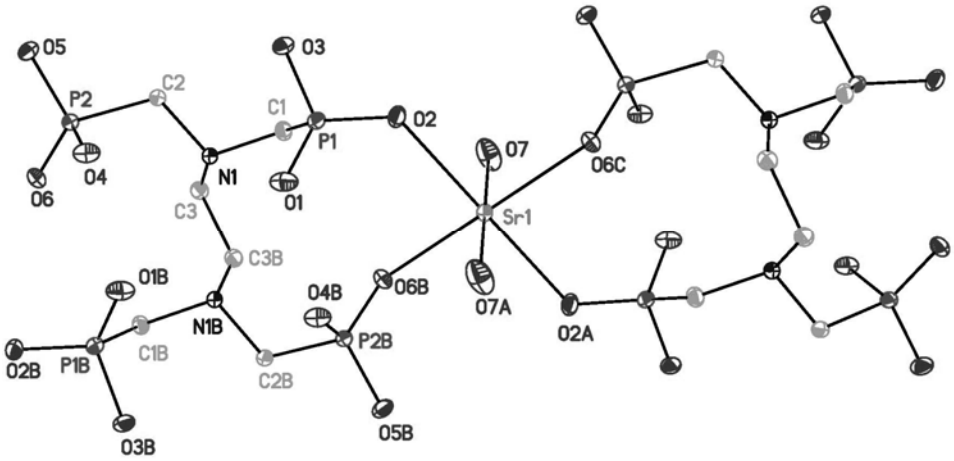

Figure 26. The asymmetric unit of Sr-EDTMP coordination polymer

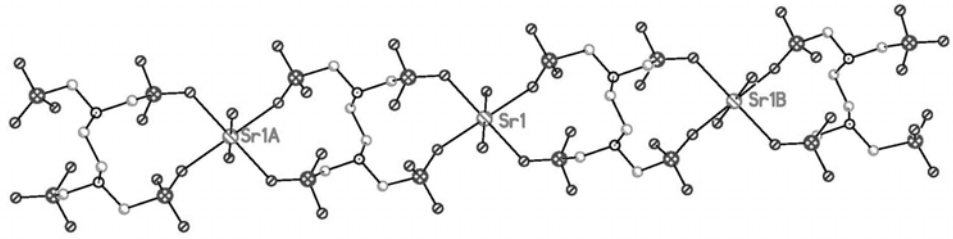

Figure 27. One-dimensional "rods" in the structure of Sr-EDTMP

2.12. Barium-PMIDA

PMIDA is a "mixed" phosphonate/carboxylate that possesses two carboxylate and one aminomethylenephosphonate groups. Its reaction with soluble Ba salts at pH ~ 6 affords a 2D coordination polymer, Ba_2-PMIDA (Figure 28). The ligand is completely deprotonated with a "4-" charge that coordinated two crystallographically independent Ba ions. Both Ba centers are 8-coordinated. Ba-O bond distances are in the range 2.739(3)-3.056(3) Å for Ba(1) and 2.655(3)-2.968(3) Å for Ba(2). Ba(1) and Ba(2) are 4.798 Å apart.

The structure of Ba_2-PMIDA can be viewed as 1D linear rods that run along the b axis (Figure 29). These one-dimensional "polymers" are held together via hydrogen bonding mediated by waters of crystallization positioned in the space between the rods. Metal-PMIDA materials have been reported in the literature.[37]

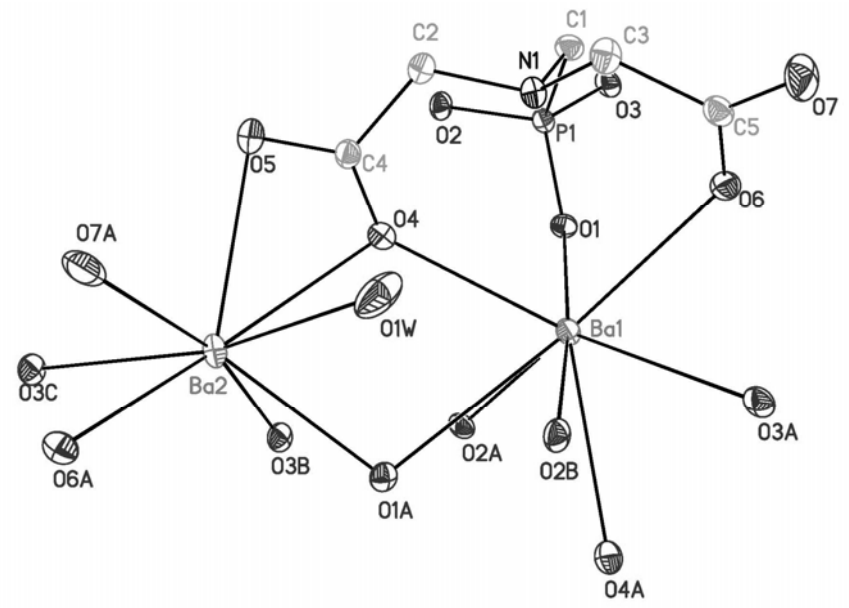

Figure 28. The asymmetric unit of Ba-PMIDA.

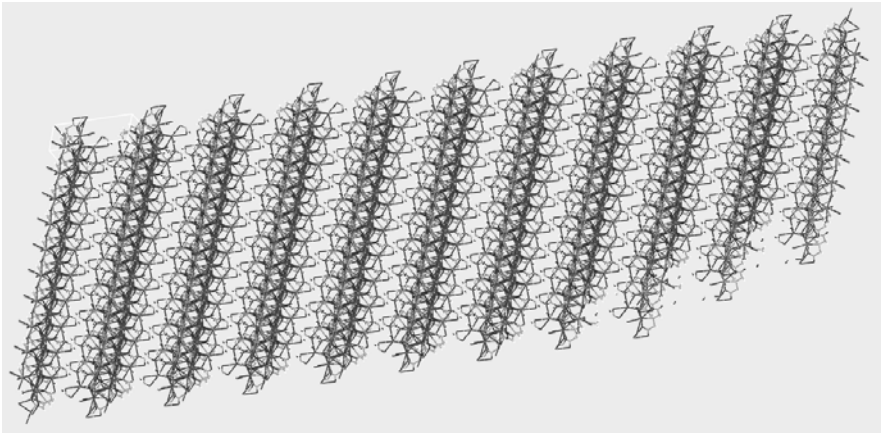

Figure 29. One-dimensional chains that run parallel to the b-axis in the structure of Ba-PMIDA

2.13. Tetrasodium-HEABMP [38]

The crystal structure of Na_4-HEABMP could be described as two-dimensional polymeric layered structure hydrogen bonded into a 3D supramolecular polymeric network. Symmetry independent part of Na_4-HEABMP and the coordination mode of the HEABMP tetraanion are shown in Figures 30 and 31.

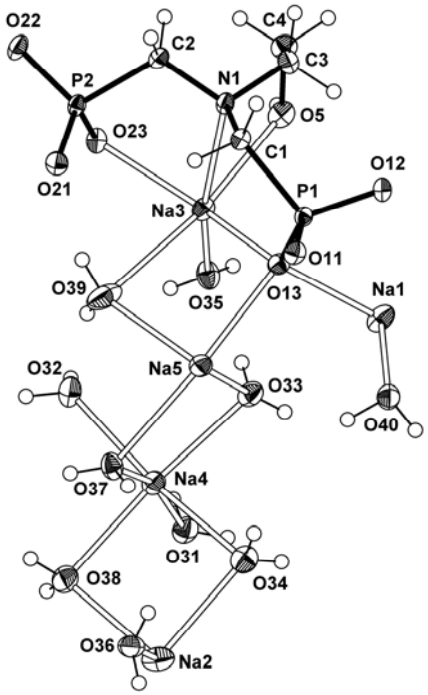

Figure 30. ORTEP diagram (50 % ellipsoids) showing symmetry independent part of Na_4-HEABMP

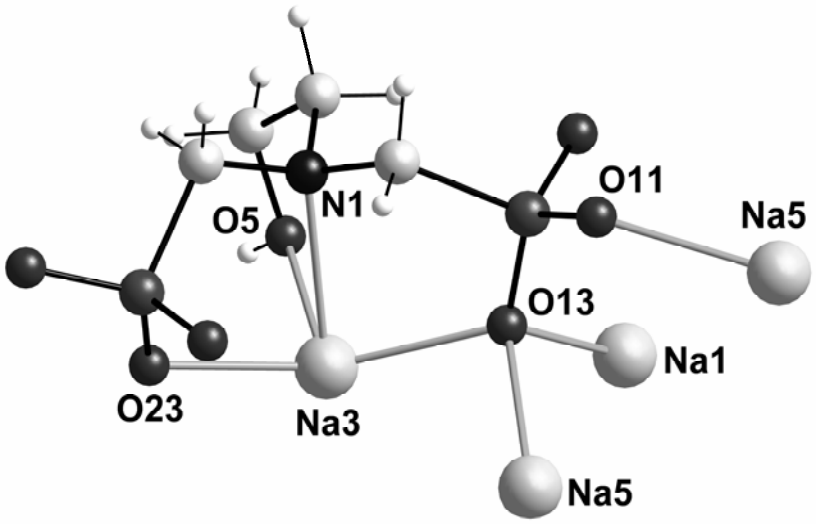

Figure 31. "Ball and stick" representation showing a coordination mode of HEABMP tetraanionic ligand.

Its structure consists of a "three-arm" backbone stemming from the N atom. Two "arms" are fully deprotonated methylene phosphonate ($-CH_2PO_3^{2-}$) moieties and the third is a hydroxyethyl ($-CH_2CH_2OH$) moiety. One of the methylene phosphonate arms uses only one oxygen donor atom (O23) to coordinate terminaly Na3 atom. Other arm uses two O donors

(O11 and O13) to coordinate four Na cations. Donor O11 acts as monodentate and terminally coordinates Na5 from the adjacent formula unit, while O13 is triply bridging Na1, Na3 and Na5 with very similar Na-O distances. O5 atom of the hydroxyethyl arm and the N1 atom are involved in the coordination of Na3. HEABMP tetraanion acts in 1 as a heptadentate chelating and concurrently as bridging ligand, which forms three five-membered metallocycles (-O23-P2-C2-N1-Na3-, -O5-C4-C3-N1-Na3- and –O13-P1-C1-N1-Na3-) all involving Na3. Detailed discussion of important geometrical aspects of HEABMP tetraanion coordination is warranted. Such discussion follows the general description of the crystal structure of 1 below. The role of water molecules is to mediate interactions between Na^+ forming a 2D polymeric sheet-like structure (Figure 32). Interactions between water molecules and Na^+ need to be discussed in more depth in order to understand the complexity of the structure.

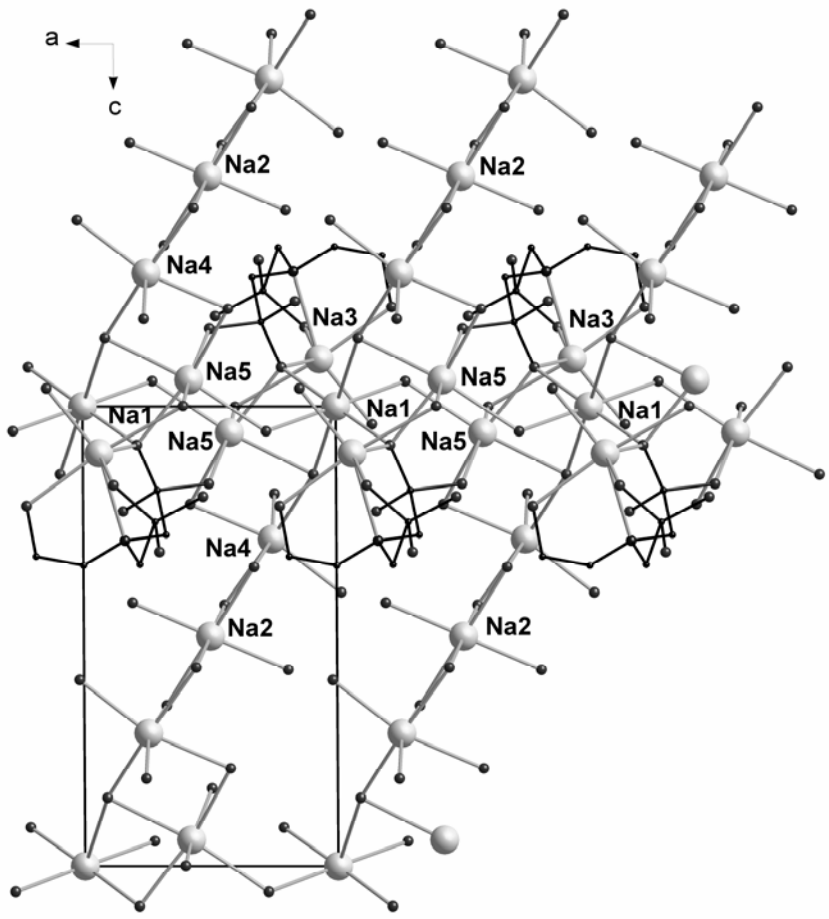

Figure 32. Packing diagram showing 2D polymeric structure propagating in direction of both axes, a and c. Hydrogen atoms are omitted for clarity

Na5 is "nested" in an octahedral environment formed by four H_2O lattice molecules and two O atoms from PO_3 groups, coming from adjacent molecules. Na-O(H_2O) interactions (all of them of bridging origin) are in the range of 2.3049(11)-2.5773(15) Å. Na-O(PO_3)

interactions are 2.3656(9) and 2.3772(9) Å. O33 and O37 provide bridges between Na5 and Na4, stretching the structure along ac diagonal, while O40 makes a bridge between Na5 and Na1 propagating the structure along the b axis.

Na1 could be considered as a ‘‘nozzle’’ linking in a axis direction diagonally propagating zigzag chains (–Na3–Na5–Na4–Na2–N4–Na5–Na3–) into 2D polymeric sheets which are parallel to ac faces. Using this kind of terminology, the tetraanion of HEABMP acts as ‘‘protecting elbow’’ protruding from 2D polymeric sheet and preventing direct links between layers (Figure 33).

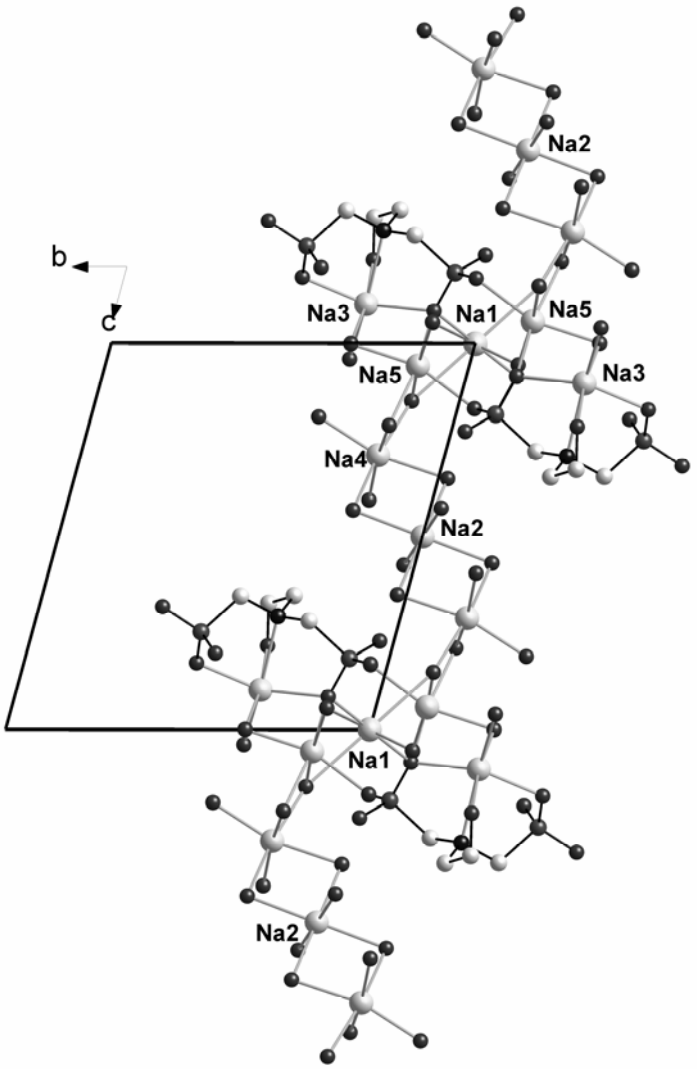

Figure 33. Packing diagram showing a side view of 2D polymeric structure as it propagates along the c axis. Hydrogen atoms are omitted for clarity

Both phosphonate groups in HEABMP are fully deprotonated. P-O bond lengths are nearly equivalent in both groups showing rather minor differences, and range from 1.5141(8) Å to 1.5368(8) Å. P-O bond length equivalency implies even distribution of the negative

charge over *all three* oxygens per -PO_3 group. P-C bond lengths fall in the normal range (1.8-1.9 Å) and are 1.8375(11) Å and 1.8279(12) Å.

The N atom is not protonated as expected due to the high pH of crystal preparation. It forms a rather long interaction of 2.5613(11) Å with Na(3). N-C bond lengths are 1.4713(14) and 1.4809(14) Å for the methylene phosphonate "arms" and 1.4680(15) Å for the "ethanol arm". The ∠ C-N-C are ~ 111° and ∠ Na3-N-C are 103.78(7), 109.16(7) and 108.10(7)°.

2.14. Calcium-PBTC [39, 40]

Crystalline $Ca(PBTC)(H_2O)_2{\cdot}2H_2O$ is obtained by reacting $CaCl_2{\cdot}2H_2O$ and PBTC in a 1:1 molar ratio. It can also be prepared in high yields from CaO or $Ca(OH)_2$ and PBTC in heterogeneous aqueous medium. Its crystal structure reveals a polymeric material with PBTC acting as a tetradentate chelate, Figure 34.

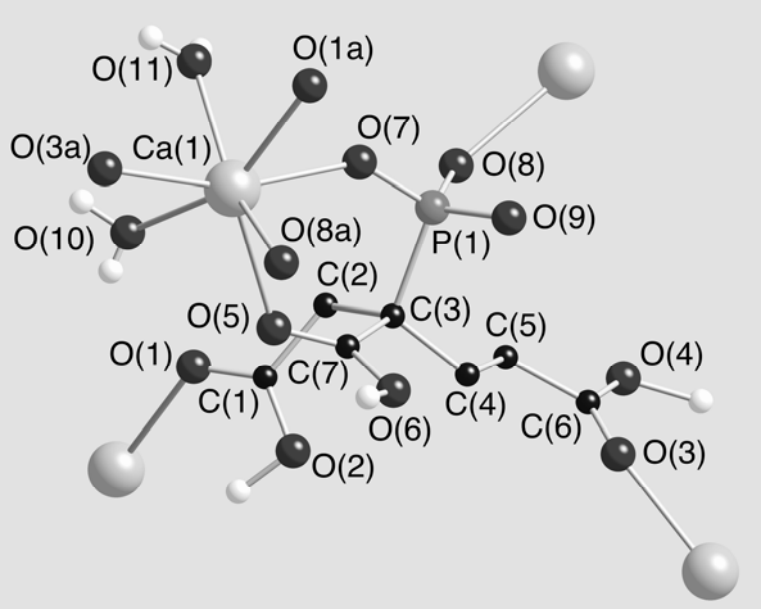

Figure 34. Fragment of the $[Ca(H_3PBTC)(H_2O)_2{\cdot}2H_2O]_n$ coordination polymer, showing the coordination environment of the seven-coordinated Ca^{2+} and the tetradentate chelation mode of H_3PBTC^{2-} to four Ca^{2+} centers

The Ca^{2+} center is 7-coordinated in a capped octahedral environment, bound by two phosphonate oxygens, three carboxylate oxygens and two water molecules. The phosphonate oxygens act as bridges between two neighboring Ca^{2+} centers located 6.781 Å apart. The protonation state of the phosphonate and carboxylate groups in H_3PBTC^{2-} warrants some discussion. X-ray crystallography cannot give accurate H atom positions, so our arguments are based on P-O, C-O and Ca-O bond distances. All P-O bond lengths are essentially equivalent (1.521 Å, 1.517Å, and 1.521 Å). In contrast, C-O bond lengths are well separated into "short" (1.208 – 1.230 Å) and "long" (1.305 – 1.310 Å). The "long" C-O bonds correspond to the oxygen atoms that are protonated, and thus, non-coordinated. On the other

hand, the "short" C-O bonds correspond to the oxygen atoms that are part of the carbonyl group and are coordinated to the Ca^{2+} center. There are several literature examples of metal phosphonate structures that have monodeprotonated, metal-coordinated phosphonate groups.[41] Careful examination of these structures reveals a consistent observation: the P-O bonds, P=O or P-O(-M), of the phosphoryl group are of approximately equal length and shorter than the P-O(H) bond of the protonated oxygen atom. The above is also true for non-coordinated phosphonates. Based on these arguments we propose that the structure of $[Ca(H_3PBTC)(H_2O)_2{\bullet}2H_2O]_n$ is best described as having a doubly deprotonated phosphonate with all three carboxylate groups protonated. The latter are coordinated to the Ca^{2+} center through their carbonyl moieties. It should be pointed out that all three phosphonate O-atoms are involved in –P-O…HO-C(=O) H-bonding to three carboxylate moieties.

This is consistent with the long Ca-O(dC) distances of Ca-(1)-O(1) 2.470(2) and Ca(1)-O(5) 2.448(2) Å. Such Ca-O=C(OH) coordination mode is rare.[42] Fully deprotonated, metal-coordinated phosphonate groups in the presence of protonated carboxylate groups have been recently observed in the structure of $Sm[(O_3PCH_2)_2NH\text{-}CH_2C_6H_4\text{-}COOH]{\bullet}H_2O$.[43] The phosphonate group and the carboxylate group oxygen atoms at the 2 position form a six-membered chelate with the Ca^{2+} center. As mentioned above, the phosphonate group is doubly deprotonated. The -O-P-O- moiety bridges two Ca2+ centers. On the basis of the similar Ca-O(phosphonate) bond distances of 2.378(2) and 2.385(2) Å the negative charge is delocalized over the entire O-P-O moiety. Ca-O_{water} distances, Ca(1)-O(11) 2.352(3) and Ca(1)-O(10) 2.445(3) Å, are consistent with those reported in the literature. There are numerous hydrogen bonding interactions in the structure of $Ca(H_3PBTC)(H_2O)_2{\bullet}2H_2O$. Twelve out of 13 oxygens in the structure (except O(3)) participate in an intricate network of hydrogen bonds. The shortest O•••O interactions are $O_{carboxylate}(2)$•••O(8)phosphonate = 2.518 Å, $O_{carboxylate}(4)$•••$O(9)_{phosphonate}$ = 2.510 Å and $O_{carboxylate}(6)$•••$O(7)_{phosphonate}$ = 2.652 Å.

Interstitial water molecules are clustered close to the ab-plane. They are hydrogen-bonded to Ca-coordinated water molecules and carboxylate O-atoms, phosphate O-atoms, as well as to each other with O•••O distances from 2.711 to 2.852 Å. The bridging -PO_3 tetrahedra and the CaO_7 polyhedra are arranged in a zig-zag chain configuration that runs parallel to the b-axis. This is depicted in Figure 35. The molecular structure of free H_5PBTC (crystallized as the monohydrate, $H_5PBTC{\bullet}H_2O$) shows both optical isomers R and S according to the Cahn-Ingold-Prelog sequence. Both R and S stereoisomers are also included in the structure of $[Ca(H_3PBTC)(H_2O)_2{\bullet}2H_2O]n$ in a regular pattern. Each chain shown in Figure 35 contains only one PBTC stereoisomer.

Uncomplexed PBTC shows three intense bands in the IR spectrum due to the ν(C=O) asymmetric stretch (1750, 1717 and 1636 cm^{-1}) and the ν(P=O) asymmetric stretch at 1075 cm^{-1}. $Ca(PBTC)(H_2O)_2{\cdot}2H_2O$ shows an intense ν(C=O) asymmetric stretch (1570 cm^{-1}) and a ν(P=O) asymmetric stretch (1080 cm^{-1}). It is noteworthy that the ν(C=O) stretch is profoundly shifted to lower frequency due to the weakening of the C=O bond due to H-bonding. A group of bands in 510-610 cm^{-1} region are assigned to Ca-O stetching vibrations.

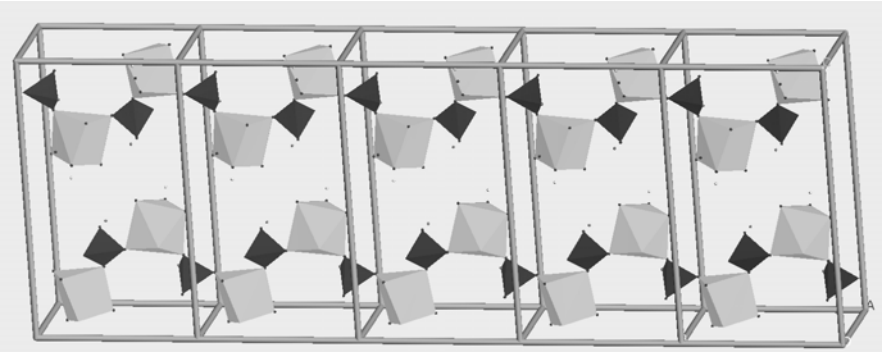

Figure 35. View of two zig-zag chains over five unit cells formed by CaO_7 polyhedra (black) and PO_3C tetrahedra (grey) that run parallel to the b axis

2.15. Ca-Na-Phosphocitrate [44]

Strictly speaking phosphocitrate (PC, Figure 36) is not a phosphonate, but a phosphate ester of citric acid. However, because of the great significance that the phosphate group imparts on its properties, it is reasonable to discuss it herein.

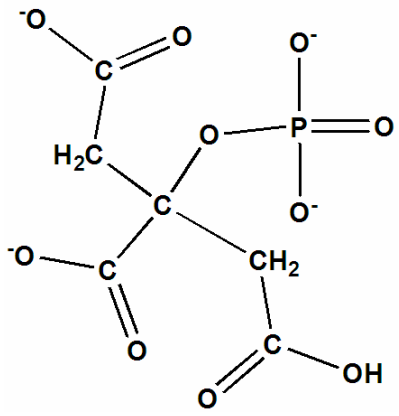

Figure 36. Schematic structure of phosphocitrate (PC) in its fully deprotonated form.

Reaction of NaPC and $CaCl_2$ at pH ~ 2 gives CaNaPC according to the equation 1 (proton content on PC also shown):

$$CaCl_2 \cdot 2H_2O + 2Na_4(HPC) \cdot 3H_2O + 5HCl \rightarrow CaNa(H_3PC)(H_4PC)(H_2O) + 7NaCl + 4H_2O$$

The structure of CaNaPC (Figure 37) is polymeric with $Ca(PC)_2(H_2O)$ “monomers” connected through Na^+ bridges. The Ca cation occupies the center of an irregular polyhedron defined by four phosphate, four carbonyl, and one water O-atoms. Coordination number 9 for Ca is rather rare. [45] In that regard, the unexpected presence of a coordinated H_2O is the result of the strain imposed by the PC ligand on the coordination geometry, making a wide

site available to H_2O. Two examples of 9-coordinate, biologically relevant Ca are in the structures of β-calcium-pyrophosphate [46] and hydroxyapatite minerals. [47] An interesting structural feature is the short distance of 2.477(1) Å between Ca and the ester *O* from C–*O*–PO_3H_2. For comparison, the Ca–O(pyrophosphate ester) distance in β-$Ca_2(P_2O_7)$ is 2.855 Å. Interestingly, this is consistent with the apparent resistance of the P–O–C moiety to hydrolysis in an acidic environment, suggesting that strong calcium coordination exerts a "protective" effect on the overall molecule. Ca–O(=C) distances are in the 2.446(2)–2.586(2) Å range, much shorter than those in Ca hydrogen citrate trihydrate (2.37–2.49 Å).[48] Similarly, the Ca–O(PO_2H) distance is 2.527(2) Å, much longer than Ca–O distances in related complexes (2.3–2.4 Å).[49]

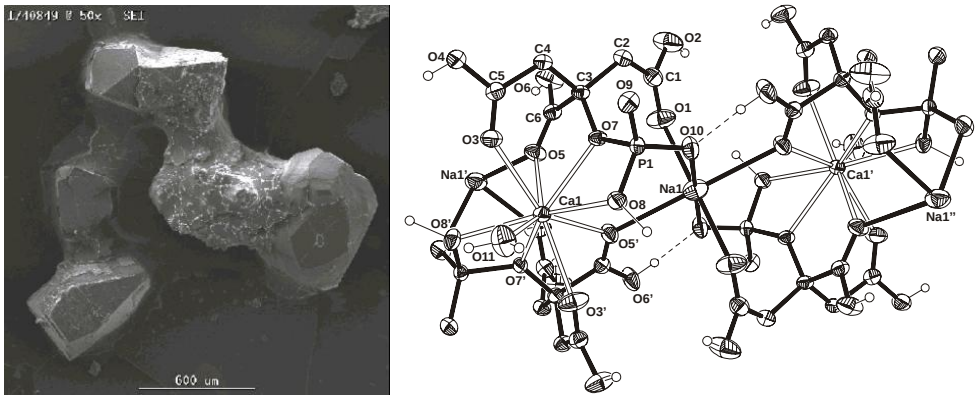

Figure 37. Single crystals of CaNaPC (left). Partial ORTEP diagram of the CaNaPC polymeric structure (50 % probability ellipsoids, right). O-attached protons and two H-bonds (dashed lines) are shown. Relevant bond lengths and distances (Å): Ca···Ca 8.794(1), Ca···Na 4.3972(5), Ca(1)-O(11) 2.388(2), Ca(1)-O(3) 2.446(2), Ca(1)-O(7) 2.477(1), Ca(1)-O(8) 2.527(2), Ca(1)-O(5) 2.586(2)

As coordination number increases Ca–O distances become elongated. Ca–O distances in CaNaPC are consistent with these observations. All –COOH groups are protonated. There are three dissociated protons *per two PC molecules*, all coming from $–PO_3H_2$. pKa values for PC have been measured (dissociating protons in italics): < 2.0 (*H*–O–P(OH)(O)O–); 3.67 (α–COO*H*); 5.15 ($^-$O–P(O–*H*)(O)O–); 7.69 (β–COO*H*); 13.56 (γ–COO*H*).[50] The second proton from $–PO_3$ is dissociated before that from α–COOH and is involved in a short hydrogen bond (2.453(3) Å) connecting adjacent polymeric "ribbons". An oxygen from PO_4 acts as a bridge between Ca^{2+} and Na^+. Na ions are 6-coordinated, a feature commonly found in Na–carboxylate salts.[51] Other structural features of CaNaPC compare well with those of NaPC.[52] In Figure 38 the structures of PC and CaNaPC are shown for comparison.

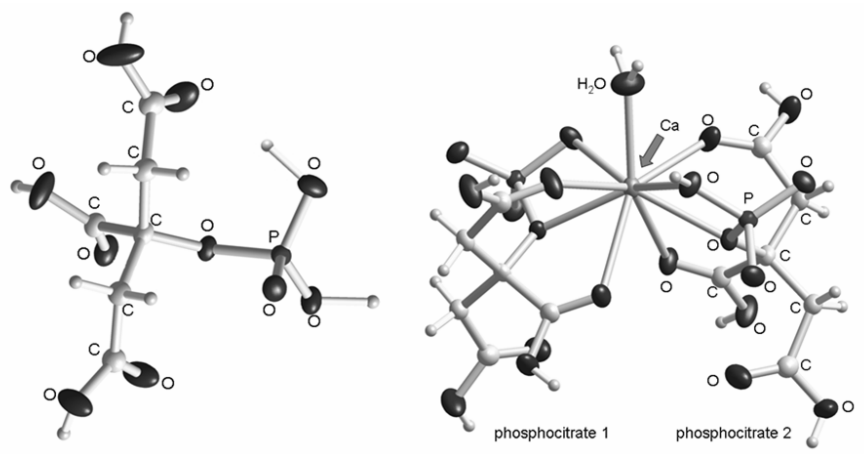

Figure 38. Comparison of the crystal structures of PC (Na salt) and CaNaPC.

CaNaPC can be described as 1D coordination polymer with one-dimensional chains that run parallel to the c axis (Figure 39). These chains are held together *via* hydrogen bonding between a protonated phosphate group and a deprotonated phosphate group (Figure 40). The FT-IR spectrum (KBr pellets, Figure 41) shows several characteristic bands: $\nu_{C=O}$ 1717, 1636 cm^{-1}, ν_{O-H} 3573, 3496 cm^{-1}, $\nu_{P=O}$(asym) 1260, 1230 cm^{-1}, and $\nu_{P=O}$(sym) 1090, 1075 cm^{-1}

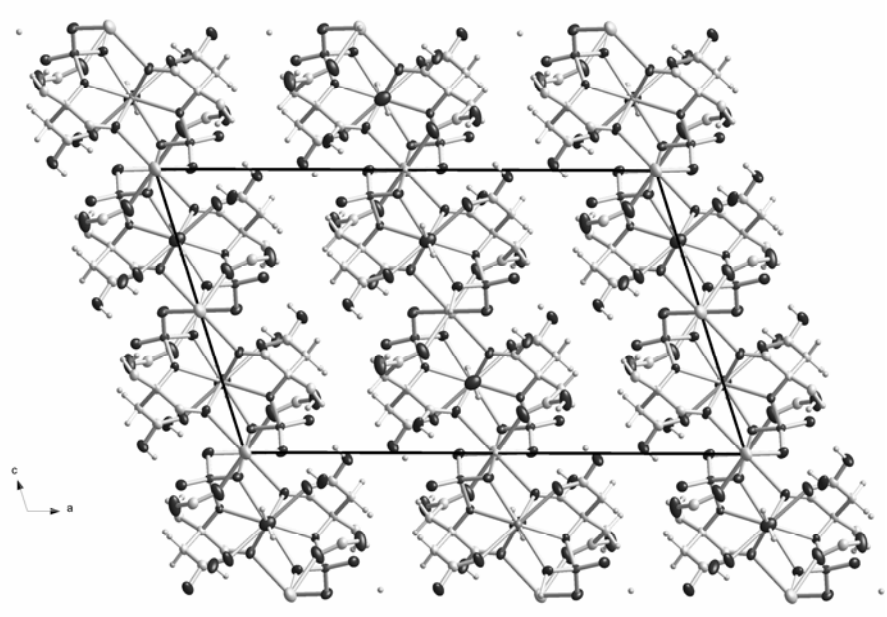

Figure 39. One-dimensional chains in the crystal structure of CaNaPC that run parallel to the c-axis

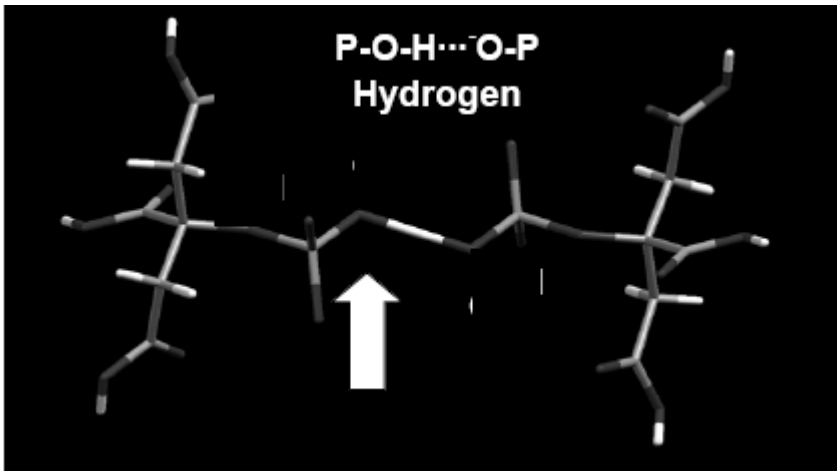

Figure 40. Hydrogen bonding interactions that hold the one-dimensional chains (Figure 39) together

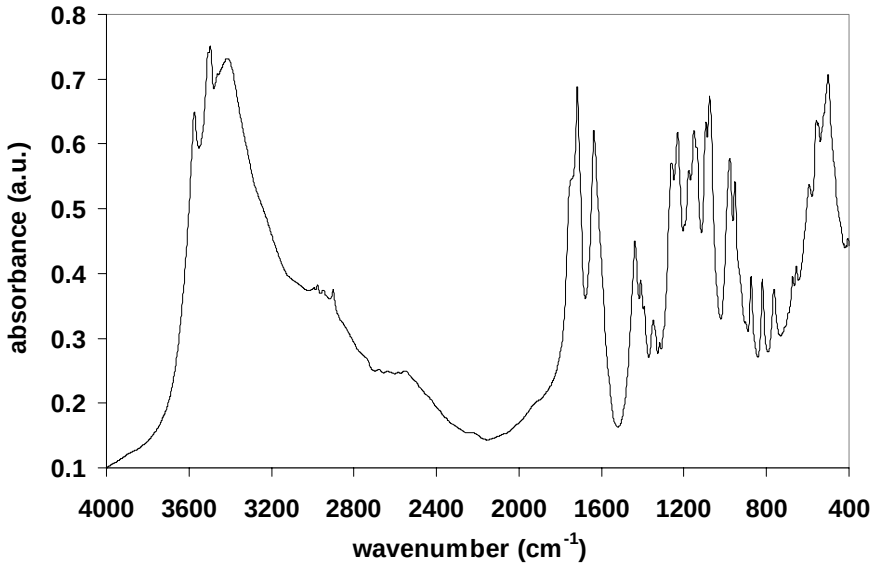

Figure 41. FT-IR spectrum of CaNaPC. Intense bands due to the asymmetric ν(C=O) stretching vibration in the region 1600-1750 cm^{-1} and due to the ν(P=O) stretching vibration in the region 1000-1100 cm^{-1} are observed

3. APPLICATIONS

3.1. Corrosion Control

Corrosion has been defined in many ways. Definitions, although different in expression, have all emphasized the changing of the mechanical properties of metals in an undesirable way. ISO 8044 defines corrosion as "Physico-chemical interaction, which is usually of an electrochemical nature, between a metal and its environment which results in changes in the properties of the metal and which may often lead to impairment of the function of the metal, the environment, or the technical system of which these form a part".[53] The cost of corrosion has been reported from many studies to be in the order of 1 to 5 % of Gross National Product for any country. The cost of corrosion for the Shell Company has been calculated to be equivalent to $400 million in 1995. World-wide cost of corrosion for the production of all grades of pulp is about $3 billion/year. These numbers do not include the cost of lost production, shutdowns to make repairs to corroded equipment etc. British Petroleum (BP) has reported that the cost of corrosion is equivalent to 6 % of the net asset value of the company. Corrosion cost in the USA electric power industry reaches $10 billion each year, according to the Electric Power Research Institute (EPRI). Also, it has been reported by EPRI that corrosion is the cause for more than 55 % of all unplanned outages and it adds over 10 % to the average annual household electricity bill. The impact of corrosion on all branches of industry in almost all countries can be observed. For example, in 1993 it was estimated that 60 % of all maintenance costs for North Sea oil production platforms were related to corrosion either directly or indirectly. A report on inspection results of several offshore production plants showed that corrosion was a factor in 35 % of structures, 33 % of process systems and 25 % of pipelines. Every year microbiologically influenced corrosion causes well impediment. Removal of defective pipelines required production to cease for at least 5 days. It is therefore apparent that corrosion control is of significant economical and technical interest. Corrosion management can be achieved in several ways, one of which is based on corrosion inhibitors. These are chemical additives that delay or (ideally) stop metallic corrosion.[54]

Corrosion inhibitors are effective for the decrease of metal corrosion in nearly neutral conditions by forming weakly soluble compounds with the metal ion existing in the solution which precipitates on to the surface to form a three-dimensional protective layer. Such inhibitors (often called interphase inhibitors) for cooling water treatment technology in the last decades comprise different types of phosphonic acids.[55] Widely used examples of organic phosphonic acids are 1-hydroxyethane-1,1-diphosphonic acid (HEDP), amino-tris(methylenephosphonic acid) (AMP), hydroxyphosphonoacetic acid (HPA), etc. Phosphonates are introduced into the system to be protected in the acid form or as alkali metal soluble salts, but readily form more stable complexes with other metal cations found in the process stream (most commonly Ca, Mg, Sr or Ba), depending on the particular application. Research in this area has been stimulated by the need to develop inhibitor formulations that are free from chromates, nitrates, nitrites, inorganic phosphorus compounds, etc. Phosphonates when blended with certain metal cations and polymers reduce the optimal inhibitor concentration needed for inhibition due to synergistic effects.[56] Synergism is one

of the important effects in the inhibition process and serves as the basis for the development of all modern corrosion inhibitor formulations.

In spite of the significant body of literature, evidence about the molecular identity of the thin protective metal-phosphonate films lags behind. In this paragraph, the corrosion inhibition performance of three metal-phosphonate materials is reported. These exhibit dramatically different anticorrosion efficiencies, which are linked to their molecular structure. These metal-phosphonates are Zn-AMP, $\{Zn[(HO_3PCH_2)_3N(H)]\cdot 3H_2O\}_n$, Zn-HDTMP, $\{Zn[(HO_3PCH_2)_2N(H)(CH_2)_6N(H)(CH_2PO_3H)_2]\cdot H_2O\}_n$, and Ca-PBTC, $\{Ca(HOOCCH_2\text{-}C(COO)(PO_3H)CH_2CH_2COOH)(H_2O)_2\cdot 2H_2O\}_n$.

Synergistic combinations of 1:1 molar ratio Zn^{2+} and AMP are reported to exhibit superior inhibition performance than either Zn^{2+} or AMP alone.[57] However, no mention is made regarding the identity of the inhibitor species involved in corrosion inhibition. Therefore, a corrosion experiment is designed in order to verify the literature results and prove that the protective material acting as a corrosion barrier is an organic-inorganic hybrid composed of Zn and AMP. A synergistic combination of Zn^{2+} and AMP in a 1:1 ratio (under identical conditions used to prepare crystalline Zn-AMP) offers excellent corrosion protection for carbon steel (see Figure 42). Although differentiation between the "control" and "Zn-AMP" protected specimens is evident within the first hours, the corrosion experiment is left to proceed over a 3-day period. Based on mass loss measurements the corrosion rate for the "control" sample is 2.5 mm/year, whereas for the Zn-AMP protected sample 0.9 mm/year, a 270 % reduction in corrosion rate. The filming material is collected and subjected to FT-IR, XRF and EDS studies.

These show that the inhibiting film is a material containing Zn (from added Zn^{2+}) and P (from added AMP) in an approximately 1:3 ratio, as expected. Fe was also present apparently originating from the steel specimen. FT-IR showed multiple bands associated with the phosphonate groups that closely resemble those of an authentically prepared Zn-AMP material. For comparison, EDS and XRF spectra of a "protected" and an "unprotected" region show presence of Zn and P in the former, but complete absence in the latter.

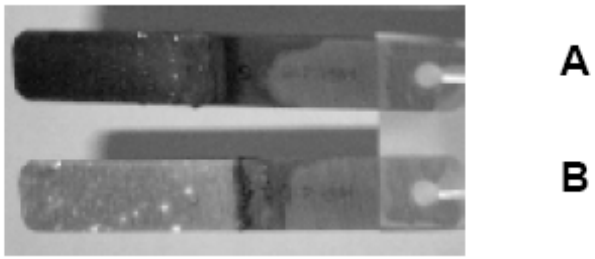

Figure 42. Corrosion inhibition by Zn-AMP. The upper specimen (A) is the control, no inhibitor present; the lower specimen (B) is with Zn^{2+}/AMP combination present, both in 1 mM. Corrosion inhibition is dramatically demonstrated at pH 3.0. Formation of Zn-AMP can be clearly seen on the steel specimen as a thin white layer, with additional material accumulated at certain locations, appearing as white spots

A combination of Zn^{2+} and HDTMP in a 1:1 ratio (under identical conditions used to prepare crystalline Zn-HDTMP) offers excellent corrosion protection for carbon steel (Figure 43). Although differentiation between the "control" and "Zn-HDTMP" protected specimens is

profound within the first hours, the corrosion experiment is left to proceed over a 3-day period. Based on mass loss measurements the corrosion rate for the "control" sample is 7.28 mm/year, whereas for the Zn-HDTMP protected sample 2.11 mm/year, a ~ 170 % reduction in corrosion rate. The filming material is collected and subjected to FT-IR, XRF and EDS studies.

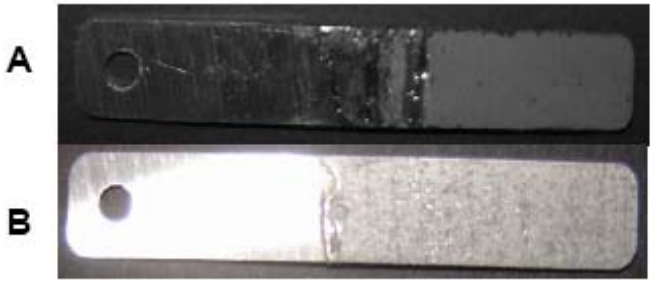

Figure 43. The anticorrosive effect of Zn-HDTMP films on carbon steel. The upper specimen is the "control" (A), no inhibitor present. Corrosion inhibition in the lower specimen (B) by a 1 mM Zn^{2+}/HDTMP synergistic combination is dramatically demonstrated

These show that the corrosion inhibiting film is a material containing Zn^{2+} (from externally added Zn^{2+}) and P (from added HDTMP) in an approximate 1:4 ratio. Fe was also present apparently originating from the carbon steel specimen. FT-IR of the filming material showed multiple bands associated with the phosphonate groups in the 950-1200 cm^{-1} region that closely resemble those of the authentically prepared Zn-HDTMP material (Figure 44). For comparison, EDS and XRF spectra of a "protected" and an "unprotected" region show presence of Zn and P in the former, but complete absence in the latter.

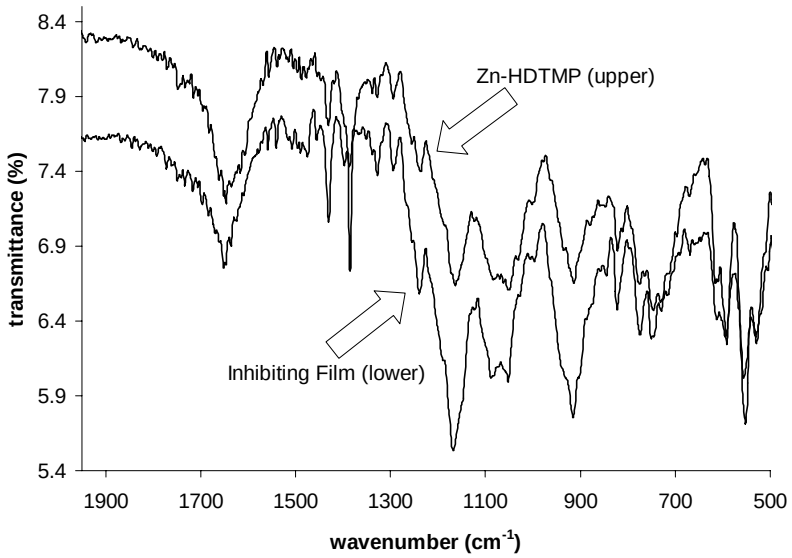

Figure 44. FT-IR spectra of "authentic" Zn-HDTMP and of the corrosion inhibiting film formed in situ from a 1:1 Zn^{2+}:HDTMP synergistic combination

A synergistic combination of Ca^{2+} and PBTC in a 1:1 molar ratio (under identical conditions used to prepare crystalline $Ca(PBTC)(H_2O)_2 \cdot 2H_2O$ seems to offer excellent corrosion protection for carbon steel (Figure 45) based on visual observations. However, based on mass loss measurements the corrosion rate for the "control" sample is 0.16 mm/year, whereas for the Ca-PBTC protected sample 1.17 mm/year, a ~ 10-fold increase in corrosion rate. Therefore, PBTC essentially enhances the dissolution of bare metal, presumably forming soluble Fe-PBTC complexes. In contrast to aminomethylene-*tris*-phosphonate, AMP, PBTC does not form stable metal-phosphonate protective films. This is consistent with the low complex formation constant for Ca-PBTC, 4.4.[58]

Figure 45. Phenomenology of the anticorrosive effect of Ca-PBTC films on carbon steel. The upper specimen is the "control" (A), no inhibitor present. Surface "cleanliness" in the lower specimen (B) by a 1 mM Ca^{2+}/PBTC synergistic combination is demonstrated, but metal loss is enhanced (see text)

Phosphonic acids are better known for their antiscaling/antifouling properties,[25] rather than their anticorrosion efficiency. However, the latter can be substantially improved in the presence of metal ions. This synergistic phenomenon has been extensively and elegantly studied mostly by electrochemical methods.[59] Notably, the work of Telegdi *et al.* has given insight into the possible mechanism of corrosion protection.[60] Kuznetsov has extensively and systematically studied a variety of inhibitors that have complexing properties.[61]

An ideal phosphonate corrosion inhibitor of the "complexing type" is required to possess the following significant features: (a) it must be capable of generating metal-phosphonate thin films on the surface to be protected (b) it should not form very soluble metal complexes, because these will not eventually "deposit" onto the metal surface, but will remain soluble in the bulk (c) it should not form sparingly soluble metal complexes because these may never reach the metal surface to achieve inhibition, but may generate undesirable deposits in the bulk or on other critical system surfaces (d) its metal complexes generated by controlled deposition on the metal surface must create dense thin films with robust structure. If the anticorrosion film is non-uniform or porous, then uneven oxygen permeation may create sites for localized attack, leading to pitting of the metal surface.

The results described herein are geared towards understanding corrosion inhibition at the molecular level, rather than proving the anticorrosion performance of the above-mentioned inhibitors. There are several hypotheses found in the literature on the mechanism of corrosion inhibition by metal-inhibitor complexes and are supported by a variety of spectroscopic and electrochemical techniques. None of these, however, has unequivocally proven the molecular identity of the metal-inhibitor complex.

The corrosion inhibition results are presented in Table 2 and Figure 46. It is apparent that pH plays a profound role in corrosion inhibition. A decrease of 2 pH units causes a 45-fold increase in corrosion rates and an operational range of 0.16 to 7.28 mm/year. This is consistent with well established observations in the literature and in the field. Presence of a metal phosphonates causes dramatic decrease in corrosion rates overall. Again, lower operational pH favors higher corrosion rates, but the operational range is now much narrower, 0.90 to 2.11. This translates in an ability to operate lower pH process waters with acceptable corrosion rates, but presence of a metal phosphonate corrosion inhibitor is necessary. The results with Ca-PBTC and Zn-PBTC warrant further discussion. Corrosion rates in the presence of inhibitor are higher than those for the control (no inhibitor). This, at a first glance, is contrary to results obtained with the Zn-HDTMP and Zn-AMP inhibitors. This may be explained by several arguments. First, the metal-phosphonate film may not be robust, but porous in its microscopic nature. This, as mentioned before, would lead to localized attack and metal pitting. Such phenomena have not been observed upon examination of the metal specimens after the corrosion experiments. Second, the metal phosphonate (Ca, or Zn-PBTC) is too soluble to deposit onto the metal surface, so it does not form a protective and anticorrosion thin film. This argument would be consistent with literature data on Metal-PBTC complex formation constants (4.4 for Ca-PBTC and 8.3 for Zn-PBTC) that are considered to be very low.[58] The difference in complex formation constants between Ca and Zn-PBTC would be consistent with the fact that Zn-PBTC is a more effective corrosion inhibitor than Ca-PBTC, as long as both inhibitors form films (albeit unstable) on the metal surface. If film formation does not take place, then corrosion rates in the presence of Ca-PBTC or Zn-PBTC would be the same as the control, which is not the case.

Therefore, the results obtained with Ca-PBTC and Zn-PBTC, indicate that these materials are soluble and due to their acidic nature they actually act as metal dissolvers rather than corrosion inhibitors. A careful look at the molecular structure of Ca-PBTC reveals that PBTC is doubly deprotonated (at the phosphonate group and at the carboxyl group at the 6 position). The remaining two carboxylate groups are protonated, but coordinated to the Ca^{2+} center through the C=O moiety. This increases the acididy of the non-coordinated –OH group of the carboxylate. The final result could be thought as formation of a Ca-PBTC soluble acidic complex at the proximity or on the metal surface, which acts as Fe oxide dissolver. Alternatively, this acidic complex may create local low pH regions that would certainly increase corrosion rates.

Table 2. Comparative corrosion rates of metal surfaces protected by metal-phosphonate corrosion inhibitors

Metal-Phosphonate	Control corrosion rates (mm/year)	Corrosion rates in the presence of metal-phosphonates (mm/year)	Corrosion pH
Zn-HDTMP	7.28	2.11	2.2
Zn-AMP	2.50	0.90	3.0
Ca-PBTC	0.16	1.17	4.0
Zn-PBTC	0.16	0.46	4.0

The two Zn-phosphonates have distinctly different crystal and molecular structures. The Zn-HDTMP material by virtue of its long chain linker between the two amino-

bis(methylenephosphonate) moieties might be thought of as a porous material. However, porosity measurements on this and the other phosphonates show absence of any porous structure. Therefore, differences in porosity cannot be invoked to explain the various anticorrosion properties of these metal-phosphonate materials.

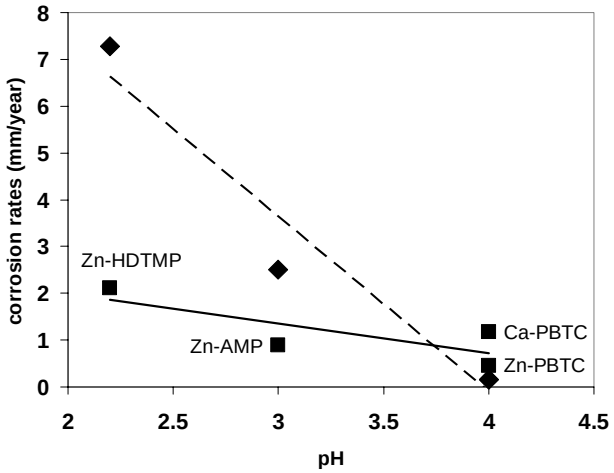

Figure 46. Corrosion rates of metal phosphonate-protected surfaces as a function of pH

Lastly, the ability of a metal-phosphonate corrosion inhibitor to adhere onto the metal surface plays a vital role in corrosion efficacy. Bulk precipitation of a metal-phosphonate complex will lead to loss of active inhibitor to precipitation, leading to insufficient levels for thin film formation. Surface adherence of the inhibitor films is a property that cannot be precisely predicted. However, it is a necessary condition for acceptable inhibition. In addition, the metal-phosphonate protective layer has to be robust and uniform. A characteristic example of a Zn-AMP film is shown in Figure 47 and is compared to a "bear" iron metal surface. Zn-HDTMP forms thin anticorrosive films similar in morphology.

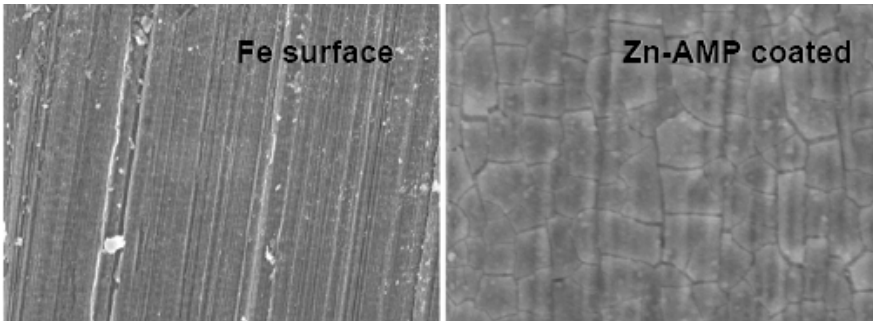

Figure 47. SEM images of a "clean" carbon steel surface (upper, bar = 100 microns) and a Zn-AMP protected steel surface (lower, bar = 10 microns). Deposition of an anticorrosive Zn-AMP thin film is obvious. Film cracking is due to drying

3.2. Biomedical Applications

Phosphocitrate (PC) is a naturally occurring compound found in mammalian mitochondria.[62] Tew *et al.* speculated that PC prevents calcium phosphate precipitation in cells or cellular compartments maintaining high concentration of Ca^{2+} and PO_4^{3-}.[62] Moro *et al.* suggested that PC arises from the cytosolic phosphorylation of citric acid, which explains why it is non-toxic and environmentally friendly.[63] *In vitro* studies suggested that concentration up to 1.5 mM PC (4.5 mg/ml) does not affect normal basal cellular functions including DNA and protein synthesis.[64] PC specifically inhibits crystal-induced MMP synthesis and mitogenesis in cells while it has no effect on similar processes induced by growth factors or serum.[65] This blocking effect is likely explained by the influence of PC on calcium crystals interaction with biomembranes.[66] PC is a potent *in vitro* inhibitor of hydroxyapatite crystal formation.[67] PC prevents soft tissue calcification *in vivo* and does not produce any significant toxic side effect in rats or mice when given in doses up to 150 mmole/Kg/day.[68] PC specifically inhibits crystal-induced proto-oncogenes, MMP synthesis, mitogenesis, signal transduction, and cyclo-oxygenase synthesis but PC exerts no effect on similar processes induced by growth factors or serum in cultured cells.[69] Although PC does not have any effect on basal or TGF-β–induced inorganic pyrophosphate elaboration and nucleotide triphosphate pyrophosphohydrolases activity, PC blocks calcification in matrix vesicles and cartilage in an *in vitro* model of chondrocalcinosis, nitric oxide-induced calcification of cartilage and apoptotic bodies.[70] In short, PC is the only agent examined so far that blocks the deleterious biologic effects of crystals and also prevents calcification.[71] As described in paragraph 2.15, a new mixed salt of calcium and sodium of PC (CaNaPC) has been synthesized. [44] Like its precursor, NaPC, CaNaPC is a potent and specific inhibitor of the biological effects of the calcium-containing crystals but CaNaPC is a significantly more potent anti-mineralization agent. This increased in potency to block biomineralization and biological effect, make PC to be a potential salutary agent for crystal deposition diseases. The Hartley strain guinea pigs develop an arthropathy that histologically mimics human osteoarthritis. The joints of this animal model have been characterized both histologically,[72] and radiographically.[73] Osteoarthritis begins in the knee joints of the Hartley guinea pig around 3 month of age, reaching an advance stage by 12 months. Histologically, osteoarthritis is characterized by chondrocyte and proteoglycan loss, fibrillation, chondrocyte cloning, osteophyte formation, and subchondral sclerosis. By 12 months of age, extensive degeneration of the articular cartilage of central medial tibial plateau, femoral condylar and meniscal cartilage has occurred. Huebner et al reported that both MMP-1 and MMP-13 played an active role in the cartilage degeneration in this animal.[74] Significant calcification of medial menisci appears to correlate with the disease and age.[75]

Two sets (n=16 animals/set) of 4-month old guinea pigs were used in the study. One set of animals received weekly IP injection of CaNaPC (40mg/kg) and the control set was injected with PBS. Animals were sacrificed after 3 months of treatment with either CaNaPC or PBS. The hind legs were removed and the joints were opened for gross examination. Cartilage surfaces of the knees were examined grossly after coating cartilage surfaces with carbon black to determine the extent of degeneration, pitting, and ulcer formation, as previously described. CaNaPC-treated cartilage surface was white and glistening with few erosions, little carbon black retention, and little synovial thickening. The Control cartilage

demonstrated discolored surface, surface ulcerations, pitting lesions in all animals, and retention of carbon black staining with an erythematous thickened synovium (Figure 48).

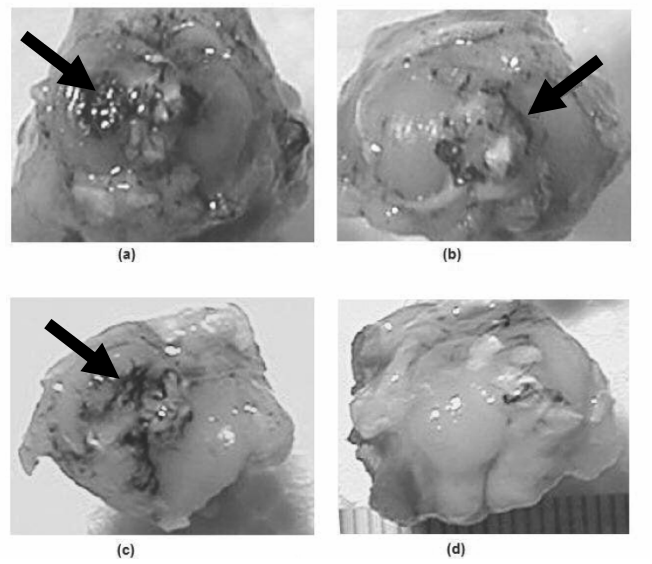

Figure 48. Gross examination of cartilage surface after coating with carbon black: (a) control femoral condyle; (b) CaNaPC treated femoral condyle; (c) control tibial plateau; and (d) CaNaPC treated tibial plateau. CaNaPC-treated cartilage surface was white and glistening with few erosions, little carbon black retention, and little synovial thickening. The Control saline-treated cartilage demonstrated discolored surface, surface ulcerations, pitting lesions in all animals, and retention of carbon black staining with an erythematous thickened synovium. Arrows point to damage area coated with carbon black on the surfaces

The Mankin 14 point grading system was used to evaluate cartilage degeneration. Histochemical examination of treated cartilage appeared normal (Figure 49) with a Mankin score of 1.6 ± 0.8. In contrast, control cartilage was either eroded or badly fibrillated (Figure 49B) demonstrated by Mankin score of 6.3 ± 1.4 (mean ± SEM, n=4, P> 0.01). A significant decrease ($p>0.01$) in calcific deposit was found for treated animals compared to control animals. Based on the calcium content of the menisci, CaNaPC treatment resulted in reduction of approximately 50% of the calcific deposit. The calcium content of menisci isolated from the treated animals was 498 ± 133 μg while those of control animals was 970 ± 221 μg [N=6, a mean ± SEM, P>0.01]. Histochemical examination with the calcium specific Von Kossa stain confirmed this observation (Figure 49 c and d). The horn of the menisci of the treated animals appeared to be intact while the one from saline-treated animals was badly fibrillated (Figure 48c and d).

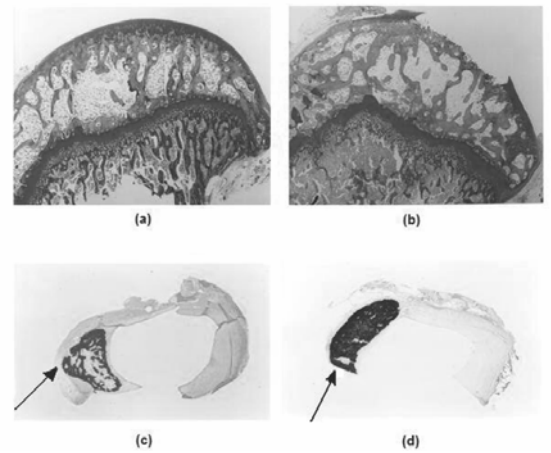

Figure 49. The efficacy of CaNaPC on the guinea pig model of osteoarthritis. Animals were sacrificed after completed 3 months of treatment IP with CaNaPC (40 mg/kg/wk). Significant decrease in the calcified deposit in the meniscus of treated animals compared to control and the cartilage on femoral condyle appeared normal while cartilage on the femoral condyle of untreated controls were either eroded or badly fibrillated. (a) Histology of 6- month old guinea pig tibial plateau after treatment with CaNaPC (40 mg/wk) for 3 months. (b) Histology of untreated control 6-month old guinea pig tibial plateau. (c) Cross-section of meniscus of 6-month old guinea treated with CaNaPC (40 mg/kg//wk) for 3 months. Note the significant reduction of the calcified deposits (dark brown color). (d) Cross section of meniscus of untreated control 6-month guinea pig. Arrows point the massive calcification in the meniscus as compared to the treated animals

The present findings lead to the proposal that there are two potential mechanisms by which articular calcification can cause cartilage degeneration. The first involves changes in joint biomechanics. Articular calcification may lead to altered loading of the joint causing injury to the cartilage matrix, which fails under normal loading and chondrocytes respond by elaborating MMPs and developing inappropriate repair responses. The second mechanism involves the biological effect of crystals on articular cells.[76] In advance stages of the disease, crystals shedding from the meniscus or cartilage into synovium induce synoviocyte proliferation and MMP synthesis, which amplify the osteoarthritis disease progression in the guinea pig osteoarthritis model [77] PC treatment has no therapeutic effect in the hemi-meniscectomy model [78] that has no known crystal involvement. Taken together with previous findings on the therapeutic effect of PC on MPA [79] and the known *in vitro* specific inhibitory effect of the biological effect of calcium-containing crystals of PC, we conclude that PC has *no* therapeutic effect on cartilage degeneration in osteoarthritis *not* associated with calcium-containing crystals. We proposed that CaNaPC blocks calcification-induced cartilage degeneration and arrests osteoarthritis disease progression by two related mechanisms. First, PC causes resorption of existing calcium deposits and inhibits new calcification of the menisci, thus prevents abnormal joint loading. Second, PC specifically inhibits crystal-induced cellular response damage.[80] However, it is still possible that the therapeutic effect may come from other as-yet identified effects of PC.

It is well known in the literature that PC's biological excretion is rapid.[81] This presents one of the problems associated with wide application of PC as calcification inhibitor. An alternative form of PC that exhibits slower, more sustained release could offer substantial therapeutic benefits. Solubility of Ca^{2+} salts is typically much lower than that of the

analogous Na^+ salts. This prompted a comparative study between the efficiencies of the Ca and Na salts of PC to inhibit hardening of an induced plaque in rats.[82] This model has been used before to demonstrate anticalcification potency of PC.[83] Results from the animal study are presented in Table 3 and Figure 50.

NaPC is an effective plaque inhibitor but at higher and more frequently administered doses than those described herein.[84] However, as shown in results from Group B, its effectiveness is greatly diminished when a lower dose is used (9.7 mg as H_5PC), resulting in only 30 % plaque reduction. Superior inhibition activity becomes evident by following treatment with CaNaPC (Group C), at an equal dose (9.6 mg as H_5PC) giving nearly quantitative (95 %) plaque inhibition. Possible explanations for the improved anticalcification efficiency of CaNaPC compared to that of NaPC could be relevant to: (a) the slower and more sustained release of "active PC", thus ensuring its bioavailability at all times by limiting the excreted amount; (b) the more effective stereospecific interaction between CaNaPC and crystal face(s) of hydroxyapatite. This latter probability could be resolved through molecular modeling. Such studies are underway, following similar ones on interactions of NaPC with other calcium minerals.[85]

Table 3. Inhibition of plaque growth using NaPC and CaNaPC as calcification inhibitors.[a]

Treatment groups	Treatment dosage (as mg H_5PC)	Plaque weight (mg)[b]	Plaque weight reduction (%)
A (control)	0	211 ± 9.244	0
B (NaPC)	9.7	147 ± 8.825	30
C (CaNaPC)	9.6	11 ± 4.444	95

[a] Data were processed to establish One Way Analysis of Variance with significance determined as pair-wise comparison (Student-Newman-Keuls method). [b] Results are expressed as mean ± SEM for 10 plaques. Statistical significance was determined at the level of $P < 0.001$ for single groups and pair-wise group comparisons

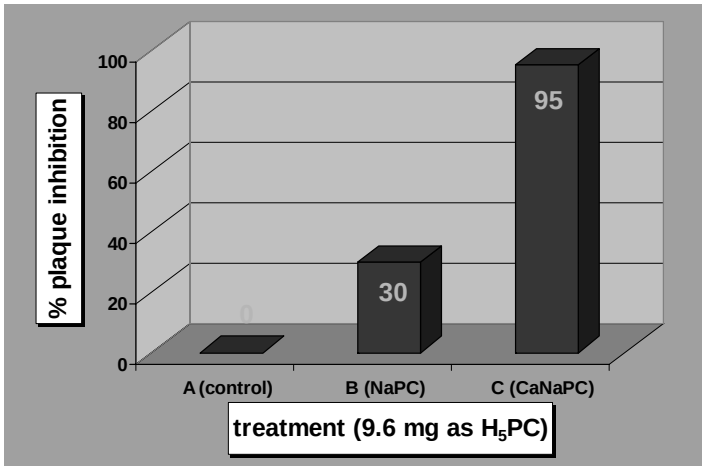

Figure 50. Comparison of *in vivo* anticalcification activities of NaPC and CaNaPC

In summary, examination of the role of pathologic calcification in articular tissue in osteoarthritis disease progression and in induced calcification model will be revealing. Study of CaNaPC as a potential therapeutic agent has generated data that confirm that meniscal calcification appears to correlate with the cartilage degeneration in this Guinea Pig osteoarthritis model, suggesting this is a good model to examine the role of calcification in osteoarthritis. PC treatment led to significant resorption of calcium deposits in menisci and arrested osteoarthritis disease progress. Similar PC treatment has no therapeutic effect in the hemi-meniscectomy model that has no known articular calcification. This supports the hypothesis that calcification plays an important role in the osteoarthritis disease progression and that CaNaPC is a potential therapeutic agent for this animal model and possibly for human Chondrocalcinosis and BCP Deposition Disease. Moreover the present observation may have broader implications. Tissue trauma or abnormal fluctuations in intracellular calcium ion concentrations can trigger formation of calcium-containing deposits. Initially, calcium salts may accumulate in an amorphous state but under continuing favorable environmental conditions, nucleation and transformation to an insoluble, crystalline salt that can activate cellular responses leading to the development of the specific pathological disease state. This scenario prevails in diseases such as renal calcinosis, urinary lithiasis, arteriosclerosis, heart valve calcification, soft tissue and tumor calcification. Whether PC has any potential therapeutic effect on any of these diseases remains an open question.

Recently, an important application of metal phosphonates to biotechnologies was reported.[86] The authors highlighted a fundamentally different route for covalently attaching DNA probes to surfaces via metal-phosphonate coordination for array applications. The new approach uses a mixed organic/inorganic monolayer to derivatize the glass and generate a reactive surface. Probe attachment is then through a highly specific coordination covalent linkage between a terminal phosphate group on the probe molecules and the inorganic ions on the glass surface. An advantage over other methods currently in use is that phosphate is a naturally occurring function that does not alter the intrinsic nature of the probe, and it can be introduced chemically or with enzymatic routes, offering the possibility of using PCR products as starting materials. Furthermore, the DNA grafting process is simple, performed in a single step instead of multiple chemical coupling reactions.

The zirconium phosphonate-modified surfaces can be prepared in different ways, but often involve binding of Zr^{4+} ions to phosphorylated groups deposited onto silica or gold. Exceptionally smooth and uniform films can be generated on hydrophobic supports by using Langmuir–Blodgett (LB) methods. The LB process begins with an octadecylphosphonic acid (ODPA) Langmuir monolayer that is deposited onto the hydrophobic solid support in such a way that the hydrophilic acid group ($-PO_3H_2$) is directed away from the support. The substrate is then removed from the LB trough and exposed to a solution of Zr^{4+} ions that bind to give a monolayer of the zirconated octadecylphosphonic acid (ODPA-Zr). In solid-state zirconium phosphonates, each Zr^{4+} ion is coordinated by oxygen atoms from different molecules, thus linking them together. The same situation arises in the zirconated LB films. The strongly binding zirconium ions cross-link the original monolayer, providing a well-defined interface of zirconium phosphonate sites that sticks strongly to the surface, because it is no longer a traditional LB film of individual molecules physisorbed to the surface but rather a network or monolayer tape in which adhesion comes from the sum of all molecules in a cross-linked array. The zirconium phosphonate films are not soluble in organic solvents, and dissolve in

water only below pH 1. Glass slides coated with the ODPA-Zr monolayers can be stored in water for months and retain activity with no evidence of desorption.

3.3 Crystal modification of Inorganic Materials and Biomaterials

3.3.1. Calcium Carbonate

Industrial water systems face several challenges related to formation of sparingly soluble electrolytes.[87] Cooling water systems, in particular, may suffer from a multitude of problems. Utility plants, manufacturing facilities, air-conditioning systems (to mention a few) use "hot" processes in their operations. These processes have to be cooled. Water is the universal cooling medium because it is cost effective and has a high heat capacity.[88] "Spent" cooling water needs to be re-cooled for reuse. This cooling is achieved by partial evaporation. The end result of this process is the concentration of all the species found in the water until they reach a critical point of "scaling", leading to precipitation, and ultimately deposition of mineral salts. The species usually associated with these deposits (depending on the water chemistry) are calcium carbonate, calcium phosphate(s), silica/metal silicates etc. Such undesirable deposition issues can be avoided by careful application of chemical water treatment techniques. [89]

Prevention of scale formation is greatly preferred by industrial water users to the more costly (and often potentially hazardous) chemical cleaning [90] of the adhered scale, in the aftermath of a scaling event. Common examples of scales that require laborious (mechanical) and potentially dangerous (hydrofluoric acid) cleaning are silica and silicate salts.[91] Prevention of the scale deposits can also benefit the water operator by eliminating (or at least by minimizing) unexpected production shut-downs and by offering substantial savings through water conservation (especially in areas with high water costs).

Organic phosphonates are an integral part of a chemicals-based water treatment program.[92] They function as scale inhibitors by adsorbing onto crystal surfaces of insoluble salts and prevent further crystal growth.[93] At high calcium levels phosphonates can precipitate out of solution as Ca salts. Unfortunately this is a very common problem in cooling water systems.[94] Such precipitates can be detrimental to the entire cooling water treatment program because:

a) They cause depletion of soluble inhibitor, and, subsequently, poor scale control because there is little or no inhibitor available in solution to inhibit scale formation.
b) They can act as potential nucleation sites for other scales.
c) They can deposit onto heat transfer surfaces (they usually have inverse solubility properties) and cause poor heat flux, much like other known scales, such as calcium carbonate, calcium phosphate, etc.).
d) If the phosphonate inhibitor in the treatment program has the purpose of corrosion inhibition, its precipitation as a Ca salt will eventually lead to poor corrosion control.

In other applications, such as oilfield drilling,[95] precipitation of scale inhibitors as Ca, Ba, or Sr salts is desirable. Large amounts of inhibitor are "squeezed" in the oilfield well and remain there for a specified amount of time, during which the inhibitor precipitates with

alkaline earth metals found in the high-salinity brine and eventually deposits onto the rock formation. Once the well is opened again for operation the metal-inhibitor salts slowly dissolve to provide adequate levels of scale inhibitor in solution.[96] Controlled dissolution of these salts is essential, as fast dissolution will lead to chemical wastage and slower dissolution will result in inefficient scale control. Knowledge of the chemistry of Ca-phosphonate salts under varying conditions of temperature and ionic strength can provide valuable information. Wise and effective use of such knowledge can lead to the discovery of new and better performing scale inhibitors.

Phosphonates are most commonly found in their deprotonated form, due to the particular pH range of operation (usually in the range 7.0 to 9.8). These additives perform scale inhibition in ppm quantities and usually work synergistically with dispersant polymers. Aminomethylene phosphonates in particular are used extensively in cooling water treatment programs, [97] oilfied applications [95] and corrosion control. [98] AMP is one of the most common aminomethylene phosphonates and is a very effective scale inhibitor. [99] However, under certain conditions (high calcium concentrations, high pH) it can form Ca-AMP precipitates which have the detrimental effects mentioned above. Some patented technologies based on polymers have been reported to effectively control Ca-AMP scale.[100]

Understanding the intimate mechanisms of scale inhibition by phosphonates requires a closer look at the molecular level of their possible function. Herein, results on the properties of AMP as a $CaCO_3$ scale inhibitor in synergy with dispersant polymers are reported. Specifically, polymers A and B are acrylate/acrylamide/alkylsulfonate terpolymers with different degree of sulfonate groups. A has higher number of acrylate and lower degree of sulfonate groups than B and both have molecular weights of ~ 18,000 daltons.[101]

The Scale Inhibition Test [25] was used to investigate the effect of AMP as $CaCO_3$ inhibitor at high Ca^{2+} and CO_3^{2-} levels, as well as high temperatures and pH. $CaCO_3$ has increased tendency to precipitate at higher temperatures, a phenomenon known as "inverse solubility". The experiments were run at 43 ºC. Bulk water temperatures in the range 40-50 ºC are commonly found in industrial applications.

According to the results in Table 4 and Figure 51, AMP is an effective $CaCO_3$ scale inhibitor. It can maintain 400 ppm (of 800 ppm) of soluble calcium in solution at high supersaturation and temperature (run 1). Furthermore, its performance is assisted by the dispersant properties of polymers A and B. At Ca^{2+}/HCO_3^- of 800/800 $CaCO_3$ inhibition is assisted by both polymers A and B. The blend AMP/polymer A achieves 64 % inhibition (run 4) and the blend AMP/polymer B is more effective with 74 % inhibition (run 5). At lower supersaturations (Ca^{2+}/HCO_3^- of 700/700) the blend with polymer B performs better than the one with polymer A, 82 % inhibition for the former (run 3) vs. 75 % for the latter (run 2). At higher supersaturations however, (Ca^{2+}/HCO_3^- of 900/900) the performance of both blends is about the same ~ 60 % (runs 6 and 7).

The dispersant properties of polymers A and B seem to be very similar based on measurements of dispersed Ca^{2+} (Table 4). Both blends achieve quantitative dispersion of $CaCO_3$ at Ca^{2+}/HCO_3^- levels of 700/700 (runs 2 and 3). At higher stress conditions (Ca^{2+}/HCO_3^- of 800/800) the dispersion performance is still high at ~ 90 % (runs 4 and 5), but drops to ~ 80 % at Ca^{2+}/HCO_3^- of 900/900 (runs 6 and 7).

Table 4. Scale Inhibition Test conditions and experimental results

Experiment	Ca (ppm)	Malk (ppm)	Mg (ppm)	AMP (ppm)	polymer (ppm)	Soluble Ca (ppm), 2h	% Inhibition, 2h	Dispersed Ca (ppm), 24h	% Dispersion, 24h
0	800	800	200	0	0	5	< 1	0	0
1	800	800	200	30	0	409	51	354	44
2	700	700	200	30	30 of A	522	75	692	99
3	700	700	200	30	30 of B	572	82	715	102
4	800	800	200	30	30 of A	510	64	716	90
5	800	800	200	30	30 of B	596	74	726	91
6	900	900	200	30	30 of A	557	62	734	82
7	900	900	200	30	30 of B	553	61	757	84

An additional point that warrants some discussion is the way AMP (together with polymers A or B) affects crystal and particle morphology of the resulting $CaCO_3$ scale deposits. In order to examine that more carefully, samples of those $CaCO_3$ deposits were analyzed by SEM. The images are given in Figure 52.

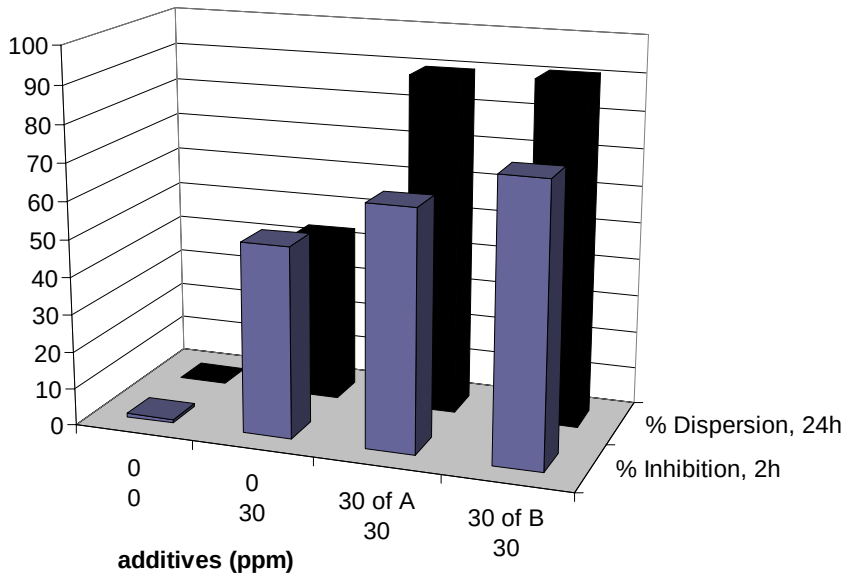

Figure 51. Effects of AMP/polymer blends on inhibition and dispersion of $CaCO_3$

Upon examination of the morphology of the $CaCO_3$ scale deposits, it becomes evident that there are obvious differences. $CaCO_3$ solids that precipitate from solutions containing AMP and polymer A (Figure 52, upper) are amorphous (non-crystalline) spheres and have little tendency to "stick" to each other. Their approximate size is 6 μm. On the other hand, $CaCO_3$ precipitates from AMP and polymer B solutions (Figure 52, lower) have well defined crystalline morphology, and, apparently, tend to agglomerate and form larger aggregates. The size of those particles is ~ 10 μm.

Dubin performed similar studies on $CaCO_3$ crystallization in the presence of organic phosphorous compounds or polymers.[102] His results showed that structural variations in organophosphonate or dispersant polymer additives used in supersaturated solutions of $CaCO_3$ caused dramatic effects on the crystal/particle morphology and size of the precipitated deposits.

Both polymers A and B show virtually the same good synergistic effects with AMP scale inhibition. However, polymer A causes the precipitated $CaCO_3$ to form amorphous (and, consequently, more easily removed) scale, whereas polymer B allows the formation of larger agglomerates composed of crystalline microparticles.

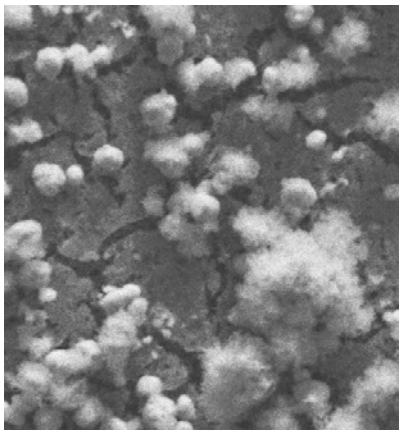

polymer A, Bar = 20 μm

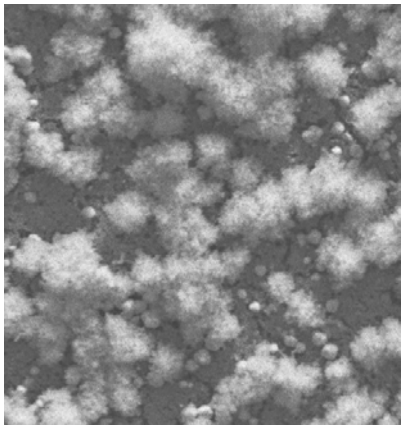

polymer A, Bar = 40 μm

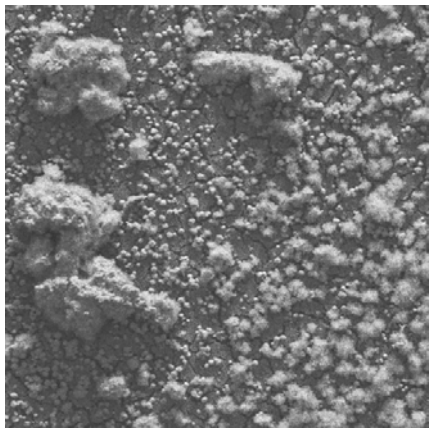

polymer A, Bar = 100 μm

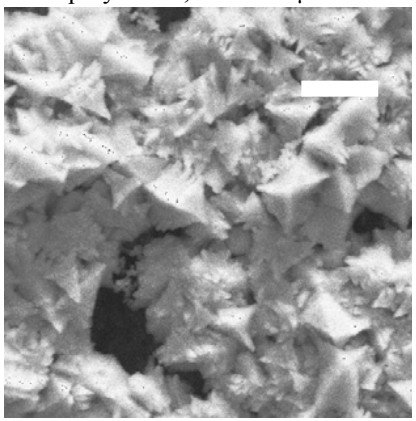

polymer A, Bar = 20 μm

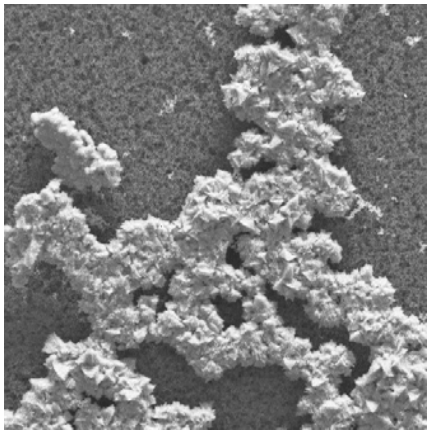

polymer A, Bar = 40 μm

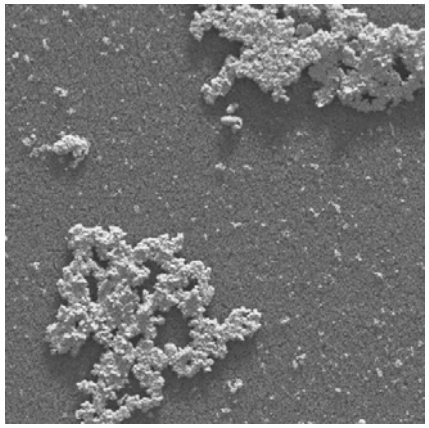

polymer A, Bar = 100 μm

Figure 52. $CaCO_3$ precipitates from solutions containing AMP and polymers A or B as additives

3.3.2. Barium Sulfate (Barite)

Barium sulfate is a common but unwanted crystallization product in the production of oil from off-shore rigs.[103] It is also a simple crystallization system that has been useful as a model for theoretical and applied studies.[104] Phosphonate additives are often used to inhibit either nucleation and/or growth of barium sulfate in order to avoid the formation of scale and several studies have shown that a complex relationship between structure, functional groups and ionization state of the phosphonate additive impacts on this inhibition.[105] More specifically, it has suggested that there is a link between the mineral lattice and the functional group spacing (the so called 'lattice matching' criteria) on the additive that dominates inhibitory power. Similarly, for multi-functional molecules it was suggested that only two functional groups were required for barite inhibition to occur.

Herein, the inhibition efficacies of two tetraphosphonates, namely EDTMP and HEDTMP, for barite are presented and compared. It should be pointed out that these additives are similar in that they both possess two aminobis(methylenephosphonate) moieties, but are different in that these groups are separated by a two methylene chain in EDTMP and by a six methylene chain in HDTMP. Results based on conductivity measurements are presented in Figure 53 in terms of their inhibitory efficacy on barium sulfate crystallization. As can be seen, in terms of conductivity, EDTMP is able to inhibit barium sulfate crystallization at lower concentrations than HEDTMP. However, both inhibit crystallization completely at this S value at relatively low concentrations (~0.001 mM for EDTMP and ~0.002 mM for HEDTMP).

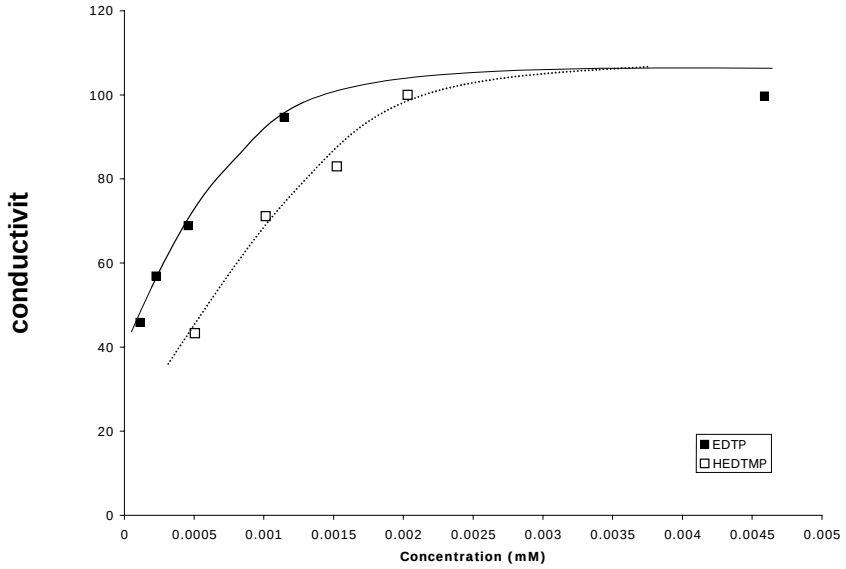

Figure 53. % Inhibition of barium sulfate precipitation de-supersaturation rate vs. concentration of additives (HEDTMP and EDTMP)

The morphology of the particles in the case of HEDTMP can be seen in Figure 54. The effect of EDTMP on barite morphology has been shown before to form long fibres at higher concentrations and elongated hexagonal particles at lower concentrations.

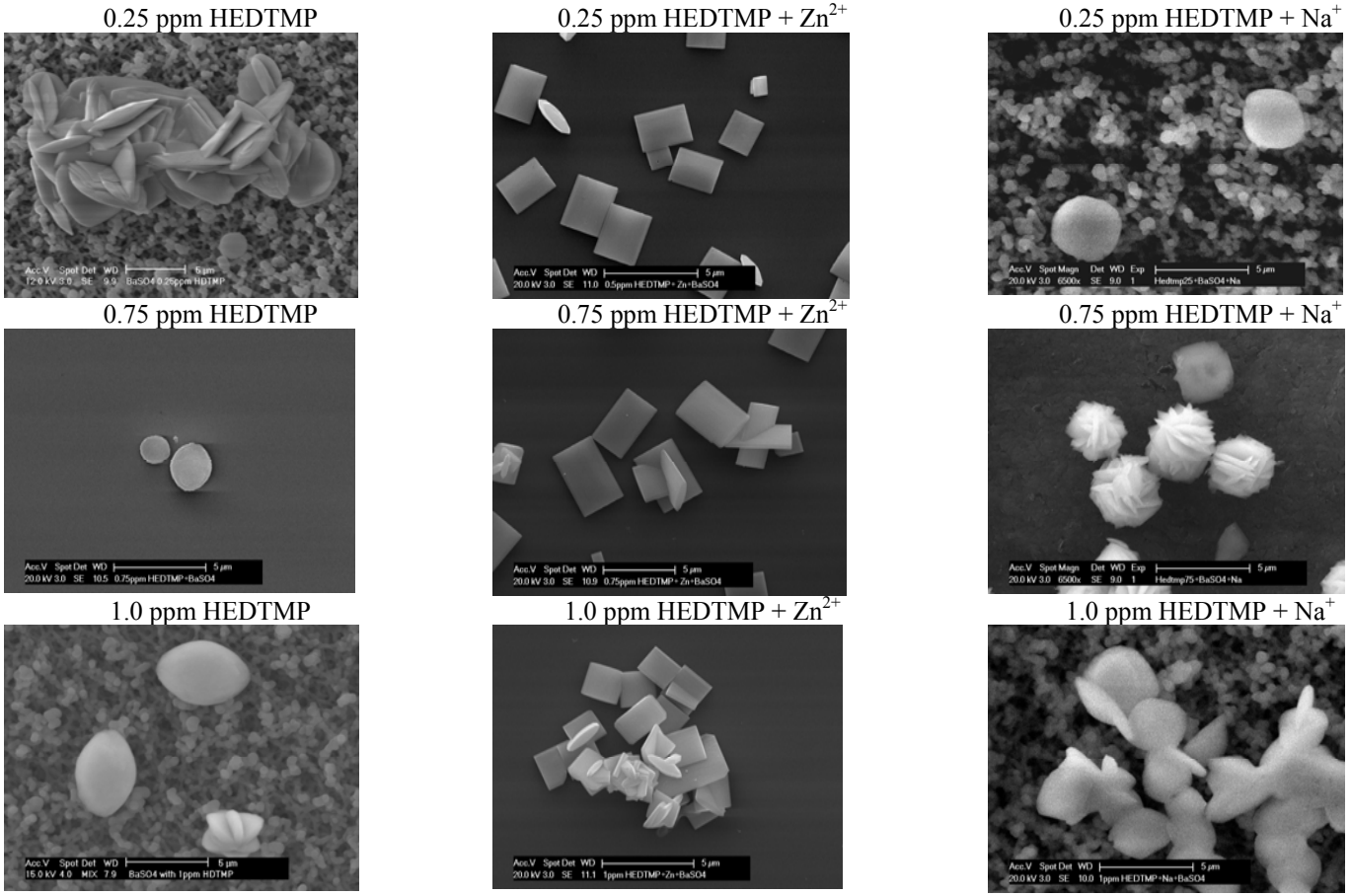

Figure 54. SEM images of barium sulfate precipitated in the presence of HEDTMP at various concentrations and with Zn^{2+} ions or Na^{+} ions present

In comparison, the HEDTMP showed a rounded morphology similar to that observed in the presence of the triphosphonate AMP (amino-tris(methylenephosphonate)).

The SEM images of barite precipitated in the presence of Zn^{2+} ions and HEDTMP show an interesting result (see Figure 54). As previously found for EDTA,[106] the presence of HEDTMP with Zn^{2+} ions shows that the barite morphology reverts to that expected for the presence of Zn^{2+} ions alone. Given that the Zn^{2+} ions, HEDTMP and Ba^{2+} ions are all present prior to sulfate addition, this cannot be due to surface adsorption of Zn^{2+} onto barite particles blocking HEDTMP adsorption. It was hypothesised that for EDTA, complexation with calcium may have been the cause (implying that the complexed EDTA either did not interact with the barite or was completely incorporated at a very early stage of precipitation). It is hypothesized that something similar is occurring to the HEDTMP + Zn^{2+} ion system.

In terms of induction times, EDTMP and HEDTMP show similar trends but at different concentrations, supporting the conductivity results. Roughly, ten times the concentration of HEDTMP was required to observe the same effect as EDTMP. This is shown in Figures 55 and 56. This is probably a consequence of the turbidity probe only detecting particles once they have reached a certain size. In this sense, the turbidity probe is less sensitive than conductivity.

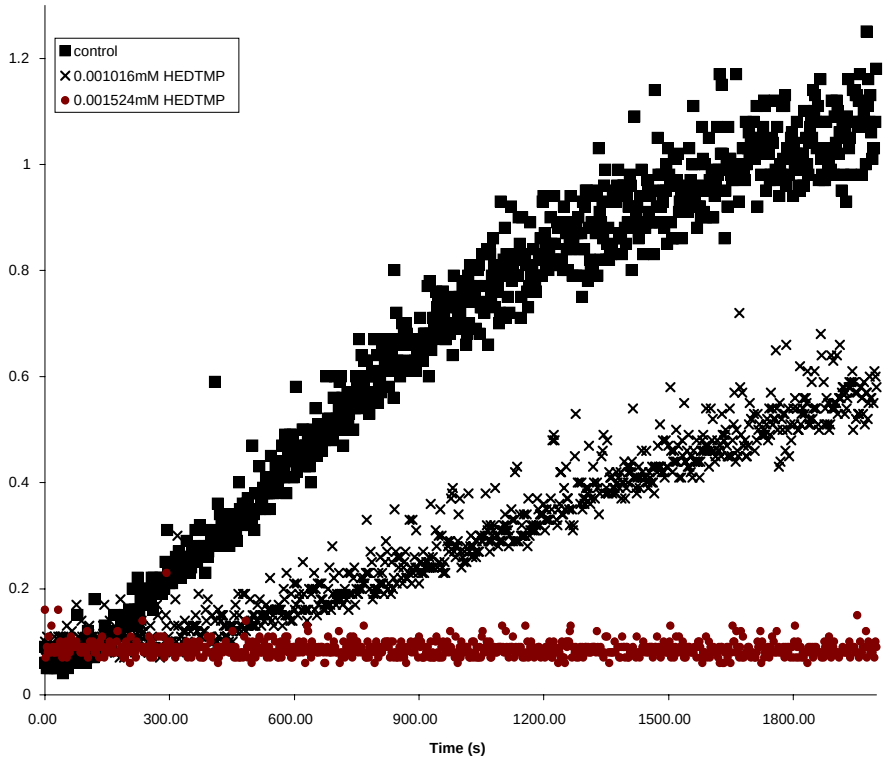

Figure 55. Turbidity (Normalised Turbidity Units, NTU) versus time for barium sulfate precipitation in the presence of HEDTMP at different concentrations

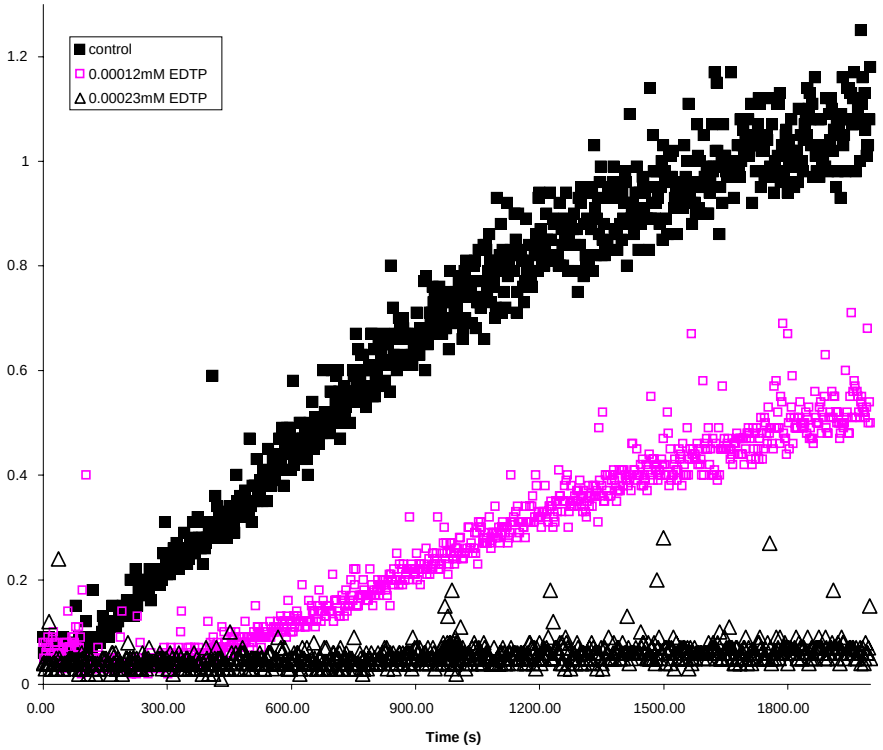

Figure 56. Turbidity (Normalised Turbidity Units, NTU) versus time for barium sulfate precipitation in the presence of EDTMP at different concentrations

The barium sulfate crystal morphology in the presence of both EDTMP and Zn^{2+} ions is *not* dramatically different to that in the absence of Zn^{2+} or EDTMP (see Figure 57). However, at higher concentrations there is perhaps a lengthening of the c axis but the morphology is essentially equivalent to the "control" conditions. In the presence of Na^{+} ions and EDTMP this is true at low additive concentrations but at higher concentrations where inhibition is significant, particles are much smaller and it also appears that they align to some extent at this concentration.

In summary, the presence of inorganic ions can have a significant effect on precipitation when additives are present. Interestingly, HEDTMP is a slightly weaker inhibitor of barium sulfate than EDTMP despite the similarity of the two additives and the fact that both contain four phosphonate groups. Clearly, the spacing between the amino-bis(methylenephosphonate) moieties of the additive backbone is playing a significant role. This is interesting in itself as Davey et al. suggested that only a minimum length between functional groups was required rather than an optimal length.[107] Obviously, experimental investigations with tetraphosphonates possessing longer chained linkers will be revealing. The interpretation of these results is that either the two phosphonate groups adsorbing are not on the same amino group or that more than two functional groups are adsorbing onto the barite surface.

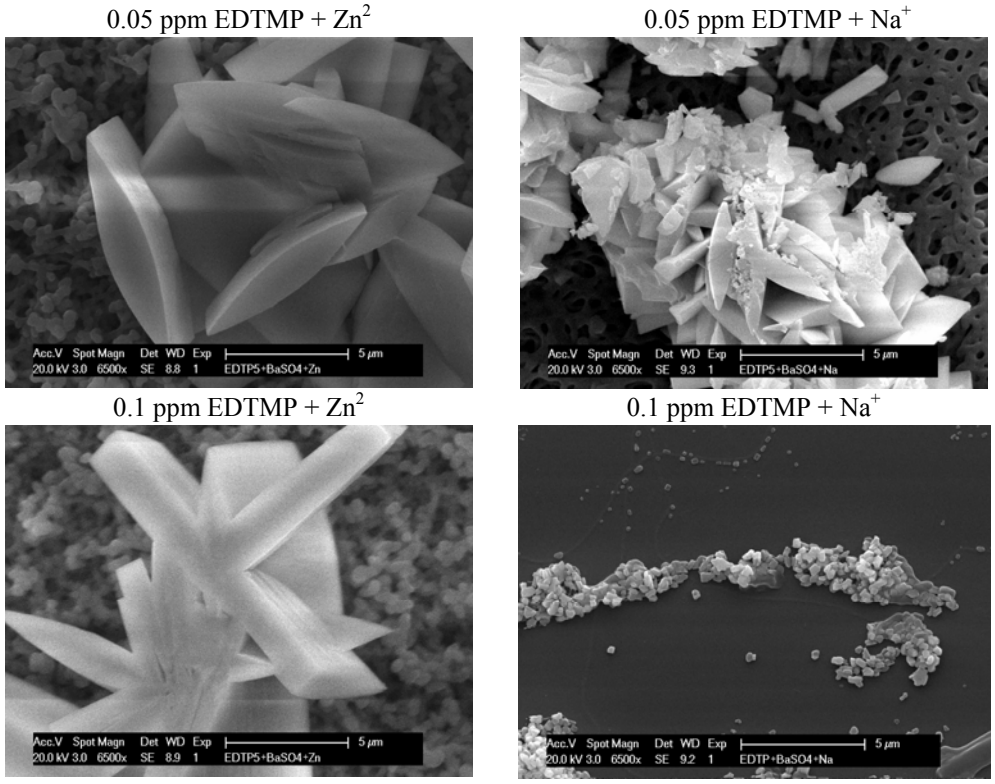

Figure 57. SEM images of barium sulfate particles precipitated in the presence of EDTMP and either Zn^{2+} or Na^{+} ions

Furthermore, the presence of Zn^{2+} ions in the presence of HEDTMP can be seen to increase the precipitation rate rather than inhibit it when compared to the equivalent ionic strength situation. Whether this effect is due to less inhibitor being available to interact (a solution complexation mechanism) or whether the complex actually increases the precipitation rate is yet to be definitively answered. A film of this precipitate has been previously observed to protect carbon steel from excessive corrosion. The effect of Zn^{2+} ions on EDTMP inhibitory activity was weaker. Additionally, in the case of either EDTMP or HEDTMP and Zn^{2+} ions being present, the morphology of barium sulfate was unaffected. This was also observed for EDTA previously and appears to be related to the complexation of the organic additive with the inorganic ion. It is not known how general this phenomenon is. Do all divalent cations promote precipitation in the presence of organic additives? If this is true, how might trivalent cations behave in the presence of phosphonates?

3.3.3. Octacalcium Phosphate

Octacalcium phosphate (OCP) has a great biological significance due to its possible involvement as a precursor during the deposition of carbonated apatite in the hard tissues of vertebrates.[108] OCP synthesis is dramatically affected by the presence of additives. Its formation was studied in the presence of NaPC and CaNaPC in order to examine whether these two similar materials will have varying effects on OCP formation. No reduction in the total amount of obtained product was observed as a function of additive concentration. On the

other hand, addition of CaNaPC provokes a modest variation of the X-ray patterns, which exhibit a minor presence of hydroxyapatite (HA), whereas the presence of HA is much more evident in the patterns of the products obtained in the presence of NaPC. Moreover, the results of SEM investigations indicate that the presence of both additives induce a drastic variation in the morphology of the products, which show a great tendency to aggregation and clustering and to assume spherical shapes. This trend is enhanced at low speed of stirring, whereas stirring at high speed seems to promote the formation of well-separated crystals. NaPC is much more effective in promoting crystal aggregation and clustering, leading to the formation of spherical structures, whereas the dimensions of the crystals obtained in the presence of CaNaPC are considerably reduced with respect to those of the control OCP. These results are presented in Table 5 and Figures 58 and 59.

Table 5. Visual observations on precipitated OCP in the presence of NaPC and CaNaPC additives and under different stirring conditions

		experimental conditions		
		No stirring	2.5 turns/sec	10 turns/sec
additives	control	Crystals about 20 μm long, 2 μm wide	Crystals and aggregates of crystals, 150-200 μm long, 5-10 μm wide	Crystals and aggregates of crystals, 80-130 μm long, 5-8 μm wide
	NaPC 3.0 mg/L	Aggregates of crystals and smooth spheres	Smooth spheres with overgrowth of crystals	Crystals and aggregates of crystals, 150-200 μm long, 2-4 μm wide
	NaPC 6.0 mg/L		Aggregates of crystals and smooth spheres	Smooth spheres and aggregates of crystals
	CaNaPC 3.0 mg/L	crystals	Aggregates of crystals, 160μm long	Crystals and aggregates of crystals, 25-40 μm long, 1-2 μm wide
	CaNaPC 6.0 mg/L	Smooth spheres, spherulites and aggregates of crystals	Smooth spheres with overgrowth of crystals	Crystals and aggregates of crystals, 25-45 μm long, 2-3 μm wide

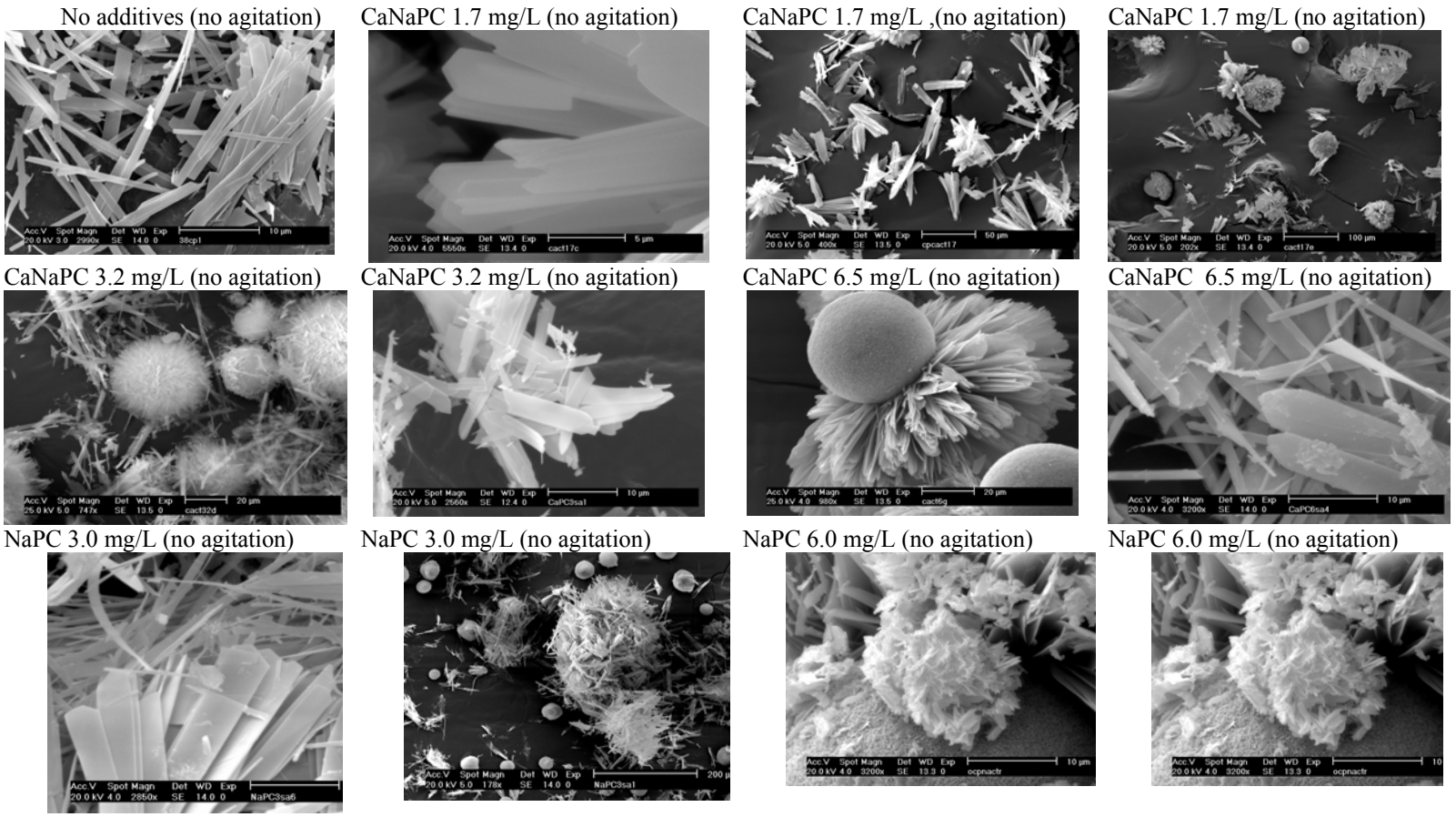

Figure 58. SEM images of OCP in the absence and presence of NaPC and CaNaPC under “no stirring” conditions. Note the difference in scale in the various images

3.3.4. Dissolution of Colloidal Silica

Colloidal silica is one of the most problematic deposits that plague industrial water systems. Its inhibition and removal still remain significant challenges in industrial water control technologies. Although phosphonates are not effective inhibitors in controlling silica formation they are moderate to good silica dissolvers. The solubility of SiO2 increases as pH increases.[109] Therefore, high pH regions are desirable for silica scale dissolution. However, silica chemical cleanings have to be performed at pH regions that do not compromise system integrity and personnel safety. In the experiments reported herein a pH of 10.00 was selected. Various additives were tested, but the results presented are for a tricarboxylate (citric acid), a structurally similar, mixed monophosphonate/tricarboxylate (2-phosphonobutane-1,2,4-tricarboxylic acid). Ammonium bifluoride, NH4F•HF is currently practiced for cleaning SiO_2/silicate deposits in industrial water systems. Hazards associated with generating HF in situ, as well as the low pH of the dissolution process and the resulting high metallic corrosion rates during cleaning, are some of the reasons that alternative, safer and more effective chemical approaches are sought for SiO_2/silicate deposit dissolution.

Results are presented in Figures 60 and 61. Silica dissolution in the absence of additives proceeds fairly slowly with time, reaching ~200 ppm soluble silica. There exists some variability in results that is most likely due to small differences in solution stirring. Citric acid accelerates silica dissolution, eventually dissolving ~ 230 ppm after 72 h. 2-phosphonobutane-1,2,4-tricarboxylic acid is more effective cleaner than citric acid. When used in 11000 ppm dosage it dissolves 333 ppm silica, a 67 % dissolution efficiency.

Systematic studies on the effect of various additives in silica dissolution have been reported elsewhere.[110]

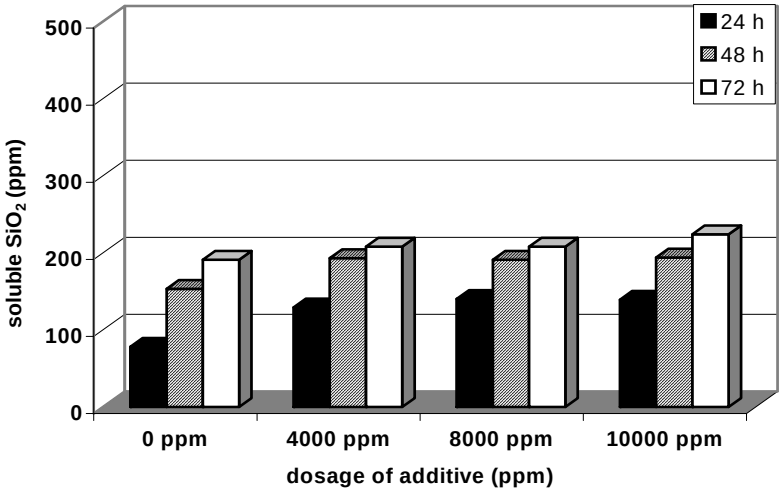

Figure 60. Collolidal silica dissolution by citric acid

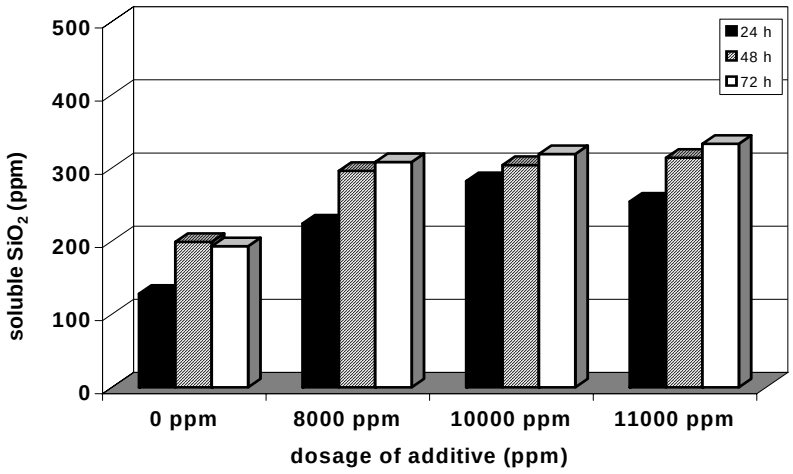

Figure 61. Collolidal silica dissolution by PBTC.

ACKNOWLEDGMENTS

A number of hard-working students and enthusiastic collaborators have greatly contributed to the research described herein. A sincere "thank you" goes to my students Eleftheria Mavredaki, Stella Katarachia, Chris Mantzaridis, Panos Lykoudis, Zoe Petraki, Eleni Barouda, Magia Papadaki and my collaborators Prof. Raphael G. Raptis (University of Puerto Rico), Prof. Herman Cheung (Miami Medical School), Prof. John Sallis (Ret., University of Tasmania), Prof. Petros G. Koutsoukos (University of Patras), Prof. Peter Baran (Juniatta College), Dr. Hong Zhao (University of Puerto Rico), Dr. Franca Jones (Curtin University of Technology).

REFERENCES

[1] (a) A. Clearfield, *Curr. Opin. Solid State Mater. Sci*. 1998, 1, 268. (b) A. Clearfield, *Curr. Opin. Solid State Mater. Sci*. 2002, 6, 495. (c) C.M. Bell, S.W. Keller, V.M. Lynch, T.E. Mallouk, *Mater. Chem. Phys*. 1993, 35, 225. (d) K. Maeda, *Microporous Mesoporous Mater*. 2004, 73, 47. (e) R.W. Sparidans, I.M. Twiss, S. Talbot, *Pharm. World Sci*. 1998, 20, 206. (f) G. Alberti, M. Casciola, U. Costantino, R. Vivani, *Adv. Mater.* 1996, 8, 291.

[2] (a) M.A. Petruska, B.C. Watson, M.W. Meisel, D.R. Talham, D. *Chem. Mater*. 2002, 14, 2011. (b) G.A. Neff, M.R. Helfrich, M.C. Clifton, C.J. Page, *Chem. Mater*. 2000, 12, 2363.

[3] (a) T.E. Mallouk, J.A. Gavin, *Acc. Chem. Res*. 1998, 31, 209. (b) A. Clearfield, Chem. Mater. 1998, 10, 2801. (c) T. Kimura, *Chem. Mater*. 2003, 15, 3742.

[4] C.Y. Ortiz-Avila, C. Bhardwaj, A. Clearfield, *Inorg. Chem*. 1994, 33, 2499.

[5] (a) L.C. Brousseau III, T.E. Mallouk, *Anal. Chem*. 1997, 69, 679. (b) L.C. Brousseau III, D.J. Aurentz, A.J. Benesi, T.E. Mallouk, *Anal. Chem*. 1997, 69, 688.

[6] (a) K. Maeda, Y. Kiyozumi, F.J. Mizukami, *Phys. Chem*. B 1997, 101, 4402. (b) F. Odobel, B. Bujoli, D. Massiot, *Chem. Mater*. 2001, 13, 163.

[7] (a) I.O. Benitez, B. Bujoli, L.J. Camus, C.M. Lee, F. Odobel, D.R. Talham, *J. Am. Chem. Soc*. 2002, 124, 4363. (b) G.E. Fanucci, J. Krzystek, M.W. Meisel, L.-C. Brunel, D.R. Talham, *J. Am. Chem. Soc*. 1998, 120, 5469.

[8] G. Cao, H.G. Hong, M.E. Thompson, *Acc. Chem. Res*. 1992, 25, 420.

[9] (a) J. Wu, W. Sun, X. Sun, H.-G. Xia, *Green Chem*., 2006, 8, 365. (b) L.S. Hollis, A.V. Miller, A.R. Amundsen, J.E. Schurig, E.W. Stern, *J. Med. Chem*. 1990, 33, 105. (c) K. Moedritzer, R.R. Irani, *Inorg. Chem*. 1966, 31, 1603.

[10] (a) C.V. Krishnamohan, A. Clearfield, *J. Am. Chem. Soc*. 2000, 122, 4394. (b) R. Vivani, U. Costantino, M. Nocchetti, *J. Mater. Chem*. 2002, 12, 3254. (c) H.-C. Yao, J.-J. Wang, Y.-S. Ma, O. Waldmann, W.-X. Du, Y. Song, Y.-Z. Li, L.-M. Zheng, S. Decurtins, X.-Q. Xin, Chem. Commun. 2006, 1745. (d) G.J. Halder, C.J. Kepert, B. Moubaraki, K.S. Murray, J.D. Cashion, *Science* 2002, 298, 1762. (e)

[11] (a) E. Lee, Y. Kim, D.-Y. Jung, *Inorg. Chem*. 2002, 41, 501. (b) V. Stavila, A. Gulea, N. Popa, S. Shova, A. Merbach, Y.A. Simonov, J. Lipkowski, *Inorg. Chem. Commun*. 2004, 7, 634. (c) A. Erxleben, *Coord. Chem. Rev*. 2003, 246, 203. (d) C. Janiak, *Dalton Trans*. 2003, 2781. (e) Y. Kim, D.-Y. Jung, *Inorg. Chem*. 2000, 39, 1470. (f) Y. Guo, D. Xiao, E. Wang, Y. Lu, J. Lu, X. Xu, L. Xu, *J. Solid State Chem*. 2005, 178, 776.

[12] K. Popov, H. Rönkkömäki, L.H.J. Lajunen, *Pure Appl. Chem*. 2001, 73, 1641.

[13] (a) Hix, G. B.; Wragg, D. S.; Wright, P. A.; Morris, R. E. *J. Chem. Soc*. Dalton Trans. 1998, 3359. (b) Slepokura, K.; Lis, T. Acta Crystallogr. 2003, C59, m76. (c) Stock, N.; Frey, S. A.; Stucky, G.D.; Cheetham, A. K. *J. Chem. Soc*., Dalton Trans. 2000, 4292. (d) Yang, B.-P.; Mao, J.-G.; Sun, Y.-Q.; Zhao, H.-H.; Clearfield, A. *Eur. J. Inorg. Chem*. 2003, 4211. (e) R. Fu, H. Zhang, L. Wang, S. Hu, Y. Li, X. Huang, X. Wu, *Eur. J. Inorg. Chem*. 2005, 3211.

[14] See http://www.phosphonate.com (accessed April 6, 2006).

[15] K.D. Demadis, P. Lykoudis, *Bioinorg. Chem. Appl*. 2005, 3, 135.

[16] (a) Silvestre, J.-P.; N. Q. Dao, N. Q.; Salvini, P. *Phosphorus, Sulfur Silicon* 2002, *177*, 771. (b) Clearfield, A. *Prog. Inorg. Chem.*1998, *47*, 371. (c) Clearfield, A.; Krishnamohan Sharma, C. V.; Zhang, B. *Chem. Mater.* 2001, *13,* 3099. (d) Dines, M. B.; Cooksey, R. E.; Griffith, P. C.; Lane, R. H. *Inorg. Chem.* 1983, *22*, 1003. (e) Yang, H. C.; Aoki, K.; Hong, H.-G.; Sackett, D. D.; Arendt, M. F.; Yau, S.-L.; Bell, C. M.; Mallouk, T. E. *J. Am. Chem. Soc*. 1993, *115*, 11855. (f) Penicaud, V.; Massiot, D.; Gelbard, G.; Odobel, F.; Bujoli, B. *J. Mol. Struct*. 1998, *470*, 31. (g) Serre, C.; Ferey, G. *Inorg. Chem*. 1999, *38*, 5370. (h) Serpaggi, S.; Ferey, G. *J. Mater. Chem.* 1998, 8, 2749. (i) Distler, A.; Lohse, D. L.; Sevov, S. C. *J. Chem. Soc., Dalton Trans.* 1999, 1805. (j) Poojary, D. M.; Zhang, B.; Clearfield, A. *J. Am. Chem. Soc*. 1997, *119*, 12550. (k) Poojary, D. M.; Zhang, B.; Belling-Hausen, P.; Clearfield, A. *Inorg. Chem*. 1996, *35*, 4942. (l) Alberti, G.; Vivani, R.; Murcia Mascaros, S. *J. Mol. Struct*. 1998, *470*, 81. (m) Alberti, G.; Marcia-Mascaros, S.; Vivani, R. *J. Am. Chem. So*c. 1998, *12*0, 9291.

[17] (a) P.G. Klepetsanis, P.G. Koutsoukos, *J. Cryst. Growth* 1998, 193, 156. (b) N.G. Harmandas, E. Navarro Fernandez, P.G. Koutsoukos, *Langmuir* 1998, 14, 1250. (c) A. Zieba, G. Sethuraman, F. Perez, G.H. Nancollas, D. Cameron, *Langmuir* 1996, 12,

2853. (d) M.M. Reddy, G.H. Nancollas, *Desalination* 1973, 12, 61. (e) R.A. Bochner, A. Abdul-Rahman, G.H. Nancollas, *J. Chem. Soc. Faraday Trans. I*, 1984, 80, 217. (f) I. Drela, P. Falewicz, S. Kuczkowska, *Wat. Res.* 1998, 32, 3188. (g) L. Dubin, *NACE Conference* 1980, Corrosion/80, Paper number 222.

[18] R.P. Carter Jr., R. L. Carroll, R.R. Irani, *Inorg. Chem*. 1967, 6, 939.

[19] V.S. Sergienko, *Russ. J. Coord. Chem*. 2001, 27, 681.

[20] J.E. Bollinger, D.M. Roundhill, *Inorg. Chem*. 1993, *32*, 2821.

[21] U. Kortz, M.T. Pope, *Inorg. Chem*. 1995, 34, 3848.

[22] K.D. Demadis, S.D. Katarachia, M. Koutmos, *Inorg. Chem. Comm*. 2005, 8, 254.

[23] K.D. Demadis, S.D. Katarachia, H. Zhao, R.G. Raptis, P. Baran, *Cryst. Growth Des*. 2006, 6, 836.

[24] (a) C.V.K. Sharma, A. Clearfield, A. Cabeza, M.A.G. Aranda, S. Bruque, *J. Am. Chem. Soc.* 2001, 123, 2885 (b) A. Cabeza, X. Ouyang, C.V.K. Sharma, M.A.G. Aranda, S.J. Bruque, A. Clearfield, *Inorg. Chem*. 2002, 41, 2325.

[25] K.D. Demadis, S.D. Katarachia, *Phosphorus, Sulfur, Silicon*, 2004, 179, 627.

[26] J.J. Daly, P.J. Wheatley, *J. Chem. Soc A* 1967, 212.

[27] D.A. Sagatys, C. Dahlgren, G. Smith, R.C. Bott, A.C. Willis, *Aust. J. Chem.* 2000, *53*, 77.

[28] K.D. Demadis, C. Mantzaridis, R.G. Raptis, G. Mezei, *Inorg. Chem*. 2005, 44, 4469.

[29] (a) Gomez-Alcantara, M.; Cabeza, A.; Martınez-Lara, M.; Aranda, M.A.G.; Suau, R.; Bhuvanesh, N.; Clearfield, A. *Inorg. Chem*. 2004, 43, 5283. (b) Song, H.-H.; Zheng, L.-M.; Wang, Z.; Yan, C.-H.; Xin, X.-Q. *Inorg. Chem*. 2001, 40, 5024. (c) Drumel, S.; Janvier, P.; Deniaud, D.; Bujoli, B. *J. Chem. Soc., Chem. Commun*. 1995, 1051. (d) Hartman, S. J.; Todorov, E.; Cruz, C.; Sevov, S. C. *Chem. Comm*. 2000, 1213. (e) Mao, J.-G.; Clearfield, A. *Inorg. Chem.* 2002, 41, 2319. (f) Yang, B.-P.; Mao, J.-G.; Sun, Y.-Q.; Zhao, H.-H.; Clearfield, A. *Eur. J. Inorg. Chem*. 2003, 4211.

[30] (a) Sharma, C.V.K.; Clearfield, A.; Cabeza, A.; Aranda, M.A.G.; Bruque, S. *J. Am. Chem. Soc*. 2001, 123, 2885. (b) Cabeza, A.; Ouyang, X.; Sharma, C.V.K.; Aranda, M.A.G.; Bruque, S. J.; Clearfield, A. *Inorg. Chem*. 2002, 41, 2325. (c) Demadis, K.D.; Katarachia, S.D.; Koutmos, M. *Inorg. Chem. Comm*. 2005, 8, 254. (d) Bishop, M.; Bott, S.G.; Barron, A.G. *Chem. Mater*. 2003, 15, 3074.

[31] Zheng, G.-L.; Ma, J.-F.; Yang, J. *J. Chem. Res*. 2004, 387.

[32] Stock, N.; Stoll, A.; Bein, T. *Angew. Chem. Int. Ed*. 2004, 43, 749.

[33] Stock, N.; Stoll, A.; Bein, T. *Microporous Mesoporous Mater.* 2004, 69, 65.

[34] Stock, N.; Rauscher, M.; Bein, T. *J. Solid State Chem*. 2004, 177, 642.

[35] K.D. Demadis, E. Barouda, H. Zhao, R.G. Raptis, *manuscript in preparation*.

[36] (a) A. Schier, S. Gamper, G. Müller, *Inorg. Chim. Acta*, 1990, 177, 179. (b) B.H. Lee, V.M. Lynch, G. Cao, T.E. Mallouk, *Acta Cryst*. 1988, C44, 365. (c) J. Yang, J.-F. Ma, G.-L. Zheng, L. Li, F.-F. Li, Y.-M. Zhang, J.-F. Liu, *J. Solid State Chem*. 2003, 174, 116. (d) C. Lei, J.-G. Mao, Y.-Q. Sun, H.-Y. Zeng, A. Clearfield, *Inorg. Chem*. 2003, 42, 6157.

[37] (a) L.M. Shkol'nikova, M.A. Porai-Koshits, N.M. Dyatlova, G.F.Yaroshenko, M.V. Rudomino, E.K. Kolova, *Zh. Strukt. Khim. (Russ. J. Struct. Chem.)* 1982, 23, 98. (b) D.C. Crans, F. Jiang, O.P. Anderson, S.M. Miller, *Inorg. Chem*. 1998, 37, 6645. (c) S.O.H. Gutschke, D.J. Price, A.K. Powell, P.T. Wood, *Angew. Chem. Int. Ed. Engl*. 1999, 38, 1088. (d) B. Zhang, D.M. Poojary, A. Clearfield, *Inorg. Chem*. 1998, 37, 249.

(e) J.-G. Mao, Z. Wang, A. Clearfield, *Inorg. Chem*. 2002, 41, 6106. (f) J.-G. Mao, A. Clearfield, *Inorg. Chem*. 2002, 41, 2319. (g) K.F. Bowes, G. Ferguson, C. Glidewell, A.J. Lough (2002) *Acta Cryst. C.* 2002, C58, o467. (h) D.M. Poojary, B. Zhang, A. Clearfield, *Angew. Chem. Int. Ed. Engl*. 1994, 33, 2324. (i) D.M. Poojary, A. Clearfield, *J. Organomet. Chem*. 1996, 512, 237. (j) F.A. Paz, F.-N. Shi, J. Klinowski, J. Rocha, T. Trindade, *Eur. J. Inorg. Chem*. 2004, 2759. (k) J.-L. Song, A.V. Prosvirin, H.-H. Zhao, J.-G. Mao, *Eur. J. Inorg. Chem*. 2004, 3706.

[38] K.D. Demadis, P. Baran, *J. Solid State Chem*. 2004, 177, 4768.

[39] K.D. Demadis, R.G. Raptis, P. Baran, *Bioinorg. Chem. Appl*. 2005, 3, 119.

[40] (a) K.D. Demadis, P. Lykoudis, R.G. Raptis, G. Mezei, *Cryst. Growth Des*. 2006, 6, 1064.

[41] (a) Song, J.-L.; Mao, J.-G.; Sun, Y.-Q.; Zeng, H.-Y. Kremer, R. K.; Clearfield, A. *J. Solid State Chem.* 2004, 177, 633. (b) Stock, N. *Solid State Sci*. 2002, 4, 1089. (c) Gutschke, S. O. H.; Price, D. J.; Powell, A. K.; Wood, P. T. *Angew. Chem., Int. Ed. Engl.* 1999, 38, 1088. (d) Fan, Y.; Li, G.; Shi, Z.; Zhang, D.; Xu, J.; Song, T.; Feng, S. *J. Solid State Chem*. 2004, 177, 4346. (e) Bauer, S.; Bein, T.; Stock, N. *J. Solid State Chem.* 2006, 179, 145. (f) Hix, G. B.; Wragg, D. S.; Wright, P. A.; Morris, R. E. *J. Chem. Soc.* Dalton Trans. 1998, 3359. (g) Slepokura, K.; Lis, T. *Acta Crystallogr*. 2003, C59, m76. (h) Stock, N.; Frey, S. A.; Stucky, G.D.; Cheetham, A. K. *J. Chem. Soc., Dalton Trans.* 2000, 4292. (i) Yang, B.-P.; Mao, J.-G.; Sun, Y.-Q.; Zhao, H.-H.; Clearfield, A. *Eur. J. Inorg. Chem*. 2003, 4211.

[42] Y. Kato, L.M. Toledo, J. Rebek, Jr., *J. Am. Chem. Soc*. 1996, 118, 8575. (b) G. Swarnabala, M.V. Rajasekharan, *Inorg. Chem*. 1998, 37, 1483. (c) M.J. Platers, R.A. Howie, A.J. Roberts, *Chem. Commun*. 1997, 893.

[43] Bauer, S.; Bein, T.; Stock, N. *J. Solid State Chem*. 2006, 179, 145.

[44] (a) Demadis, K. D.; Sallis, J. D.; Raptis, R. G.; Baran, P. *J. Am. Chem. Soc*. 2001, 123, 10129. (b) Demadis, K. D.; Katarachia, S. D.; Koutmos, M. *Inorg. Chem. Commun*. 2005, 8, 254.

[45] G. Chiari, *Acta Cryst*. 1990, B46, 717.

[46] N.C. Webb, *Acta Cryst*. 1966, 21, 942.

[47] M.I. Kay, R.A. Young, A.S. Posner, *Nature* 1964, 204, 1050.

[48] B. Sheldrick, *Acta Cryst*. 1974, B30, 2056.

[49] A. Clearfield, *Prog. Inorg. Chem*. 1998, 47, 371.

[50] L.C. Ward, R. Shankar, J.D. Sallis, *Atherosclerosis* 1987, 65, 117.

[51] B.L. Barnett, V.A. Uchtman, *Inorg. Chem*. 1979, 18, 2674.

[52] A. Wierzbicki, C.S. Sikes, J.D. Sallis, J.D. Madura, E.D. Stevens, K.L. Martin, *Calcif. Tissue Int.* 1995, 56, 297.

[53] Mattson, E. (1989), *Basic Corrosion Technology for Scientists and Engineers*, Ellis Horwood Publishers.

[54] R. Javaherdashti, *Anti-Corrosion Methods and Materials* 2000, 47(1), 30.

[55] G. Gunasekaran, R. Natarajan, V.S. Muralidharan, N. Palaniswamy and B.V. Appa Rao, *Anti-Corrosion Methods and Materials* 1997, 44(4), 248.

[56] S. Rajendran, B.V. Appa Rao and N. Palaniswamy, *Anti-Corrosion Methods and Materials* 1999, 46(1), 23.

[57] (a) Kalman, E.; Lukovits, I.; Palinkas, G. *ACH-Models in Chemistry* 1995, 132, 527. (b) Bofardi, B.P. in *Reviews on Corrosion Inhibitor Science and Technology*, Raman, A.;

Labine, P. Eds., NACE International: Houston, TX, 1993, p. II-6. (c) Sastri, V.S. *Corrosion Inhibitors*: *Principles and Applications*, John Wiley and Sons: Chichester, 1998, p. 720.

[58] Knepper, T.P. *Trends Anal. Chem*. 2003, 22, 708.

[59] (a) S. Rajendran, B.V. Apparao and N. Palaniswamy, *Anti-Corrosion Methods and Materials* 1998, 45(5), 338. (b) Gunasekaran, G.; Palanisamy, N.; Appa Rao, B.V.; Muralidharan, V.S. *Electrochim. Acta* 1997, 42, 1427.

[60] E. Kalman, F.H. Karman, J. Telegdi, B. Varhegyi, J. Balla, T. Kiss, *Corrosion Sci*. 1993, 35, 1477.

[61] Kuznetsov, Y.I.; Kazanskaya, G.Y.; Tsirulnikova, N.V. *Prot. Met*. 2003, 39, 120.

[62] Tew WP, Malis CD, Howard JE, Lehninger AL. *Proc. Natl. Acad. Sci. USA* 1981, 78, 5528.

[63] Moro L, Stagni N, Luxich E, Sallis JD, DeBernard B. *Biochem. Biophys. Res. Commun.* 1990, 170, 251.

[64] (a) Cheung HS, Sallis JD, Mitchell P, Struve JA. *Biochem. Biophys. Res. Commun.* 1990, 171, 20. (b) Cheung HS, Kurup IV, Sallis JD, Ryan LM. *J. Biol. Chem.* 1996, 271, 28082. (c) Nair D, Misra RP, Sallis JD, Cheung HS. *J. Biol. Chem.* 1997, 272, 18920.

[65] (a) Reuben PM, Wenger L, Cruz M, Cheung HS. *Connective Tissue Research* 2001, 42, 1. (b) Cheung HS, Sallis JD, Struve JA. *Biochem. Biophys. Acta* 1996, 1315, 105. (c) Cheung HS. *Rev. Bras. Rheum.* 1994, 34, S117.

[66] (a) Dalal P, Zannotti A, Wierzbicki A, Madura JD, Cheung HS. *Biophysical J.* 2005, 89, 1. (b) Wierzbicki A, Dalal P, Madura JD, Cheung HS. *J. Phys. Chem.* B 2003, 107, 12346.

[67] Tew WP, Mahle CD, Benavides J, Howard JE, Lehninger AL. *Biochemistry* 1980, 19, 1983.

[68] (a) Shankar R, Crowden S, Sallis JD. Atherosclerosis 1985, 50, 191.. (b) Sallis JD, Cheung HS. *Curr. Opin. Biol.* 2003, 15, 321.

[69] (a) Cheung HS. *Front. Biosci.* 2005, 10, 1336. (b) Reuben P, Brogley M, Sun Y, Cheung HS. *J. Biol. Chem.* 2002, 277, 15190. (c) Morgan MP, Whelan LC, Sallis JD, McCarthy JC, Fitzgerald DJ, McCarthy GM. *Arthritis Rheum.* 2004, 50, 1642.

[70] Cheung HS, Ryan LM. *Osteoarthritis and Cartilage* 1999, 7, 409.

[71] Cheung, H.S.; Sallis, J.D.; Demadis, K.D.; Wierzbicki, A. *Arthritis Rheum*. 2006, 54, 2452.

[72] (a) Bendele AM, White SL, Hulman JF. *Lab. Animal Sci.* 1989, 39, 115. (b) Bendele AM, Hulman JF. *Arthritis Rheum.* 1988, 31, 561.

[73] Watson PJ, Hall LD, Malcolm A, Tyler JA. *Arthritis Rheum*. 1996, 36, 1327.

[74] Huebner JL, Otterness IG, Freund EM, Caterson B, Krause VB. *Arthritis Rheum*. 1998, 41, 877.

[75] Kapadia RD, Badger AM, Levin JM, Swift B, Bhattacharya A, Dodds RA et al. *Osteoarthritis and Cartilage* 2000, 8, 374.

[76] Cheung HS. *Curr. Opin. Rheum.* 2005, 17, 336.

[77] Bennett RM, Lehr JRM, McCarty DJ. *Arthritis Rheum*. 1976, 19, 93.

[78] Moskowitz RW, Davis W, Sammarco J, Martens M, Baker J, Mayor M. *Arthritis Rheum.* 1973, 16, 397.

[79] Krug HE, Mahowald ML, Halverson PB, Sallis JD, Cheung HS. *Arthritis Rheum.* 1993, 36, 1603.
[80] Cheung HS. *Current Rheumatology Reports* 2001, 3, 24.
[81] N.F.G. Parry, J.D. Sallis, in *Urolithiasis* 2000; A.L. Rodger, B.E. Hibbert, B. Hess, S.R. Khan, G.M. Preminger, Eds.; University of Cape Town Publications: South Africa, 2000, p. 204.
[82] Chemical induction of calcergy has been described previously in D.V. Doyle, C.J. Dunn, D.A. Willoughby, *J. Path.* 1979, 128, 63.
[83] There is a direct relationship between plaque weight and precipitation of hydroxyapatite, as shown in C.M. Cooper, J.D. Sallis, Int. *J. Pharm*. 1993, 98, 165.
[84] J.D. Sallis, J.D. Meehan, H. Kamperman, M.E. Anderson, *Phosphorus Sulfur Silicon* 1993, 76, 281.
[85] (a) Wierzbicki A, Cheung HS. J. Mol. Struct. *THEOCHEM* 1998, 454, 287. (b) Wierzbicki A, Cheung HS. J. Mol. Struct. *THEOCHEM* 2000, 529, 73.
[86] B. Bujoli, S.M. Lane, G. Nonglaton, M. Pipelier, J. Leger, D.R. Talham, C. Tellier, *Chem. Eur. J*. 2005, 11, 1980.
[87] (a) *Water-Formed Scale Deposits,* Cowan, J.C.; Weintritt, D.J. Water-Formed Scale Deposits, Gulf Publishing Co. Houston, TX, 1976. (b) *Mineral Scale Formation and Inhibition,* Amjad, Z. Ed.; Plenum Press: New York, 1995 and references therein. (c) *Calcium Phosphates in Biological and Industrial Systems,* Amjad, Z. Ed.; Kluwer Academic Publishers: Boston, 1998 and references therein. (d) Amjad, Z.; Hooley, J.P. *Tenside. Surf. Det.* 1994, *31*, 12. (e) Amjad, Z.; *Can. J. Chem.* 1988, *66*, 2180. (f) Oddo, J.E.; Tomson, M.B. *SPE Production and Facilities* 1994, *February*, 47.
[88] *(a) The Nalco Water Handbook*, Kemmer, F.N., McGraw-Hill Company, New York, 1988. (b) *Betz handbook of industrial water conditioning*, Betz Laboratories, Inc, Betz: Trevose, Pennsylvania, 1980.
[89] *(a) Procedures of Industrial Water Treatment*, Tanis, J.N. Ltan Inc., Ridgefield, CT: 1987. (b) J. Katzel, *Plant Engineering* 1989, *27*, 32. (c) Power Special Report *Power* 1973, *March*, S-1. (d) E.C. Elliot, *Power* 1985, *December*, S-1. (e) *Rules of Thumb for Chemical Engineers*, Branan, C.R.; Gulf Publishing Co. Houston, TX, 1994, p. 127.
[90] *(a) Technology for Chemical Cleaning of Industrial Equipment*, Frenier, W.W., NACE Press: Houston, TX, 2001, and references therein. (b) *Industrial Chemical Cleaning*, McCoy, J.W., Chemical Publishing: New York, 1984.
[91] (a) Poff, G. *Mater. Perform.* 1978, *10*, 24. (b) Wohlberg, C.; Buchholz, J.R. Corrosion/75, Paper No. 143, National Association of Corrosion Engineers, Houston, TX, 1975. (b) Smith, C.W. *Industrial Water Treatment* 1993, *July/August*, 20. (c) Midkiff, W.S.; Foyt, H.P. *Materials Performance* 1979, *August,* 39. (d) Midkiff, W.S.; Foyt, H.P. *Materials Performance,* 1978, *February,* p. 17. (e) Midkiff, W.S.; Foyt, H.P. Cooling Technology Institute, TP77-16 (TP-169A). (f) Midkiff, W.S.; Foyt, H.P. Los Alamos Scientific Laboratory, Report LA-UR-76-660 (1976). (g) Midkiff, W.S. Los Alamos Scientific Laboratory, Report LA-5508-MS (March 1974).
[92] (a) Dequest: *Phosphonates by Solutia* (Introductory Guide), Publication # 7459151B. (b) Dequest: *Phosphonates by Solutia* (2054 Phosphonates for scale and corrosion control, chelation, dispersion), Publication # 7450006A. (c) *Dequest: Phosphonates by Solutia* (2060-S, 2066 and 2066-A Phosphonates: metal ion control agents), Publication

7459369. (d) *Dequest: Phosphonates by Solutia* (2000 and 2006 Phosphonates for scale and corrosion control, chelation, dispersion), Publication # 7459023B.

[93] (a) Gill, J.; Varsanik, R.G. *J. Cryst. Growth* 1986, *76*, 57. (b) Matty, J.M.; Tomson, M.B. *Appl. Geochem.* 1988, 3, 549. (c) Tomson, M.B. *J. Cryst. Growth* 1983, *62*, 106. (d) Blum, H.; Christophliemk, P. *Phosphorus Sulfur Silicon* 1987, *30*, 619. (e) Amjad, Z. *J. Colloid Interface Sci.* 1988, *123*, 523.

[94] (a) Masler, W.F.; Amjad, Z. Corrosion/88, Paper No. 11, National Association of Corrosion Engineers, Houston, TX, 1988. (b) Deluchat, V.; Bollinger, J-C.; Serpaud, B.; Caullet, C. *Talanta* 1997, *44*, 897. (d) Oddo, J.E.; Tomson, M.B. *Applied Geochem.* 1990, *5*, 527.

[95] (a) Sweeney, F.M.; Cooper, S.D. *Society of Petroleum Engineers International Symposium on Oilfield Chemistry, New Orleans, LA March 2-5, 1993, paper SPE 25159.* (b) Oddo, J.E.; Tomson, M.B. Corrosion/92, Paper No. 34, National Association of Corrosion Engineers, Houston, TX, 1992. (c) Xiao, J.; Kan, A.T.; Tomson, M.B. *American Chemical Society-Division of Fuel Chemistry, Symposium Preprints* 1998, *43*, 246. (d) Browning, F.H.; Fogler, H.S. *AIChE Journal* 1996, *42*, 2883. (e) Vetter, O.J. *J. Pet. Tech.* 1973, *March*, 339. (f) Pairat, R.; Sumeath, C.; Browning, F.H.; Fogler, H.S. *Langmuir* 1997, *13*, 1791. (h) Browning, F.H.; Fogler, H.S. *AIChE Journal* 1996, *42*, 2883.

[96] (a) Carter, R.P.; Carrol, R.L.; Irani, R.R. *Inorg. Chem.* 1967, *6*, 939. (b) Hasson, D.; Semiat, R.; Bramson, D.; Busch, M.; Limoni-Relis, B. *Desalination* 1998, *118*, 285. (c) Gill, J.S. B. *Desalination* 1999, *124*, 43. (d) Hamed, O.A.; Al-Sofi, M.A.K.; Imam, M.; Mardouf, K.B.; Al-Mobayed, A.S.; Ehsan, A. B. *Desalination* 2000, *128*, 275. (e) Gill, J.S. *International Water Conference 1995, paper # 23,* p. 93.

[97] *Corrosion inhibitors: principles and applications*, Sastri, V.S., Chichester; New York: Wiley, 1998. (b) *Corrosion Inhibitors*, Nathan, C.C. Ed., NACE International: Houston, TX, 1973. (c) Organic inhibitors of corrosion of metals, Kuznetsov, Y.I., Plenum Press: New York, 1996. (d) *Corrosion Inhibitors*, European Federation of Corrosion, Publication # 11, The Institute of Metals: London, England, 1994. (e) Farooqi, I.H.; Nasir, M.A.; Quraishi *Corr. Prev. and Control* 1997, October, p. 129.

[98] (a) Reddy, M.M.; Nancollas, G.H. *Desalination* 1973, *12*, 61. (b) Tomson, M.B. *J. Cryst. Growth* 1983, *62*, 106. (c) Klepetsanis, P.G.; Koutsoukos, P.G. *J. Cryst. Growth* 1998, *193*, 156. (d) Harmandas, N. G.; Navarro Fernandez, E.; Koutsoukos, P.G. *Langmuir* 1998, *14*, 1250. (e) Dalpi, M.; Karayianni, E.; Koutsoukos, P.G. *J. Chem. Soc. Faraday Trans.* 1993, *89*, 965. (f) Xyla, A.G.; Mikroyannidis, J.; Koutsoukos, P.G. *J. Colloid Interface Sci.* 1992, *153*, 537.

[99] (a) Amjad, Z. *Tenside Surf. Det.* 1997, *34*, 102. (b) European Patent Application 0 267 597 A2. Masler, W.F., III; Amjad, Z. (c) Smyk, E.B.; Hoots, J.E.; Fivizzani, K.P.; Fulks, K.E. Corrosion/88, Paper No. 14, National Association of Corrosion Engineers, Houston, TX, 1988. (d) Hoots, J.E.; Crucil, G.A. Corrosion/86, Paper No. 13, National Association of Corrosion Engineers, Houston, TX, 1986. (e) European Patent Application 0 109 200 A1. Becker, L.W.

[100] US patents 4,983,686, 4,795,789, 4,756,881, 4,490,308, European Patent Application EP 265846, German Patent DE 3616583.

[101] (a) Dubin, L. Corrosion/80, Paper No. 222, National Association of Corrosion Engineers, Houston, TX, 1980.

[102] (a) Bartholomew, R.D. *International Water Conference, paper # 74,* p. 523 (1998). (b) Vaska, M.; Go, W. *Industrial Water Treatment* 1993, March/April, 39.

[103] (a) A.I.R. Stark, R.A. Wogelius, D.J. Vaughan, *Geophysical Research Abstracts*, Vol. 5, 14081, 2003. (b) P. Hartman, C.S. Strom, *J. Cryst. Growth* 1989, 97, 502. (c) M.C. Van Der Leeden, D. Kaschiev, G.M. Van Rosmalen, *J. Coll. Inter. Sci*. 1992, 152, 338. (d) C.M. Pina, C.V. Putnis, U. Becker, S. Biswas, E.C. Carroll, D. Bosbach, A. Putnis, *Surf. Sci*. 2004, 553, 61.

[104] (a) A. Matynia, K. Piotrowski, J. Koralewska, B. Wierzbowska, *Chem. Eng. Tech*. 2004, 27, 559. (b) L. Qi, H. Cölfen, M. Antonietti, *Chem. Mater*. 2000, 12, 2392.

[105] (a) Demadis, K.D.; Stathoulopoulou, A. *Materials Performance* 2006, 45(1), 40. (b) L. Qi, H. Cölfen, M. Antonietti, *Angew. Chem. Int. Ed*. 2000, 39, 604. (c) M.C. Van der Leeden, D. Kashchiev, G.M. van Rosmalen, *J. Cryst. Growth* 1993, 130, 221. (d) F. Jones, A. Stanley, A. Oliveira, A.L. Rohl, M.M. Reyhani, G.M. Parkinson, M.I. Ogden, *J. Cryst. Growth* 2003, 249, 584.

[106] Jones F., Oliveira A., Parkinson G.M., Rohl A.L., Stanley A., Upson T., *J. Cryst*. *Growth*, 2004, 262, 572.

[107] L.A. Bromley, D. Cottier, R.J. Davey, B. Dobbs, S. Smith, B.R. Heywood, *Langmuir* 1993, 9, 3594.

[108] (a) W.E. Brown, J.P. Smith, J.R. Lehr, A.W. Frazier, *Nature* 1962, 196, 1048. (b) A. Bigi, B. Bracci, S. Panzavolta, M. Iliescu, M. Plouet-Richard, J. Werckmann, D. *Cryst. Growth Des*. 2004, 4, 141. (c) V.K. Sharma, M. Johnsson, J.D. Sallis, G.H. Nancollas, *Langmuir* 1992, 8, 676. (d) A. Bigi, E. Boanini, G. Cojazzi, G. Falini, S. Panzavolta, *Cryst. Growth Des*. 2001, 1, 239.

[109] (a) Iler, R.K. *The chemistry of silica* (solubility, polymerization, colloid and surface properties and biochemistry), Wiley-Interscience, New York 1979. (b) Iler, R.K. *The chemistry of silica and silicates*, Cornell University Press, 1955.

[110] (a) K.D. Demadis, E. Neofotistou, E. Mavredaki, M. Tsiknakis, E.-M. Sarigiannidou, S.D. Katarachia, *Desalination* 2005, 179, 281. (b) E. Mavredaki, E. Neofotistou, K.D. Demadis, *Ind. Engin. Chem. Res*. 2005, 44, 7019. (c) K.D. Demadis, E. Mavredaki, *Env. Chem. Lett*. 2005, 3. 127.